2025

Investigating the relevance of nuclear deformability in zebrafish neuroepithelia

Mariana Maia-Gil

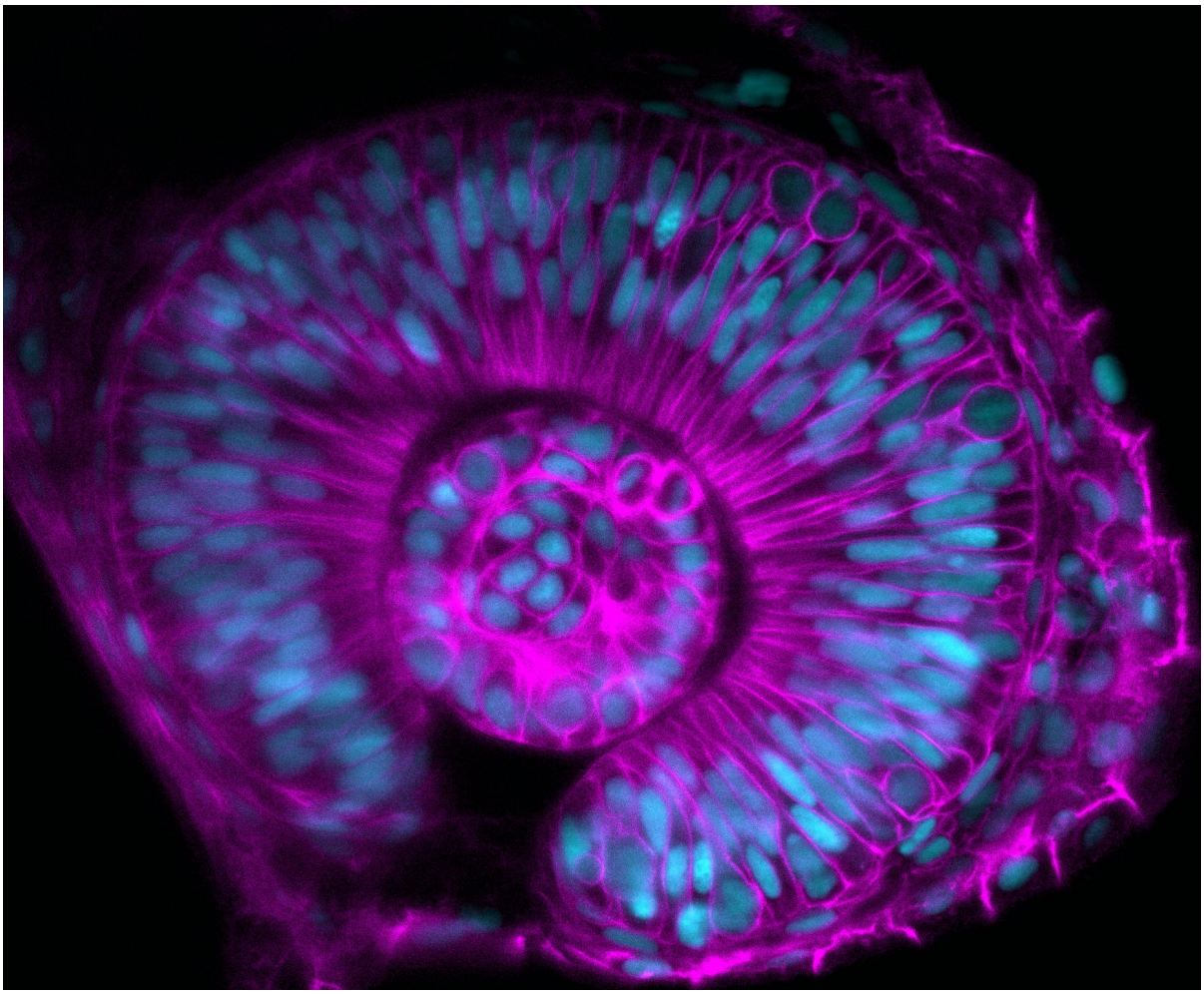

Dissertation presented to obtain the **Ph.D degree in**

Integrative Biology and Biomedicine

Oeiras, March, 2025

Acknowledgments

First and foremost, I have to thank Caren Norden for being an extraordinary supervisor and mentor. From science to life, she has always cared about me while pushing me forward. She gave me time and space when I needed it, she supported my maternity journey and, above all, she trusted me. I trust her just as much. And trust is the secret ingredient that makes her such a great leader. Caren is an incredible scientist—creative, sharp, and full of humour. She has made me laugh countless times, like the Wednesday she struggled up the stairs, saying, 'I had José in the morning.' I also learned from her cultural adjustment to Portugal. Once, when Caren was one of the directors of the institute, I had to explain that here, if we want a working computer, we actually have to buy one. Coincidence or not, soon after, everyone arriving at the institute received a computer. A lesson with many layers to reflect on! To be more precise and concise: Caren is both a scientific and personal role model, and I couldn't be more thankful for the opportunity to learn from her. As for the rest—nobody cares, Sean, nobody cares…

Doing my PhD in the Norden lab was truly an incredible experience! This was mainly because everyone cared about each other while maintaining a critical and supportive environment. It made all the difference to grow and learn in such a constructive atmosphere. I am truly grateful to all past and present members of the lab for constantly pushing my limits, both in science and in gravity: I especially appreciate Iskra Yanakieva for her support—she had the initial ideas that led to this project and kept exchanging emails with me; Tânia Ferreira, who shared lab life with me through transitions and challenges. Patrícia Ramos and João Coelho, who helped with revision experiments and always kept the fun levels high. Obrigadão ao cara Maurício Rocha Martins and kiitos ao senhor Jaakko Lehtimäki, who always had time to exchange ideas—great ideas! A harm thank you to Elisa Nerli, who taught me the beauty of Light Sheet microscopy over a video call, taught me how to swim, and made me the best parmigiana ever! Thank you to Diana Garcia Morales and Renata Cunha for all our conversations at Soya, about everything and anything—I am honored to call you my friends.

A huge thank you to Juliette Gouhier and Maria Gorjão, the amazing students I co-supervised and who taught me more than they can imagine. I was the lucky one to share my

scientific journey with you, along with our runs during incubation time and the poems shared on our commutes home.

I am also grateful to our collaborators. To Elias Barriga and Jaime Espina, who introduced me to the wonders of atomic force microscopy and helped turn a hypothesis into measurable data. And to Anna Erzberger and Roman Belousov, who patiently explained physics to me and showed how much theory can enhance our understanding.

I would also like to thank the IGC facilities for their technical support, especially the imaging and animal facilities. A special thank you to the fish girls—Liliana, Inês, Maysa, and Cristina!

Thank you to the IBB2019 cohort - Priscilla, Katia, Romana and Joana, you will always have a special place in my heart! I would also like to thank my thesis committee, Raquel Oliveira and Elias Barriga, for the great input in the project!

Thank you to my friends—the ones who have been with me since childhood and those with whom I've shared great moments over beers and dinners. I'm sorry for the beers I missed due to late lab sessions, but I'm deeply grateful for the ones we did have! Thank you for laughing with me about the broken scientific system in Portugal, for supporting me even when my choices came at a cost, and for respecting me for choosing what brings me the most joy.

I also want to thank my family—especially my father, for making me feel safe enough to dream, and my mother, for always being there no matter what. I'm incredibly lucky to have had your support through all these years!

And a huge thank you to André, who always has the happiest smile for me, gives me all the hugs I need, and keeps proving to me that "a ciência é querer adaptar o menor sonho ao maior" (Fernado Pessoa). A dream with a wagging tail and the two most beautiful retinas we have ever seen.

Science pushes the boundaries of imagination.

I dedicate this thesis to my father.

Dedico esta tese ao meu Pai.

(Por todas as conversas de mão dada, a passear à beira-mar)

Uma mosca sem valor
pousa com a mesma alegria
na careca de um doutor
como em qualquer porcaria.

António Aleixo – Este livro que vos deixo

Abstract

Nuclear positioning is a fundamental process in cellular and developmental biology. In neuroepithelia, the apical migration of nuclei before mitosis is crucial for tissue integrity and successful neurogenesis. While the cytoskeletal mechanisms driving this movement have been extensively studied, the influence of nuclear material properties on nuclear positioning remains less understood. A key determinant of nuclear deformability is Lamin A/C, an intermediate filament of the nuclear lamina. In vitro studies have shown that low Lamin A/C levels enhance nuclear deformability, facilitating cell migration in confined environments. Interestingly, during early development, including in confined neuroepithelia, Lamin A/C is expressed at low levels, suggesting a potential link between nuclear deformability and efficient nuclear positioning in developing tissues.

To investigate this, we used a zebrafish transgenic model in which Lamin A is overexpressed upon heat-shock induction. Our findings show that increased Lamin A expression leads to nuclear stiffening, reducing nuclear deformability. As a result, nuclei with high Lamin A levels move more slowly and less directly toward the apical side in the densely packed zebrafish retina. In contrast, in the less confined hindbrain neuroepithelium, these effects are minimal, indicating that the impact of nuclear stiffness on migration depends on tissue context. Moreover, even control cells that do not overexpress Lamin A exhibit impaired nuclear migration and mitotic entry when surrounded by a stiffer Lamin A-overexpressing environment, highlighting non-cell autonomous effects.

Together, this study suggests that nuclear material properties influence nuclear positioning in a tissue-dependent manner, providing new insights into the interplay between nuclear mechanics and developmental processes.

Resumo

A posição dos núcleos nas células é determinante para diversos processos da biologia celular e do desenvolvimento. No caso dos neuroepitélios, os núcleos localizam-se junto à superfície apical das células antes da mitose, garantindo a integridade do tecido e o desenvolvimento normal dos neurónios. Embora tenham sido realizados diversos estudos sobre os mecanismos do citoesqueleto que impulsionam os núcleos, ainda se sabe pouco sobre a influência das propriedades do núcleo, como a sua deformabilidade, no seu posicionamento adequado.

A Lamin A/C, um filamento intermédio da lâmina nuclear, é um dos principais elementos determinantes da deformabilidade nuclear. Estudos in vitro demonstraram que níveis baixos de Lamin A/C aumentam a deformabilidade do núcleo, facilitando a migração nuclear em ambientes confinados. Curiosamente, a expressão de Lamin A/C é geralmente baixa nas primeiras fases do desenvolvimento, o que ocorre também nos neuroepitélios, que apresentam um espaço bastante restrito. Assim, pode existir uma ligação entre a deformabilidade dos núcleos e a sua capacidade de se posicionarem corretamente em tecidos com espaço limitado.

Para explorar esta hipótese, utilizámos um modelo transgénico de peixe-zebra, no qual a Lamin A é sobrexpressa após indução por choque térmico. Os nossos resultados mostram que o aumento de Lamin A leva ao enrijecimento dos núcleos, reduzindo a sua capacidade de deformação. Verificámos que os núcleos com níveis elevados de Lamin A movem-se mais lentamente e de forma menos precisa em direção à superfície apical da retina do peixe-zebra. No entanto, no neuroepitélio do rombencéfalo, onde o espaço disponível é maior, os efeitos observados são mínimos. Isto sugere que o impacto da rigidez nuclear na migração apical depende das características do tecido em que os núcleos estão inseridos.

Adicionalmente, verificámos que células de controlo, que não sobrexpressam Lamin A, apresentam dificuldades na migração apical dos núcleos e no início da divisão celular quando estão rodeadas por um ambiente mais rígido, devido à sobrexpressão de Lamin A.

Este estudo sugere que as propriedades do núcleo influenciam a capacidade de posicionamento nuclear dentro das células, dependendo do tecido em que estão localizados. Esta conclusão abre novas perspetivas sobre a interação entre as propriedades do núcleo e os processos de desenvolvimento dos tecidos.

Contents

ACKNOWLEDGMENTS 3

ABSTRACT 9

RESUMO 10

CONTENTS 11

1. INTRODUCTION 13

1.1 Moving nuclei to the right place at the right time 13
1.2 Cytoskeleton components driving nuclear positioning 14
1.2.1 Mechanisms of cytoskeleton interaction with the nucleus 15
1.2.2 Microtubules can either push or pull nuclei 18
1.2.3 Actin-dependent mechanisms for nuclear positioning 19
1.2.3.1 Actin nucleation generates a pushing force 21
1.2.3.2 Actin-myosin creates contractile forces 22
1.2.3.3 TAN lines can couple the nucleus to the cytoskeleton 23
1.3.2 Cell and tissue morphology can define nuclear positioning mechanisms 23
1.3 The role of nuclear lamina in nuclear positioning 24
1.3.1 Lamin A regulates gene transcription 26
1.3.2 Lamin A expression levels modulate cell migration in confinement 27
1.3.3 Possible mechanical regulation of cell rounding in confined tissues 29
1.4 Lamin A expression in developmental contexts 30
1.5 Nuclear positioning in the zebrafish neuroepithelia 31
1.5.1 Overview about pseudostratified epithelia 31
1.5.2 Apical nuclear migration 32
1.5.3 Apical mitosis guarantees tissue integrity 33
1.6 Exploring the influence of nuclear mechanics on nuclear positioning in zebrafish neuroepithelia 35
1.7 Objective of the study 36

2. RESULTS 38

2.1 Lamin A expression levels increase upon overexpression in the zebrafish retina, and Lamin A integrates into the nuclear lamina 40
2.2 Lamin A overexpression in the zebrafish retinal neuroepithelia decreases nuclear volume and deformability 42
2.3 Lamin A overexpression changes nuclear and tissue stiffness: theory and experiment 45
2.4 Overexpression of Lamin A lengthens the G2 phase but not the overall cell cycle 48
2.5 Lamin A-overexpression does not delay retinal neurogenesis onset and lamination 51
2.6 Nuclei can reach the apical surface prior to mitosis despite increased Lamin A expression 53
2.7 Nuclear stochastic movements associated with S and G1 phases are not altered by Lamin A overexpression 54
2.8 Lamin A-overexpression slows apical nuclear migration by 50% and disrupts directionality before mitosis 56
2.9 Lamin A-overexpressing does not interfere with cytoskeleton arrangements 60
2.10 Reduced nuclear deformability is associated with defects in apical nuclear migration in Lamin A-overexpressing nuclei 61
2.11 Effects of Lamin A overexpression are less pronounced in the looser packed hindbrain 63
2.12 Increased nuclear stiffness impairs apical nuclear migration in a non-cell autonomous manner 67
2.13 Increased nuclear, and therefore tissue, stiffness delays nuclear envelope breakdown and mitotic rounding 70

3. DISCUSSION 74

3.1 Linking nuclear material properties and migration within the context of a developing tissue 75
3.1.1 The relevance of nuclear deformability for nuclear positioning depends on the tissue context 75
3.1.2 Nuclear deformability tissue-wide facilitate nuclear positioning and mitotic entry 76

3.1.3 Nuclear deformability can influence the material properties of pseudostratified epithelia 78
3.2 Lamin A overexpression: affects nuclear mechanics rather than gene regulation 79
3.2.1 Ruling out alternative explanations: Cytoskeleton and Nuclear Envelope 80
3.2.2 Conclusion: Nuclear mechanics are the primary effect of Lamin A overexpression in zebrafish neuroepithelia 81
3.3 Low level of Lamin A expression may facilitate morphogenesis 82
3.4 Nuclear deformability ensures robustness in densely packed tissues 84
4. FUTURE DIRECTIONS 86
4.1 The effect of nuclear properties on nuclear positioning beyond zebrafish neuroepithelium 86
4.2 How is DNA damaged prevented in the densely packed zebrafish neuroepithelia 87
5. CONCLUSIONS 89
6. MATERIAL AND METHODS 90
6.1 Experimental model and study participants details 90
6.2 DNA Cloning and Constructs used 90
6.3 DNA and RNA microinjections 91
6.4 Blastomere transplantation 91
6.5 Heat-shock treatment and screening 92
6.6 Dissection of zebrafish heads 92
6.7 Immunoblotting 93
6.8 Whole-mount immunostaining 94
6.9 Dissection of retinal pseudostratified epithelium 94
6.9.1 Atomic Force Microscopy (AFM) measurements 95
6.9.2 AFM data analysis and image treatment 95
6.10 Microscope image acquisition 96
6.10.1 Confocal scans 96
6.10.2 Time-lapse imaging using Light Sheet Fluorescent Microscopy (LSFM) 97
6.11 Image processing and analysis 97
6.12 Nuclear segmentations, volume and shape analysis 97
6.13 Nuclear deformations during S and G2 phases 98
6.14 Analysis of cell cycle nuclear dynamics 98
6.15 Sample Drift Correction 99
6.16 MIP, rotation and nuclei tracking 99
6.17 Kinetics of apical nuclear migration 99
6.18 Quantification and Statistical analysis 100
6.20 Table of experimental repeats and statistical parameters used 100
7. LIST OF FIGURES 107
8. LIST OF ABBREVIATIONS 108
9. REFERENCES 111

1. Introduction

In this thesis, I investigated whether and how nuclear deformability influences nuclear positioning during neuroepithelial development. To address this, I overexpressed Lamin A, a key nuclear lamina protein, and examined its impact on nuclear stiffness and apical migration. To provide context for this research, I will first give an overview of nuclear positioning and the forces that drive nuclear movement. I will then discuss how nuclear material properties, related to Lamin A/C expression levels, can influence nuclear dynamics in a densely packed tissue. Finally, I will explain why pseudostratified epithelia—specifically the zebrafish retina and hindbrain—serve as an ideal model system for studying the nuclear movements required for cell proliferation in this context.

1.1 Moving nuclei to the right place at the right time

Nuclear positioning plays a crucial role in organ development, tissue homeostasis, and disease prevention across various biological contexts.

The position of the nucleus within cells and unicellular organisms determines whether a division will be symmetric or asymmetric, ultimately influencing the fate of daughter cells. Proper nuclear positioning is critical in unicellular organisms, such as budding and fission yeast, where nuclei must be actively positioned at the cell midplane to ensure equal DNA segregation between daughter cells (Moore et al., 2009; Varshney and Sanyal, 2019). Similarly, in fertilised mammalian and invertebrate eggs, the nucleus is positioned relative to the plane of cell division.

Nuclear positioning is also essential for organ development and tissue organisation. In invertebrates, such as the Drosophila oocyte, the nucleus moves from the posterior to the anterior margin to establish the embryo's dorsoventral axis (Zhao et al., 2012). In multinucleated cells as found in the drosophila embryo and myofibers, nuclei are evenly spaced to ensure proper development. In Drosophila embryos, nuclear positioning regulates synchronous cell cycles and proper morphogenesis, while in vertebrate myofibres, it specifies nuclear function (reviewed in (Padilla et al., 2022). In pseudostratified epithelia, including the Drosophila wing disc and the vertebrate neuroepithelium, apical nuclear positioning before mitosis is essential for maintaining tissue integrity (Nakajima et al., 2013; Strzyz et al., 2015).

Additionally, in skeletal muscle, nuclei must relocate from the centre to the periphery of myofibres to support proper muscle function (Roman et al., 2017).

Nuclear positioning is also crucial for directed cell migration. Before migrating, cells undergo shape changes driven by cytoskeletal and organelle rearrangements, establishing polarity. In fibroblasts, muscle cells, neurons, mesenchymal cells, and many cancer cells, the nucleus typically moves towards the cell rear, influencing migration direction (Calero-Cuenca et al., 2018; Gomes et al., 2005).

Given this widespread importance, defects in nuclear positioning can have severe consequences for cell and tissue function. Mispositioned nuclei are a hallmark of several diseases, most of which are linked to mutations in the nuclear envelope and associated proteins. Muscle and neurological disorders are among the most common conditions where nuclear positioning is disrupted (reviewed in (Isermann and Lammerding, 2013)).

In Centronuclear Myopathies (CNM), nuclei fail to migrate to the periphery of muscle fibres, impairing muscle function (Jungbluth et al., 2008). Similarly, in Emery-Dreifuss Muscular Dystrophy (EDMD), mutations in nuclear envelope proteins such as Emerin and Lamin A/C disrupt nuclear movement, leading to muscle weakness and contractures (Folker and Baylies, 2013).

In the nervous system, nuclear positioning defects contribute to severe developmental disorders. Lissencephaly, a brain malformation associated with impaired neuronal migration, results in intellectual disabilities and seizures (Gleeson et al., 1998). Likewise, microcephaly arises when abnormal nuclear movement during brain development leads to reduced brain size which in turn can result in cognitive impairments (Gundersen and Worman, 2013).

These disorders often stem from defects in the cellular machinery responsible for moving nuclei to the right place at the right time. This system, which includes cytoskeletal arrangements, motor proteins, and nuclear envelope components, ensures precise nuclear positioning. When it fails, nuclei become mispositioned, disrupting normal development and tissue function (Calero-Cuenca et al., 2018).

Therefore, understanding nuclear positioning is critical for uncovering the biological mechanisms that drive organ development and maintain tissue integrity.

1.2 Cytoskeleton components driving nuclear positioning

Due to the importance of getting nuclei at the right place at the right time, several studies have explored the mechanisms that drive nuclear movements in different contexts. These research shows that nuclear positioning is a highly regulated process driven by dynamic interactions between the cytoskeleton and the nucleus or the nuclear envelope.

1.2.1 Mechanisms of cytoskeleton interaction with the nucleus

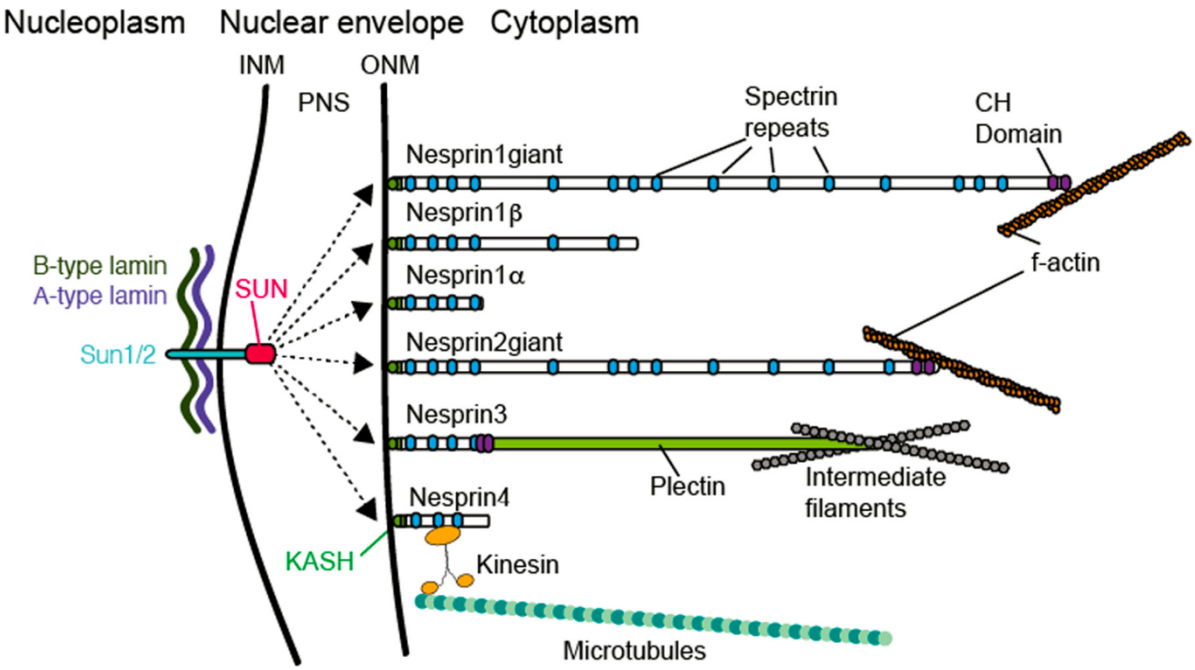

Figure 1.1 Schematic of the Linker of Nucleoskeleton and Cytoskeleton (LINC) complex

(A) TAN (Transmembrane Actin-Associated Nuclear) line: The LINC complex spans the nuclear envelope and directly connects the nucleus to the cytoskeleton through interactions in the perinuclear space (PNS). SUN-domain proteins inside the nucleus link to the nuclear lamina, while KASH-domain Nesprin proteins extend across the PNS to anchor cytoskeletal components. This mechanical coupling is crucial for nuclear positioning, movement, and transmitting mechanical signals that regulate cellular processes.
The ability of LINC complexes to bind specific cytoskeletal elements is determined by the N-termini of KASH proteins: Nesprin-1 and nesprin-2 isoforms interact with the MT motors kinesin-1 and dynein; Nesprin-3 binds the crosslinking protein plectin mediating the connection to cytoplasmic intermediate filaments; and Nesprin-4 associates with microtubules through kinesin-1. **(Adapted from (Deshpande and Telley, 2021).**

One of the cell's strategies for driving nuclear positioning relies on a molecular bridge that physically connects the nuclear envelope to the cytoskeleton—the LINC (Linker of Nucleoskeleton and Cytoskeleton) complex (Figure 1.1). This conserved protein assembly is composed of Nesprins (Nuclear Envelope Spectrin Repeat Proteins) which have KASH domain (Klarsicht, ANC1, Syne homology) proteins in the outer nuclear membrane (ONM) and a CH domain linking to cytoskeletal components such as actin filaments, microtubules, and intermediate filaments at the cytoplasm. In the inner nuclear membrane (INM), the LINC complex is composed by SUN (Sad1p, UNC-84) domain proteins (Sun1 and 2), which bind to the nuclear lamina (Figure 1.3). Through their interaction, the LINC complex enables the transmission of mechanical forces across the nuclear envelope, facilitating essential cellular processes such as nuclear positioning, migration, mechanotransduction, and chromosome organization (reviewed in (Kalukula et al., 2022)).

Nuclear movements can also be driven by interactions between the cytoskeleton and the nucleus through nuclear pores, which serve as anchoring points for cytoskeletal elements. These pores, known as nuclear pore complexes (NPCs), are large protein structures composed of nucleoporins that span both the inner and outer nuclear membranes. In addition to regulating molecular exchange between the nucleus and cytoplasm, nuclear pore complexes (NPCs) can also facilitate mechanical force transmission between the cytoskeleton and the nucleus, contributing to nuclear positioning in various cellular contexts. Actin filaments interact with nucleoporins to aid nuclear movement, while microtubule motors like dynein pull on the nucleus via NPC-anchored connections. In addition to interactions through nuclear pores, cytoskeletal elements such as microtubules can also interact with emerin and other nuclear envelope proteins, further strengthening the nucleus-cytoskeleton connection and facilitating nuclear movement (Hu et al., 2013; Kalukula et al., 2022; Salina et al., 2002) (Figure 1.2).

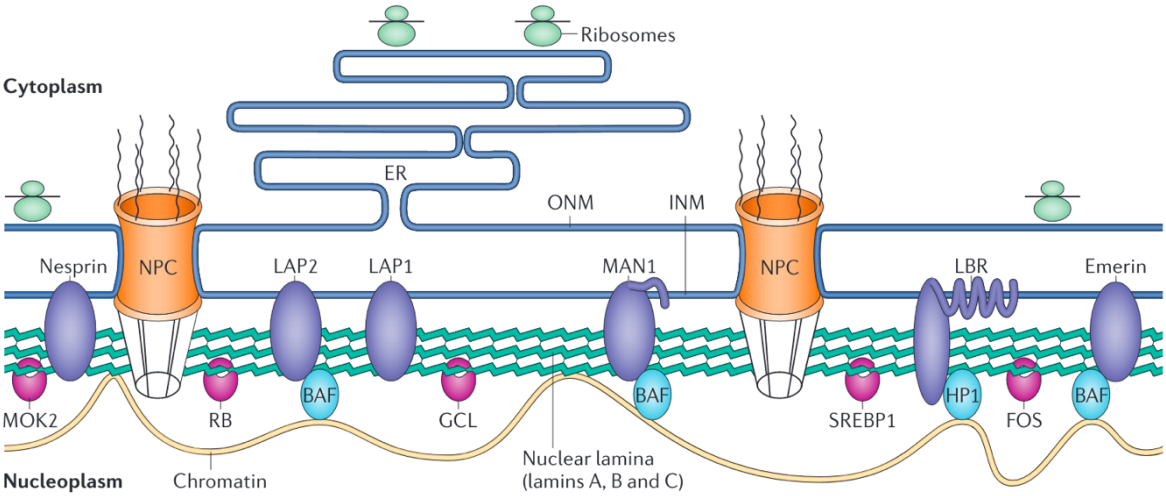

Figure 1.2 Schematic of the nuclear lamina interactions (Adapted from (Capell and Collins, 2006): The nuclear lamina lines the inner surface of the inner nuclear membrane (INM), providing structural support, chromatin organization, and anchoring sites for nuclear pore complexes (NPCs), nuclear envelope proteins, and transcription factors. Among the nuclear envelope proteins linked to the lamina are nesprin, emerin, LAP1, LAP2, lamin B receptor (LBR), and MAN1. Transcription factors that interact with the lamina include retinoblastoma (RB), germ cell-less (GCL), sterol response element binding protein (SREBP1), FOS, and MOK2. The outer nuclear membrane (ONM) connects with the endoplasmic reticulum (ER) at the cytoplasm.

Another strategy to transmit mechanical forces from the cytoskeleton to the nucleus relies on the polymerization or depolymerization of microtubules and actin filaments. In this mechanism, the growth or shrinkage of microtubules and actin that generates forces that are sufficient to drive nuclear movement. These forces can either push or pull the nucleus, depending on the direction of polymerisation or depolymerisation. For example, in oocytes, microtubules attached to centrosomes polymerize against the cell cortex, generating a pushing force that moves the nucleus away from the cortex (Figure 1.3). Similarly, in the zebrafish retina, actin polymerization beneath the nuclei generates a pushing force that drives the nuclei toward the apical surface of the cell (Yanakieva et al., 2019). Unlike the previous strategies of force transmission, this mechanism does not require direct anchoring of the cytoskeleton to the nuclear envelope.

These cytoskeleton-nucleus interactions are mediated by a variety of cytoskeletal-associated proteins, molecular motors, and nuclear envelope components, with each mechanism being context-dependent. As a result, both microtubules and actin contribute to nuclear positioning through diverse and distinct strategies (reviewed in (Deshpande and Telley,

2021)). In the following, I will first explore the role of microtubules in nuclear movement, followed by a deeper look into how actin polymerization also plays a key role in driving nuclear positioning.

1.2.2 Microtubules can either push or pull nuclei

Microtubules are involved in nuclear positioning in various biological systems, which can typical growth and shrink to push or pull nuclei. In the early C. elegans embryo, forces generated by the microtubule aster are both necessary and sufficient to centre the nucleus, ensuring proper spatial organisation before division. Similarly, in early-born migrating neurons, nuclear movement can be driven by a combination of microtubule-based pulling forces and actomyosin-generated pushing forces at the cell rear. A cage-like microtubule structure exerts a pulling force on the nucleus towards the centrosome, while actomyosin contraction at the back of the cell helps propel it forward. In early C. elegans and Xenopus embryos, the microtubule motor proteins dynein and dynactin are key players in moving the pronucleus and microtubule asters, coordinating nuclear positioning during development (Gomes et al., 2005; Gönczy et al., 1999; Skop and White, 1998).. Dynein is also crucial in migrating neurons, where it ensures coordinated movement of the nucleus and centrosome, allowing efficient nuclear translocation (Shu et al., 2004; Solecki et al., 2004; Tanaka et al., 2004). These examples demonstrate the diverse ways in which microtubules regulate nuclear positioning across different cell types and developmental contexts.

Microtubules can therefore exert pushing and pulling forces, by microtubules polymerisation and depolymerisation and by motor-driven proteins as dynein and kinesin. Microtubules, which are tube-like structures made of tubulin proteins, have inherent polarity, with a *plus end* and a *minus end*. While the plus end is more dynamic, undergoing rapid growth and shrinkage, the minus end is generally more stable and anchored within the cell in structures like the *microtubule-organising centre* (MTOC). Motor proteins interact with microtubules in a directional manner—*dynein* moves cargo toward the minus end, while *kinesin* typically moves toward the plus end. These microtubules-based mechanisms of nuclear positioning are described in the scheme of figure 1.3.

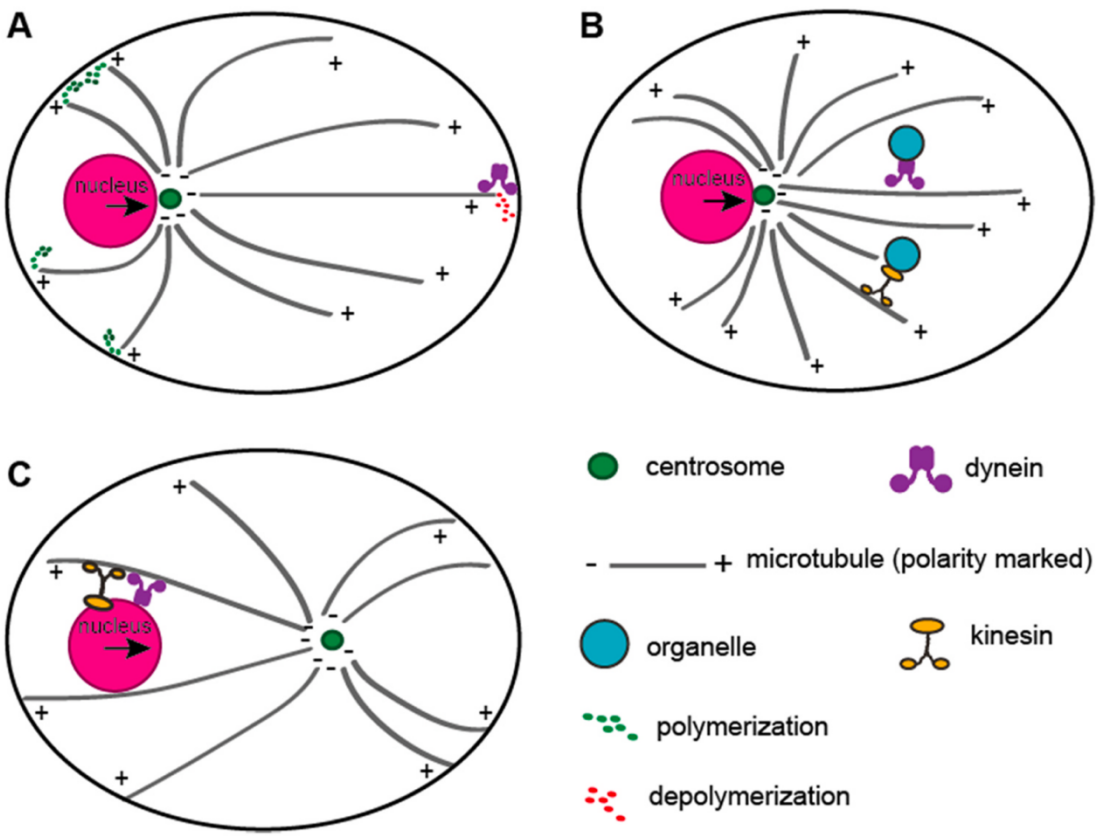

Figure 1.3 Schematic showing microtubule-based mechanisms of nuclear positioning:

(A) Polymerisation pushing force: Microtubules polymerise (+ end) generating a pushing force against the cell cortex that moves nuclei away from it. Meanwhile, the motor protein dynein, anchored at the cell cortex, pulls on microtubules, which can either counteract or assist this movement by inducing microtubule depolymerisation. (B) Pulling forces generated by motor proteins on organelles: In larger cells, where microtubules do not reach the cell cortex, the motor proteins dynein and kinesin can anchor at other organelles generating a pulling force on the microtubules that indirectly moves the nucleus and its microtubule-organising centre (MTOC). (C) Direct motor-driven pulling forces on the nucleus: Molecular motors attached to the nucleus itself generate movement. Kinesins pull towards microtubule plus ends, while dynein pulls towards minus ends, collectively directing nuclear positioning. A and B describes the typical movement of the male pronucleus and C the female one. Arrows indicate movement direction. Adapted from (Deshpande and Telley, 2021).

1.2.3 Actin-dependent mechanisms for nuclear positioning

While microtubules play a crucial role in nuclear positioning, actin-dependent mechanisms also contribute, either complementing microtubule-driven forces or acting independently in various cellular contexts. Actin is a highly conserved globular protein that polymerizes into filamentous actin (F-actin), forming key components of the cytoskeleton.

These filaments provide structural support, regulate cell shape, and drive essential processes such as migration, intracellular transport, and nuclear positioning. For example, actin facilitates the rearward movement of the nucleus during fibroblast polarization, a key step before migration (Gomes et al., 2005). In muscle development, actin-driven forces position nuclei before myoblast fusion, with TAN lines guiding nuclei behind the centrosome to establish cell polarity (Chang et al., 2015). Similarly, in developing neuroepithelia, actomyosin contractility and actin polymerization coordinate the apical movement of nuclei before cell division (Meyer et al., 2011; Norden et al., 2009; Yanakieva et al., 2019). The organisation of TAN lines and actin-driven nuclear movements are illustrated in Figure 1.4.

In the following sections, I will discuss and give examples of actin-dependent mechanisms that ensure timely and accurate nuclear positioning.

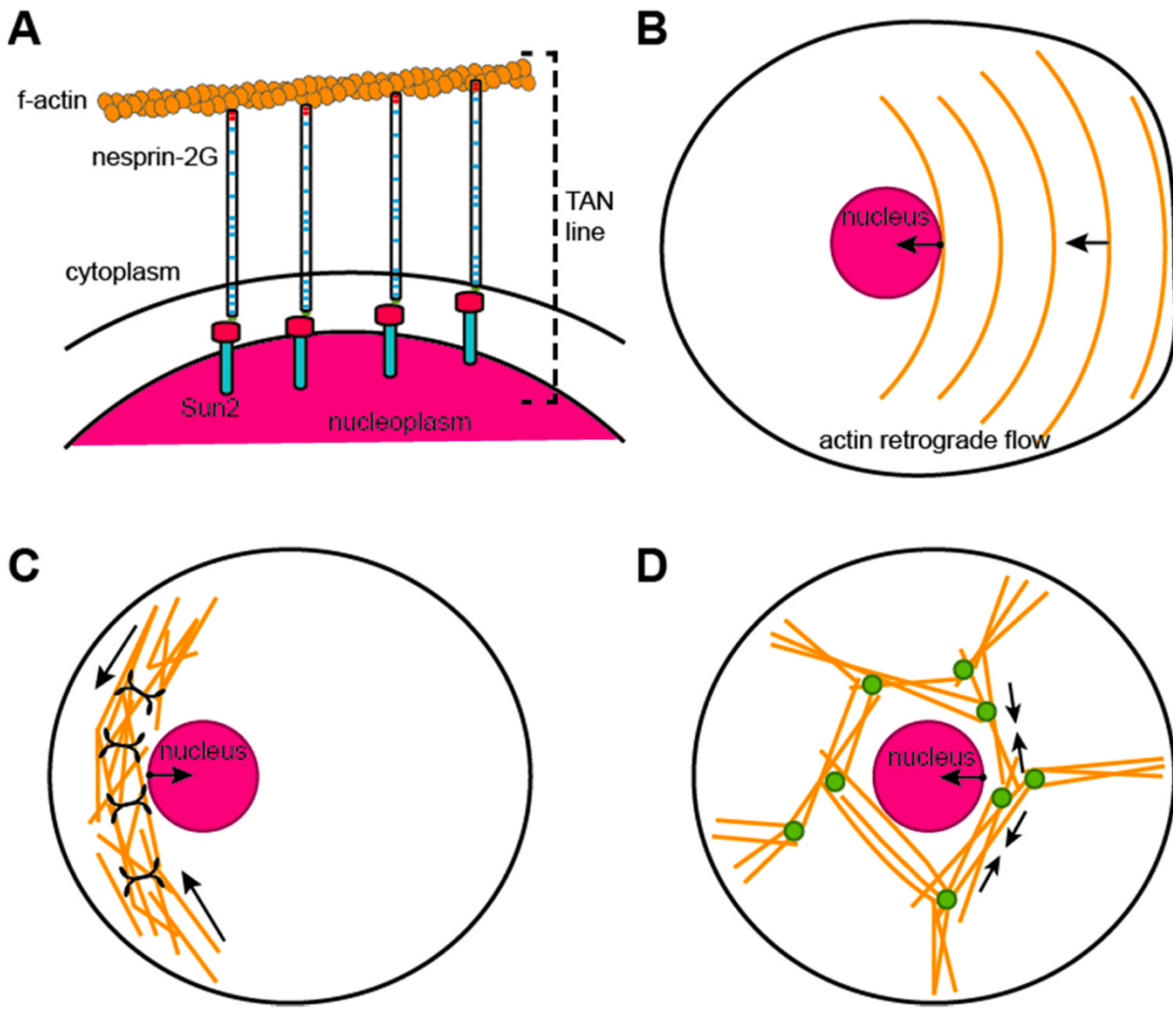

Figure 1.4 *Schematic showing Actin-based mechanisms of nuclear positioning:*

(A) TAN (Transmembrane Actin-Associated Nuclear) line: are composed of Sun-KASH (LINC) complexes, which span the nuclear envelope and physically connect the nucleus to the cytoskeleton, and of actin, which interact with the LINC complex to generate forces that move the nucleus. **(B) Actin nucleation and turn-over** generates a retrograde flow that drives nuclei movement. **(C) Actomyosin contractility** driven by non-muscle myosin-II (black) creates a pushing force that moves the nucleus. **(D) Actin-myosin cable contractions**, along with vesicle node repositioning, generate the forces that drive nuclear movement. This process is organised by nucleation factors and facilitated by vesicles (green) coated with myosin Vb. B-D describe redundant mechanisms for pronucleus positioning in mouse oocytes. Arrows indicate movement direction. **Adapted from Deshpande and Telley 2021).**

1.2.3.1 Actin nucleation generates a pushing force

Like microtubules, actin filaments can generate pushing forces through polymerization. Actin monomers assemble in a polarized manner, with a fast-growing barbed (plus) end and a slower-growing pointed (minus) end. The nucleation of new actin filaments is a tightly regulated process, as it determines where and when forces are generated within the cell. Two key regulators of actin filament nucleation are the Arp2/3 complex and formins.

The Arp2/3 complex nucleates branched actin networks by binding to the sides of pre-existing filaments, where it initiates new filaments that grow at their plus ends. This process is controlled by nucleation-promoting factors like WASP and WAVE/SCAR proteins, which trigger conformational changes in Arp2/3, facilitating actin monomer recruitment and precise spatial regulation of actin branching. An example of actin nucleation dependent on the Arp2/3 complex is the movement of nuclei to the muscle periphery during myogenesis. In muscle fibers, the Arp2/3 complex contributes to nuclear positioning by organizing desmin—an intermediate filament protein essential for maintaining muscle structural integrity—to crosslink myofibrils and determine nuclear positioning (Roman et al., 2017).

In contrast, formins drive the formation of straight, unbranched actin filaments. These dimeric proteins promote actin nucleation by bringing monomers together and remain associated with the growing plus end, working alongside profilin to accelerate filament elongation. Formins are regulated through various factors, as Diaphanous-related formins

(DRFs), Cdc12p, For3p, and Fus1p that control their activity in a spatiotemporal manner, ensuring actin filament growth occurs at the right place and time. For example, formin-dependent actin polymerization is involved in positioning nuclei at the apical side prior to cell division in the zebrafish retina (Yanakieva et al., 2019). This mechanism does not require an anchoring system between filamentous actin and the nucleus. Instead, it transmits force to the nucleus by generating a pushing force through the addition of new actin monomers to the growing actin filament.

Thus, actin nucleation is tightly regulated by distinct mechanisms to ensure accurate nuclear positioning, making it a key process to investigate in order to understand organ development.

1.2.3.2 Actin-myosin creates contractile forces

In addition to actin nucleation, actin can also generate forces for nuclear positioning through contractility. This process involves interactions with various actin-binding proteins and motor proteins like myosin, which generate contractile forces essential for cell movement and nuclear translocation. Myosin motors can cross-link or slide actin filaments to produce force.

Myosin II, a key player in this process, is a filamentous motor protein composed of two heavy chains, two essential light chains, and two myosin regulatory light chains (MRLCs) (Sellers et al., 2003). Its activity is tightly regulated, primarily through phosphorylation of two conserved residues (Ser19 and Thr18) in MRLC. This phosphorylation is mediated by different kinases, including myosin light chain kinase (MLCK), Rho-associated kinase (ROCK), and myotonic dystrophy-related Cdc42-binding kinase (MRCK), allowing precise control of actomyosin contractility during nuclear positioning. Nuclear positioning dependent on actin–myosin contractility has been observed in the zebrafish hindbrain. In these straight neuroepithelia, myosin activity—regulated via the Rho-associated kinase (ROCK) pathway—drives apical nuclear positioning prior to cell division (Yanakieva et al., 2019). Thus, understanding the mechanisms that regulate force transmission to the nucleus—such as those controlling actin nucleation or myosin contractility—is essential for uncovering how nuclear positioning is controlled across different cellular contexts.

1.2.3.3 TAN lines can couple the nucleus to the cytoskeleton

In addition to the previously discussed examples, the nucleus can, in certain contexts, be physically linked to dynamic actin filaments to facilitate its positioning. This connection occurs through transmembrane actin-associated nuclear (TAN) lines, which consist of SUN–KASH (LINC) complexes that couple the nucleus to the actin cytoskeleton. These structures play a central role in nuclear positioning by transmitting cytoskeletal forces directly to the nucleus, particularly in migrating cells such as fibroblasts and neurons (Deshpande and Telley, 2021; Luxton et al., 2011).

A well-characterized example of actin-dependent nuclear movement is observed during fibroblast polarization for migration. As the cell polarizes, the centrosome remains centrally positioned, while the nucleus is pulled rearward via actin retrograde flow. This repositioning ensures that the centrosome aligns properly between the nucleus and the cell's leading edge, a configuration critical for directed migration (Gomes et al., 2005; Luxton et al., 2010).

TAN lines, composed of nuclear envelope proteins such as nesprin-2G and SUN2, physically couple the actin cytoskeleton to the nucleus, enabling force transmission. These connections are anchored within the nuclear envelope by A-type lamins, which stabilize the interface and support effective force propagation, ultimately driving nuclear movement (Luxton et al., 2011).

The importance of placing nuclei correctly during tissue development and maintenance is reflected in the wide variety of mechanisms that have evolved to move them. Rather than relying on a single universal strategy, cells appear to tailor nuclear positioning mechanisms to their specific biological context. However, what drives the adoption of distinct mechanisms across different cells and tissues remains poorly understood.

1.3.2 Cell and tissue morphology can define nuclear positioning mechanisms

The wide range of mechanisms that drive nuclear positioning suggests that cells adapt their strategies to fit the specific challenges of their environment. While we know that forces from cytoskeletal elements like microtubules and actin can move nuclei, it's still unclear what

determines which mechanism is used in different tissues. Recent evidence points to cell and tissue morphology as a key factor shaping these choices.

A striking example comes from the zebrafish neuroepithelia, where nuclear positioning relies on different actin-based mechanisms depending on the geometry of the tissue (Yanakieva et al., 2019). In straight tissues such as the hindbrain, apical nuclear migration is driven by myosin contractility regulated by the Rho-ROCK pathway. In contrast, in the more curved retina, nuclei are pushed apically by formin-mediated actin polymerization. Here, a transient actin network forms beneath the nucleus, generating a pushing force that helps it reach the apical surface. These differences suggest that physical features—such as curvature or cell packing—can influence which molecular machinery is recruited to move the nucleus (Yanakieva et al., 2019).

Despite these insights, it remains unclear how cells select one mechanism over another. This mechanistic variety highlights not only the necessity of precise nuclear positioning but also raises broader questions about what additional parameters influence nuclear movements across diverse biological systems.

1.3 The role of nuclear lamina in nuclear positioning

In addition to the cytoskeletal arrangements that generate forces for nuclear positioning, the nucleus itself—and in particular, the nuclear lamina—plays a critical role in regulating nuclear movements. To understand how the nuclear lamina contributes to these dynamics, it is essential to first consider its composition, structure, and mechanical properties.

The nuclear lamina is a dense protein network that lines the inner nuclear membrane (INM) of the nuclear envelope (Figure 1.4). It consists of three main domains: the N-terminal head, the central coiled-coil rod, and the globular C-terminal tail. The rod domain mediates interactions between lamina proteins, while the C-terminal tail, containing a nuclear localization signal (NLS), an immunoglobulin-fold (IgG fold), and a CAAX motif, facilitates interactions with non-lamina proteins (Snider and Omary, 2014; Zheng et al., 2022). This structure not only provides mechanical stability to the nucleus but also serves as a platform for protein-protein interactions that influence gene regulation and nuclear positioning.

Lamins, the primary components of the nuclear lamina and classified as type V intermediate filaments, play a crucial role in maintaining the nuclear shape, size, and

mechanical properties. These characteristics ultimately determine whether the nucleus acts as a limiting factor for 3D cell migration, especially in confined environments (Calero-Cuenca et al., 2018; Harada et al., 2014; Yamada and Sixt, 2019). If the nucleus is too large to fit through a space or cannot deform to navigate the 3D challenges of the extracellular matrix, its physical properties can limit both cell migration and nuclear positioning. There are two main types of Lamins: A type Lamins (Lamin A and C isoforms) generated from alternative slicing of the LMNA gene; and B type Lamins (Lamin B1 and Lamin B2) encoded by LMB1 and LMB2 genes. While A-type lamins are key regulators of nuclear stiffness, Lamin B contributes to nuclear integrity but not to stiffness (Lammerding et al., 2006).

These conclusions were drawn from various in vitro studies where A-type and B-type lamins were individually knocked down, and their effects on constrained cell migration were analysed. It was observed that Lamin A/C-deficient cells, derived from mouse fibroblasts, have altered nuclear shape, reduced stiffness and decreased cell viability under strain. In contrast, Lamin B1-defficient cells have normal nuclear mechanics, but frequently exhibit blebs in confined scenarios (Lammerding et al., 2006). At the organismal level, mice deficient in both A type lamins present growth retardation and muscle and cardiac dystrophy. This is in line with human data showing that deficiencies in A type lamins are associated with Emery-Dreifuss muscular dystrophy and dilated cardiomyopathy, among other laminopathies (Capell and Collins, 2006). Interestingly, Lamin B1 deficient mice die shortly after birth due to development abnormalities and no human diseases have been linked to B type lamin, suggesting that Lamin B1 and B2 are crucial for growth and viability. These results clearly demonstrate that deficiencies in the nuclear lamina can lead to tissue-wide dysfunctions, highlighting the importance of studying lamin functions at the organismal level. While the precise mechanisms linking lamin defects to tissue dysfunction remain a subject of debate, two main hypotheses have been proposed (discussed in (Gruenbaum and Foisner, 2015; Hutchison, 2002; Lammerding et al., 2006)):

The gene regulation hypothesis suggests that lamin mutations give rise to diverse disease phenotypes by disrupting genetic regulatory networks. Since lamins typically associate with chromatin to regulate gene accessibility for transcription, mutations in these proteins could interfere with these interactions. This could lead to the misexpression of genes—activating the wrong ones at the wrong time or inhibiting the correct ones—ultimately contributing to disease.

The structural hypothesis proposes that lamin mutations weaken nuclear integrity, making nuclei more fragile and prone to cell death, particularly in mechanically stressed tissues. In this view, lamins act as a protective shield, safeguarding nuclei from mechanical forces. When lamins are mutated, this shield is compromised, leaving genetic material more vulnerable to the physical challenges of 3D tissue architecture. Unlike the gene regulation hypothesis, this perspective specifically considers the mechanical stresses experienced at the organismal level.

The phenotypic consequences of lamin mutations likely arise from a combination of disrupted gene regulation and impaired nuclear mechanics. While it remains unclear which of these mechanisms predominates in specific tissue contexts, there is experimental evidence supporting both hypotheses. The relative contribution of each may vary depending on the cellular environment and physiological demands of the tissue.

1.3.1 Lamin A regulates gene transcription

Several studies support the gene regulation hypothesis, highlighting the critical role of Lamin A in gene regulation through its influence on chromatin organization and transcription. Lamin A interacts with chromatin at lamina-associated domains (LADs), where it helps regulate DNA replication, repair, and gene expression (Gruenbaum and Foisner, 2015). Each type of Lamins can distinctly regulate gene expression (Dechat et al., 2008). By binding chromatin and nuclear proteins, Lamin A modulates which genes are accessible for transcription and ensures proper gene expression during cell differentiation. Additionally, it contributes to gene silencing by associating with heterochromatin at the nuclear periphery (Zheng et al., 2022). A- type lamins can also localize in the nucleoplasm, where they interact with splicing-factor speckles, potentially regulating gene expression at both transcriptional and post-transcriptional levels (Hutchison, 2002). Given the widespread impact of lamin-chromatin interactions on gene regulation, it is likely that defects at the transcriptomic level contribute, at least in part, to the diverse phenotypic defects observed in lamin-associated diseases. However, many of these diseases, the so called laminopathies, involve mutations in the mechanisms that drive nuclear movement, which are particularly relevant when considering the cell-environment interaction—an essential aspect that the studies supporting the gene regulation hypothesis have often overlooked.

1.3.2 Lamin A expression levels modulate cell migration in confinement

Studies supporting the structural hypothesis address the critical role of Lamin A/C in regulating nuclear stiffness, which significantly influences 3D cell migration. This is particularly important because the nucleus, as the largest and often stiffest organelle, can act as a physical barrier when cells migrate through narrow spaces such as the interstitial space or extracellular matrix (Davidson et al., 2014; Harada et al., 2014; Swift et al., 2013).

In vitro studies using microfluidic systems have demonstrated that nuclear deformability is essential for migration through spaces smaller than the nucleus itself. Cells utilize nuclear deformability to squeeze through narrow constrictions, a property directly influenced by Lamin A/C expression levels. Higher Lamin A/C expression results in a denser nuclear lamina, increasing nuclear stiffness, while lower expression leads to a more deformable nucleus. This relationship has been extensively studied in the context of 3D cell migration in confined microchannels (Davidson et al., 2014; Harada et al., 2014; Swift et al., 2013).

1.3.2.1 Reduced Lamin A/C levels enhance cell migration in confined environments

In mouse embryonic fibroblasts (MEFs), deletion of the Lmna gene, which encodes Lamin A/C, enhances migration through microfluidic channels with constrictions as small as 2–5 µm. In response to a chemoattractant gradient (PDGF), MEFs with reduced Lamin A/C levels exhibited increased nuclear deformation and faster migration through narrow constrictions compared to wild-type (Lmna+/+) cells. Wild-type cells showed impaired migration efficiency through the smallest constrictions, indicating that higher Lamin A/C expression limits nuclear deformability and restricts migration (Davidson et al., 2014; Lammerding et al., 2006).

This alteration in nuclear structure in Lamin A/C-deficient MEFs was also observed in skeletal myoblasts derived from the fore and hind limbs of Lmna−/− mice. Lmna−/− myotubes exhibited severe nuclear deformations under ~5% biaxial strain (stretch), whereas Lmna+/+ nuclei remained more stable. These findings suggest that nuclear structure defects in MEFs extend to other cell types, such as muscle cells, where Lamin A/C plays a crucial role in maintaining nuclear integrity (Lammerding et al., 2006).

Similar observations have been reported in cancer cells. In breast cancer cells that naturally express high Lamin A/C levels, shRNA-mediated depletion of Lamin A/C increased nuclear

deformability and enhanced migration through confined spaces. Using a microfluidic micropipette aspiration assay, researchers found that MDA-MB-468 cells depleted of Lamin A/C migrated significantly faster through small constrictions than control cells. However, in larger control channels, no significant difference in migration speed was observed, indicating that Lamin A/C specifically influences migration in confined environments (Bell et al., 2022). Supporting the role of Lamin A/C in breast cancer metastasis, analyses of human breast tumours revealed a significant association between lower Lamin A levels and decreased patient survival (Bell et al., 2022). This aligns with broader cancer research linking altered Lamin A/C expression to increased invasiveness and metastatic potential (Bell et al., 2022; Davidson et al., 2014). Likewise, in lung cancer cells (A549), transient knockdown of Lmna via siRNA (siLMNA) resulted in softer nuclei and increased migration through 3 µm pore Transwell filters. Moreover, in xenograft mouse models, tumours derived from A549 siLMNA cells exhibited faster initial growth (Harada et al., 2014).

These studies demonstrate that reducing Lamin A/C levels in various cell types—including MEFs, myotubes, and breast and lung cancer cells—is sufficient to enhance cell migration through confined spaces in vitro. This increased migratory ability correlates with greater nuclear deformability, suggesting that a more deformable nucleus facilitates cells' passage through narrow constrictions.

1.3.2.2 Increased Lamin A/C expression limits cell migration through constrictions

In these lines, increased Lamin A/C expression correlates with higher nuclear stiffness and reduced migration through narrow spaces. Overexpression of Lamin A/C in osteosarcoma cells decreased tumour aggressiveness by impairing migration (Urciuoli et al., 2021). Similarly, breast cancer cells with elevated Lamin A/C expression exhibited lower nuclear deformability and reduced migration efficiency in confined environments (Bell et al., 2022). Neutrophil-like cells also showed impaired migration through constricted spaces when Lamin A/C levels were high (Rowat et al., 2013).

Overall, these studies demonstrate a negative correlation between Lamin A/C levels and both nuclear deformability and the ability of cells to migrate through confined spaces. Together, these findings highlight the fundamental role of nuclear mechanics—regulated by

Lamin A/C—in enabling cell migration within the complex, constrained environments of living tissues.

1.3.2.3 Connecting Lamin A/C levels to nuclear positioning under confinement

This link between nuclear deformability, due to Lamin A/C levels, and confined cell migration raises the hypothesis that nuclear mechanics may also influence nuclear positioning. This connection is supported by two observations: first, nuclear positioning is often a prerequisite for cell migration, as seen in polarized fibroblasts (Gomes et al., 2005) which migrate to complex 3D environments; and second, nuclei frequently need to be repositioned within cells embedded in highly confined tissues—particularly during development, such as in neuroepithelia (reviewed in (Norden, 2017).

A compelling example linking nuclear mechanics to developmental nuclear positioning comes from myogenesis. In muscle cells, nuclei undergo noticeable deformation as they migrate toward the cell periphery—a process essential for muscle function. This suggests that nuclear stiffness may influence nuclear positioning. Supporting this, overexpression of Lamin A/C to increase nuclear stiffness (via mCherry-Lamin A/C) reduced the number of peripheral nuclei and correlated inversely with nuclear migration velocity (Roman et al., 2017). These results indicate that excessive nuclear stiffness can act as a mechanical barrier to nuclear movement in confined tissues.

Altogether, this points to a possible role for nuclear mechanics in guiding proper nuclear positioning during tissue development. However, the extent to which nuclear mechanics impact developmental processes remains incompletely understood and warrants further investigation.

1.3.3 Possible mechanical regulation of cell rounding in confined tissues

In addition to cell migration and nuclear positioning, confined environments can impose mechanical challenges during other key morphogenetic events. One such event is mitotic rounding, a process in which cells adopt a spherical shape to ensure accurate spindle assembly and proper chromosome segregation. Mitotic rounding requires sufficient space for cells to round correctly, and its efficiency can be compromised under mechanical constraints. For

example, in isolated HeLa cells, confinement within stiff hydrogels impairs the ability of cells to round, leading to delays in mitotic progression (Lancaster et al., 2013). This highlights that the mechanical properties of the surrounding environment can directly influence mitotic progression and successful cell division.

While the role of mechanical constraints in mitotic rounding has been explored in vitro, the contribution of nuclear mechanics in this context remains poorly understood, particularly in living, developing tissues. In particular, it is still unknown whether Lamin A/C expression—which modulates nuclear stiffness—also affects cell rounding and division efficiency in confined environments. This question is especially relevant in developmental tissues, which are inherently crowded and highly dynamic. In such contexts, tissue mechanics could impose physical limits on space-making events like mitotic rounding, potentially impacting the efficiency of cell division. However, how Lamin A/C expression levels influence tissue-wide mechanics, and how increased tissue stiffness impacts cellular processes that require space, remains largely unexplored.

1.4 Lamin A expression in developmental contexts

Natural variations in Lamin A/C expression are tissue-dependent and often correlate with specific functional requirements. One example is the low expression of Lamin A during early development, as observed in zebrafish retinal and hindbrain neuroepithelia (Yanakieva et al., 2019), the developing mouse brain (Röber et al., 1989), and both mouse and human embryonic stem cells (Constantinescu et al., 2006). In fact, A-type lamin expression follows a developmentally regulated pattern, with minimal levels in early embryonic stages and a progressive increase as differentiation advances. Eventually, Lamin A/C becomes widely expressed in most mature cells (Lammerding et al., 2006; Lehner et al., 1987), highlighting its role in reinforcing nuclear stability as cells transition from a highly plastic state to specialized functions.

Given the well-established role of Lamin A in regulating nuclear mechanics, it is reasonable to speculate that its expression levels influence both cellular and nuclear movements within confined tissues. Low Lamin A levels may facilitate migration in densely packed, morphogenetically active tissues, whereas its gradual increase could serve to stabilize tissue

architecture once extensive movement is no longer required. This suggests that reduced Lamin A/C expression, by enhancing nuclear deformability during early development, may promote the nuclear and cellular movement essential for dynamic tissue rearrangements, ultimately supporting proper organ formation.

1.5 Nuclear positioning in the zebrafish neuroepithelia

Pseudostratified epithelia (PSE) offer a compelling model to study how nuclear mechanical properties influence nuclear movements during development. These tissues are densely packed, highly proliferative, and exhibit strikingly dynamic nuclear positioning (Ferme et al., 2024; Leung et al., 2011; Matejčić et al., 2018; Norden et al., 2009; Yanakieva et al., 2019). Such characteristics create unique mechanical constraints that make PSEs particularly suited for investigating how nuclei move within confined environments. Among PSEs, the zebrafish neuroepithelium stands out due to its low nuclear Lamin A/C expression (Yanakieva et al., 2019), offering an ideal system to explore potential links between nuclear mechanics and positioning. In the following, I will first highlight the relevance and diversity of PSEs, then explore the biological significance of nuclear movements within these tissues, and finally discuss zebrafish neuroepithelia as a valuable model to investigate whether and how nuclear mechanical properties—such as those influenced by Lamin A/C—affect nuclear positioning during development.

1.5.1 Overview about pseudostratified epithelia

Pseudostratified epithelia (PSE) are found across a wide range of animals and serve as essential organ precursors throughout evolution. They appear in invertebrates, such as the embryonic ectoderm of Nematostella and Drosophila imaginal discs (Meyer et al., 2011), as well as in vertebrates, where they contribute to the development of organs like the liver, gut, and pancreas buds, the central nervous system, and form the epiblast of the gastrulating mouse embryo (reviewed in (Nakajima et al., 2013; Strzyz et al., 2016). Reflecting the diversity of organs PSE generate, PSE themselves are heterogeneous in length, architecture, and packing state (reviewed in (Norden, 2017)). These proliferative tissues consist of elongated epithelial cells attached to both the apical and basal sides of the tissue. Their cell length and density vary considerably and tend to increase as development progresses. Based on these characteristics,

PSEs are typically classified as short, intermediate, or long (reviewed in (Strzyz et al., 2016)) (Figure 1.5 A). The structural diversity of PSE presents distinct mechanical challenges for cellular and nuclear movement, which are integral to tissue morphogenesis. Given their dense nuclear packing and the fact that nuclei occupy the majority of the cell volume—and consequently much of the tissue—it is plausible that nuclear material properties influence PSE development. Understanding the biology of PSE—including how nuclear material properties contribute to their development—is therefore key to uncovering the mechanisms underlying organ formation.

1.5.2 Apical nuclear migration

Given the densely packed nature of PSEs, it is likely that nuclear mechanics influence interkinetic nuclear migration (IKNM), a defining feature of all studied pseudostratified epithelia (PSE) (Lee and Norden, 2013; Leung et al., 2011; Meyer et al., 2011; Nakajima et al., 2013; Norden et al., 2009; Sauer, 1935; Strzyz et al., 2016, 2015; Yanakieva et al., 2019). During IKNM, nuclei undergo highly dynamic apico-basal movements through the densely packed tissue, movements that are tightly linked to cell cycle progression (Figure 1.5 B):

- G2 phase: Nuclei move apically in a rapid and directed manner, just before mitosis (Kosodo et al., 2011; Norden et al., 2009; Strzyz et al., 2015; Tsai et al., 2007; Yanakieva et al., 2019);
- Post-mitosis (G1 phase): Nuclei displace basally in a stochastic manner (Kosodo et al., 2011; Leung et al., 2011).
- S phase: Nuclear positions fluctuate along the apico-basal axis (Leung et al., 2011; Norden et al., 2009).

Importantly, during the G2 phase, apical nuclear migration not only plays an active role in nuclear positioning but also passively displaces surrounding nuclei, further contributing to the dynamic nuclear positioning within the neuroepithelium (Kosodo et al., 2011; Leung et al., 2011; Strzyz et al., 2016). While it remains unexplored whether both active and passive nuclear movements can be influenced by nuclear mechanics, apical nuclear migration is essential to ensure that mitosis consistently occurs at the apical surface of the tissue (Sauer, 1935; Strzyz et al., 2016).

1.5.3 Apical mitosis guarantees tissue integrity

Several studies have investigated the significance of apical nuclear migration and its role in ensuring apical mitosis. One proposed function is the establishment of a mitotic zone at the apical surface, which may facilitate orderly cell division (Hu et al., 2013). Another hypothesis suggests that apical migration enables nuclei to encounter the centrosome, which remains positioned apically throughout the cell cycle and plays a crucial role in cell division (Hu et al., 2013; Tsai et al., 2010). However, research on the zebrafish retinal neuroepithelium challenges this view, demonstrating that mitotic entry can occur at non-apical positions and is independent of centrosomes position (Strzyz et al., 2015). When actomyosin contractility was inhibited using the myosin II inhibitor blebbistatin, nuclei entered mitosis away from the apical surface. Furthermore, centrosome positioning was not strictly required for apical nuclear migration, as seen when centriole amplification, induced by the overexpression of an overstabilized form of Plk4, caused centrosomes and nuclei to meet at non-apical locations. Even in such cases, nuclei still migrated apically taking the centrosome along, suggesting that apical nuclear movement is an independent process rather than merely a means to align with the centrosome (Strzyz et al., 2015).

Moreover, research has revealed that nuclear migration and apical mitosis play a fundamental role in tissue development. These processes are essential for maintaining proper tissue organization and ensuring successful cell proliferation and differentiation, highlighting their significance in the overall development of pseudostratified epithelia. When mitosis occurs away from the apical surface, one of the daughter cells loses its apical attachment and fails to enter neurogenesis, instead forming a cluster of proliferating cells. Experimentally, non-apical mitosis can be induced in two ways: 1) by disrupting normal actin organization, achieved by linking aPKC to a CAAX domain to target it to the membrane. In controls, F-actin is organized as filaments along the apicobasal axis; and 2) by inhibiting Plk1 activity in a subset of cells using a dominant-negative (DN) construct under a heat-shock (HS) promoter. This causes apical cells to stall in mitosis, forming a physical barrier that prevents neighbouring control cells from reaching the apical surface (Strzyz et al., 2015)(Figure 1.5 C). This effect is not exclusive to zebrafish neuroepithelia (Strzyz et al., 2015) as similar observations have been made in the Drosophila wing disc epithelium (Nakajima et al., 2013). These findings suggest that, apical nuclear migration and apical mitotic rounding may be functionally distinct processes, as apical

migration continues even when mitotic entry takes place at a non-apical position. Thus, apical migration and the consequent mitotic rounding are necessary to maintain tissue integrity and successful neurogenesis (Strzyz et al., 2016, 2015).

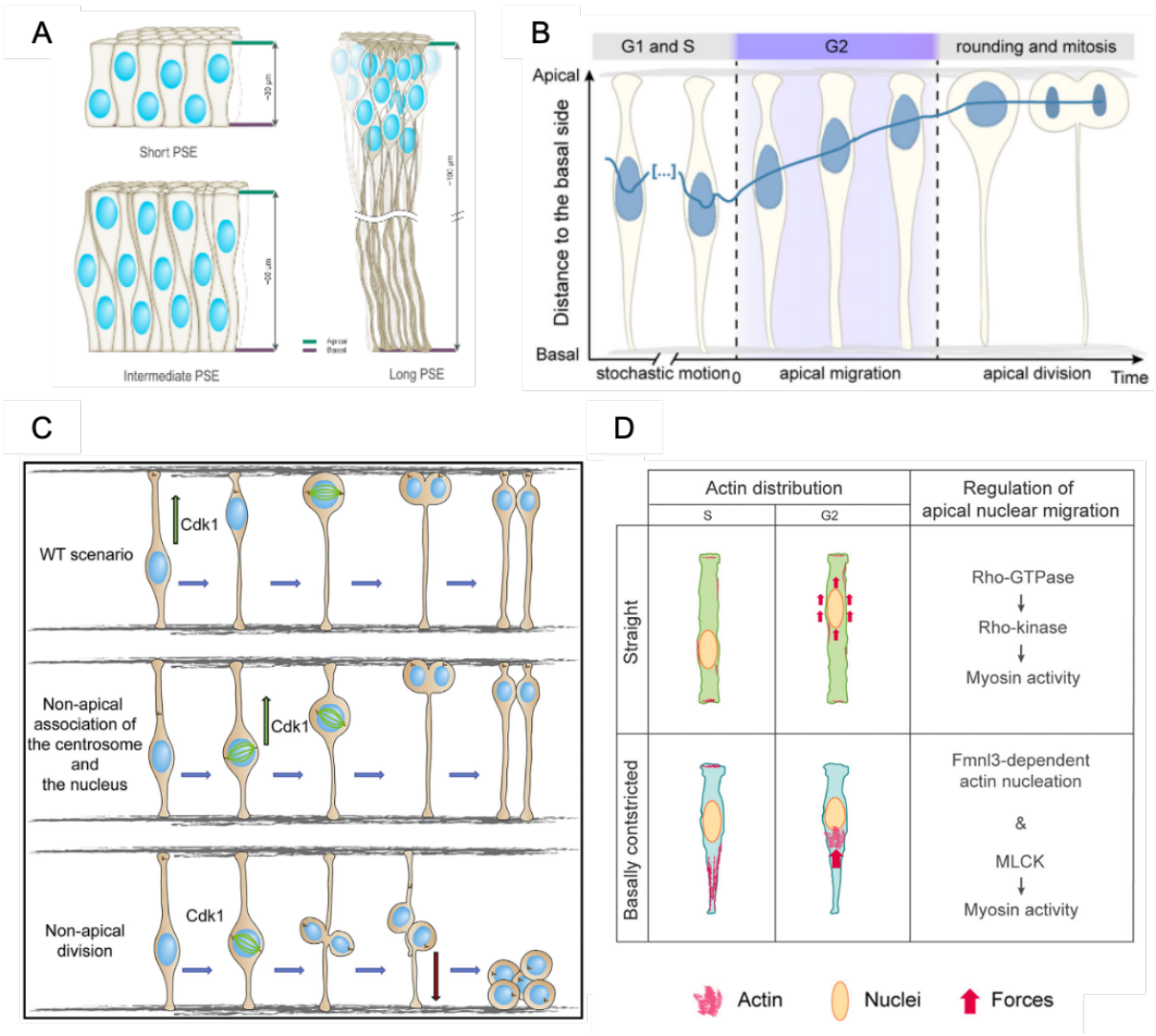

Figure 1.5 *Nuclear positioning in Pseudostratified epithelia (PSE): (A) PSE classification according to cell length and density*

(A) PSE classification according to cell length and density (Adapted from (Strzyz et al., 2015)): Short PSE (20–30 µm cells, 2–3 nuclear layers) are found in vertebrate endodermal organ buds and the Drosophila optic lobe. Intermediate PSE (up to 60 µm cells, 4–5 nuclear layers) are seen in fly imaginal discs and the zebrafish retinal and hindbrain neuroepithelia; Long PSE (up to 100 µm cells, 8+ nuclear layers) are present in the neural tube of higher vertebrates. In extreme cases, such as the developing neocortex, radial glial cells can exceed 200 µm in length. (B) Nuclear movements are cell-cycle dependent (Adapted from (Yanakieva et al., 2019)): During G1 and S phase nuclei position is stochastic along the apico-basal cell axis. In contrast, nuclei migrate apically during the G2 phase of the cell cycle, before apical mitotic entry. (C) CDK1 expression is necessary and sufficient to drive nuclear apical movement (Adapted from (Strzyz et al., 2015)): apical nuclear migration continues when the centrosome and the nucleus meet non-apically; however, when the nucleus divide non-apically, one of the daughter cells loses its apical attachment and form a cluster of proliferating cells. (D) Schematic example of actin distribution and mechanisms in a straight and a curved (basal constricted) zebrafish neuroepithelia (Adapted from (Yanakieva et al., 2019)).

1.6 Exploring the influence of nuclear mechanics on nuclear positioning in zebrafish neuroepithelia

Despite the central role of pseudostratified epithelia (PSEs) in development and the critical importance of accurate apical mitosis for organogenesis, our understanding of the factors that regulate nuclear positioning within these tissues remains incomplete. While it is well established that different cytoskeletal systems contribute to nuclear movement depending on tissue architecture—such as length and cell density (Norden, 2017; Strzyz et al., 2016; Yanakieva et al., 2019)—whether intrinsic nuclear mechanical properties, including those modulated by Lamin A/C, also play a role in this process remains largely unexplored.

The zebrafish neuroepithelium offers a compelling model to address this question. As a densely packed PSE (Matejčić et al., 2018), its organization suggests that nuclear positioning may be shaped not only by cytoskeletal activity but also by mechanical constraints imposed by tissue structure. Although nuclei are separated by plasma membranes, their close proximity and limited space could lead to physical interactions. Supporting this, neuroepithelial nuclei in zebrafish display frequent and dynamic deformations throughout the cell cycle, including

during both passive and active movement (Yanakieva et al., 2019), suggesting that mechanical forces are constantly at play.

Previous work has shown that the specific cytoskeletal mechanism responsible for apical nuclear migration in zebrafish neuroepithelia depends on cell and tissue morphology (Norden, 2017; Strzyz et al., 2016). For example, curved epithelia like the retina rely on actin-based pushing forces, while straighter tissues such as the hindbrain depend on myosin contractility (Yanakieva et al., 2019) (Figure 1.5 D). This further supports the idea that tissue architecture and biophysical constraints influence nuclear dynamics. However, it remains unclear whether, and to what extent, nuclear mechanical properties themselves modulate positioning in such environments.

Zebrafish embryos are particularly advantageous for studying these questions due to their optical transparency, rapid and external development, and genetic tractability. These features allow high-resolution live imaging of nuclear movements in developing tissues. The retina and the hindbrain, a well-characterized zebrafish PSE, displays dense nuclear packing (Ferme et al., 2024; Kim et al., 2024) and stereotypical apical movements (Yanakieva et al., 2019), closely mimicking the spatial constraints observed in other developing tissues. Moreover, retinal and hindbrain cells naturally express low levels of Lamin A/C (Yanakieva et al., 2019), providing a sensitized background to test the influence of nuclear stiffness on migration dynamics. The availability of transgenic lines for single-cell and nuclear labeling, together with established light-sheet microscopy protocols, makes it possible to track apical migration at minute-scale resolution with minimal phototoxicity (Icha et al., 2016b; Yanakieva et al., 2018). Recent advances, such as transgenic tools for heat-shock–induced modulation of tissue mechanics (Amini et al., 2022a; Kim et al., 2024), further enhance the zebrafish system's potential for dissecting the mechanical regulation of nuclear positioning. Together, these tools make the zebrafish neuroepithelia an ideal system to investigate how nuclear deformability contributes to nuclear positioning in confined developmental environments.

1.7 Objective of the study

In this thesis, I aimed to investigate whether, and to what extent, nuclear mechanical properties influence nuclear positioning during neuroepithelial development. To this end, I

used the zebrafish transgenic line Tg(hsp70:LMNA-mKate2) to overexpress Lamin A, a nuclear lamina protein whose levels inversely correlate with nuclear deformability.

To confirm that Lamin A overexpression increased nuclear stiffness in the developing zebrafish retina, I assessed both nuclear and tissue material properties using atomic force microscopy and quantified nuclear deformability from live imaging data. I then examined whether elevated Lamin A levels affect cell cycle dynamics and neuronal development.

To evaluate the impact of increased nuclear stiffness on apical nuclear positioning, I performed live imaging and detailed quantification of nuclear movements during apical migration. I first tested whether Lamin A overexpression alters nuclear dynamics in a cell-autonomous manner, and whether this effect depends on tissue packing density, by comparing the densely packed retina to the less crowded hindbrain. Next, I investigated whether tissue-wide increases in nuclear stiffness could affect movements of control nuclei in a non-cell-autonomous manner. I further explored how these mechanical changes influence additional processes such as nuclear envelope breakdown and mitotic rounding.

Altogether, this study examines how nuclear mechanical properties—specifically nuclear deformability regulated by Lamin A levels—influence nuclear positioning and mitotic entry in zebrafish neuroepithelia, underscoring the importance of nuclear mechanics in shaping cellular behaviour during organ development.

2. Results

In my PhD project, I aimed at understanding whether and how nuclear mechanical properties can influence nuclear positioning in neuroepithelial development. To achieve this, I used a genetic tool that we speculated will increase nuclear stiffness in zebrafish neuroepithelia. The Tg(hsp70:LMNA-mKate2) zebrafish transgenic line overexpresses Lamin A by heat-shock induction. We followed apical migration of control and Lamin A overexpressing nuclei using live imaging. Quantification of nuclear positions over time ill shed light on whether and how nuclear deformability influences apical nuclear migration in the densely packed zebrafish neuroepithelia.

At the beginning of this project, several key aspects of apical nuclear movement were already well-established: it was known why nuclei move apically—this movement is essential to ensure tissue integrity, as sub-apical divisions compromise tissue architecture (Strzyz et al., 2015); when this apical movement occurs—during the G2 phase of the cell cycle, with CDK1 expression being both necessary and sufficient to trigger the movement (Leung et al., 2011; Strzyz et al., 2015); how nuclei move—through an actin-dependent mechanism, which is influenced by cell and tissue morphology, with nuclear movement in straight neuroepithelia being regulated by Rho-ROCK-dependent myosin contractility, while in curved neuroepithelia, it is driven by a formin-dependent pushing mechanism (Yanakieva et al., 2019)(Norden et al. 2009; Yanakieva et al. 2019); and where nuclei move—through a dynamic and densely packed pseudostratified neuroepithelium (Ferme et al., 2024; Kim et al., 2024; Matejčić et al., 2018).

This section presents results from a published paper of which I am the lead author:

• **Mariana Maia-Gil**, Maria Gorjão, Roman Belousov, Jaime A. Espina, João Coelho, Juliette Gouhier, Ana P. Ramos, Elias H. Barriga, Anna Erzberger, and Caren Norden (2024). *Nuclear deformability facilitates apical nuclear migration in the developing zebrafish retina*. *Current Biology*, Volume 34, Issue 23, 5429–5443.e8. https://doi.org/10.1016/j.cub.2024.10.015

Some of the results were generated in collaboration with various colleagues: Juliette Gouhier, a master's student I supervised for 4 months, conducted experiments in the hindbrain; Maria Gorjão, a master's student I supervised for 1 year, worked on 3D

segmentation and explored the effects of Lamin A overexpression on the cytoskeleton and neuronal development; Dr. João Coelho, the laboratory manager, assisted with sample preparation for protein quantification and performed the Western blot experiments; and Dr. Ana Patrícia Ramos, a postdoctoral researcher, contributed to Airyscan confocal microscopy and 3D segmentation using the LimeSeg plugin.

Additionally, I established collaborations with the laboratory of Dr. Elias Barriga, at the Instituto Gulbenkian de Ciência, Oeiras, Portugal, where I worked with Dr. Jaime Espina to conduct atomic force microscopy experiments; and with the laboratory of Dr. Anna Erzberger, at the Cell Biology and Biophysics Unit, European Molecular Biology Laboratory (EMBL), Heidelberg, Germany, where Dr. Roman Belousov developed the mechanical model and analysed the 3D data. Therefore, at the beginning of each section, I mention the colleagues with whom I collaborated to produce the data presented.

2.1 Lamin A expression levels increase upon overexpression in the zebrafish retina, and Lamin A integrates into the nuclear lamina

(In this section, dissections were done with Maria Gorjão and Dr. João Coelho, Dr. João Coelho performed the Western blots and Dr. Ana Patrícia Ramos helped with the confocal airyscan imaging.)

Nuclei in zebrafish neuroepithelia are highly deformable and only express low levels of Lamin A/C, a nuclear lamina protein which expression levels positively correlate with nuclear stiffness (Yanakieva et al., 2019). To modulate nuclear mechanical properties, I used a zebrafish transgenic line previously generated in our laboratory, in which Lamin A is expressed under the control of a heat-shock promoter—Tg(hsp70:LMNA-mKate2). Following heat-shock induction, Lamin A expression increases tissue-wide, with the protein fused to the fluorescent reporter mKate2, allowing for direct visualization of its expression in vivo (Amini et al., 2022a).

The first step was to understand what Lamin A does upon overexpression. I began by analysing how much of the protein is present after heat-shock induction. Overexpression was induced by subjecting zebrafish larvae to a 30-minute heat shock at 39°C at 22 hours post-fertilization (hpf). Zebrafish heads, primarily composed of neuroepithelia, were then dissected at 2, 6, and 14 hours post-heat shock, and Lamin A expression levels were assessed using Western blot (Figures 2.1 A and B). Western blot analysis revealed that endogenous Lamin A (74 kDa) is nearly undetectable in control conditions (Tg(hsp70:LMNA-mKate2) zebrafish without heat-shock), consistent with previous immunostaining results (Yanakieva et al., 2019). As expected, endogenous Lamin A was also present at low levels in the overexpression conditions—2, 6, and 14 hours post-heat shock. In contrast, upon heat-shock induction, a distinct band at ~100 kDa corresponding to the Lamin A–mKate2 fusion protein (74 kDa + 26 kDa) was detected at all examined time points, with maximal expression observed around 6 hours post-heat shock (Figure 2.1 A). The Western blot showed another band between 74 kDa and 100 kDa, which likely corresponds to a truncated version of the Lamin A–mKate2 fusion, where amino acids near the N-terminal could be missing. Since the anti-Lamin A antibody used recognises an epitope near the C-terminal, we assume that this region remains intact. However, further investigation is required to confirm this. Importantly, Lamin A overexpression did not affect the expression levels of Lamin B1 and B2, the other major components of the nuclear lamina (Figure 2.1 B). Thus, by confirming the low endogenous levels of Lamin A and

demonstrating successful induction upon heat shock, these results validate the use of the Tg(

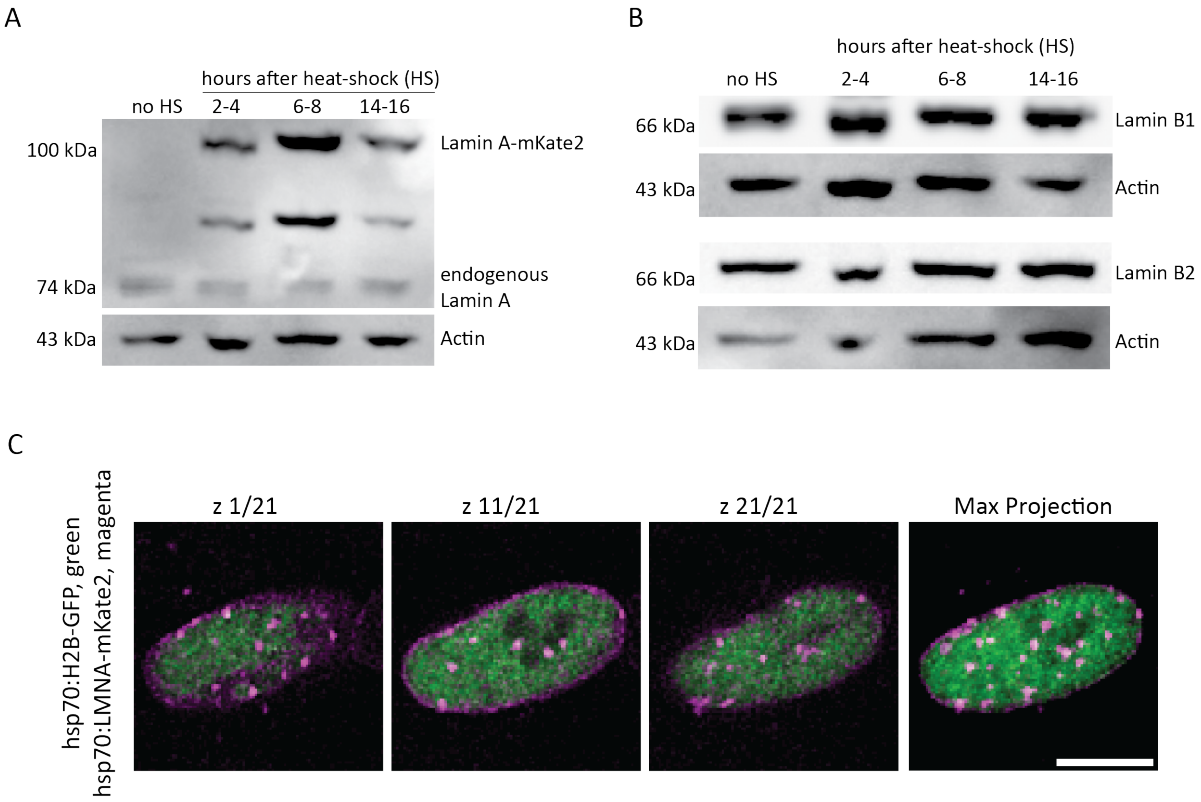

Figure 2. 1 Lamin A overexpression leads to increased Lamin A levels, which integrate into the nuclear lamina

(A) Western blot showing Lamin A levels in the Lamin A OE line Tg(hsp70:LMNA-mKate2) without heat-shock (left) and at 2, 6, and 14 hours post-heat-shock (right). (B) Western blot analysis of Lamin B1 (upper panel) and Lamin B2 (lower panel) levels in the Lamin A OE line Tg(hsp70:LMNA-mKate2) without heat-shock (left) and at 2, 6, and 14 hours post-heat-shock (right). (C) Representative images showing the typical localisation of the LMNA-mKate2 signal in comparison with the H2B-GFP nuclear marker. Z-stack images through the nucleus (left) and maximum intensity projection (right) are shown. Voxel depth: 0.17 µm. Scale bar: 5 µm.

hsp70:LMNA-mKate2) line for controlled overexpression. The detection of Lamin A-mKate2 protein at multiple time points—and its peak around 6 hours post-heat shock—establishes a clear temporal window (6–14 hours) for downstream functional analyses.

As Lamin A locates beneath the nuclear envelope and varying levels of its expression have been shown to be related to nuclear mechanical properties (Lammerding et al., 2006), we next aimed to confirm whether the overexpressed Lamin A integrates into the nuclear lamina. To do this, we induced Lamin A overexpression mosaically and co-labelled these nuclei with H2B-GFP, a histone nuclear marker. If Lamin A is properly integrated, we would expect its signal to

surround the H2B label. Indeed, confocal microscopy images using Airyscan mode revealed an accumulation of Lamin A–mKate2 at the nuclear lamina (Figure 2.1 C).

To a lesser extent, an intranuclear pool of Lamin A was also observed (Figure 2.1 C). These punctate Lamin A structures in the nucleoplasm have been reported in both endogenous and overexpression scenarios and may represent overexpressed Lamin A that has yet to be transported or cannot be incorporated into the nuclear envelope due to saturation. Nevertheless, these results suggest that the majority of overexpressed Lamin A successfully integrates into the nuclear envelope.

2.2 Lamin A overexpression in the zebrafish retinal neuroepithelia decreases nuclear volume and deformability

(In this section, DNA plasmid injections, confocal imaging, 3D segmentations, and IMARIS analysis were conducted in collaboration with Maria Gorjão. The analysis of root-mean-squared deviations resulted from a collaboration with Dr. Anna Erzberger and Dr. Roman Belousov.)

Finally, to understand whether Lamin A overexpression influences nuclear mechanical properties in the developing zebrafish retina, I first analysed its impact on nuclear morphology. Lamin A is known to modulate nuclear stiffness, which can affect both nuclear deformability and shape (Lammerding et al., 2006). To begin, I mosaically labelled nuclei with H2B-GFP and performed 3D segmentation in IMARIS software to quantify nuclear volume (Figure 2.2 A). Comparing control nuclei with nuclei from the Tg(hsp70:LMNA-mKate2) zebrafish transgenic line, we observed that on average, control nuclei had a volume of 169.8 ± 47.83 μm^3, compared to nuclei overexpressing Lamin A with 130.4 ± 27.47 μm^3 (mean ± SD) (Figure 2.2 B). This represented a 20% reduction in nuclear size compared to controls. However, as observed in figure 2.2 A, this size reduction is isometric and nuclear aspect ratios remained similar in both conditions, indicating that nuclei in both groups are elongated along the apical-basal axis (Figure 2.2 C). Interestingly, variance of nuclear volume and aspect ratio is smaller when nuclei overexpress Lamin A (variance comparison: $p_{Volume} < 0.0040$, $p_{Aspect\ Ratio} < 0.00119$, Levene's test). These findings indicate that nuclear morphology is more heterogeneous in controls, while Lamin A overexpression appears to constrain nuclear shape, consistent with increased nuclear stiffness.

Given the observed differences in nuclear morphology, I next investigated whether Lamin A overexpression alters nuclear deformability. Thus, control and Lamin A overexpressing nuclei were mosaically labelled using the nuclear envelop marker EGFP-Lap2b (Figure 2.2 D) and then 3D segmented at consecutive time points during the S phase of the cell cycle (Figure 2.2 E and F). During S phase nuclear movement is stochastic (Leung et al., 2011), and therefore, nuclear deformations in this near-equilibrium configuration are not a direct consequence of nuclear active movement. In order to evaluate small scale deformations directly from in vivo imaging data, the root mean squared deviations (RMSD) of nuclear surface was analysed from a perfect ellipsoid (scheme in Figure 2.2 E). As a proxy for nuclear deformability, the RMSD analysis quantifies how much the nuclear surface, 3D-segmented from the EGFP-Lap2b label, deviates from a perfect ellipsoid. A greater amplitude of deviations over time indicates increased nuclear deformability, while fewer deviations suggest less deformability. RMSD analysis is a novel approach developed within the scope of this project to quantify small-scale deformations, providing a direct assessment of nuclear mechanical properties from in vivo images. Analysis of the RMSD standard deviations shows that control nuclei exhibit two times larger surface fluctuations compared to Lamin A-overexpressing nuclei (Figure 2.2 F). This suggests that Lamin A overexpression increases nuclear stiffness and nuclei became more rigid than controls.

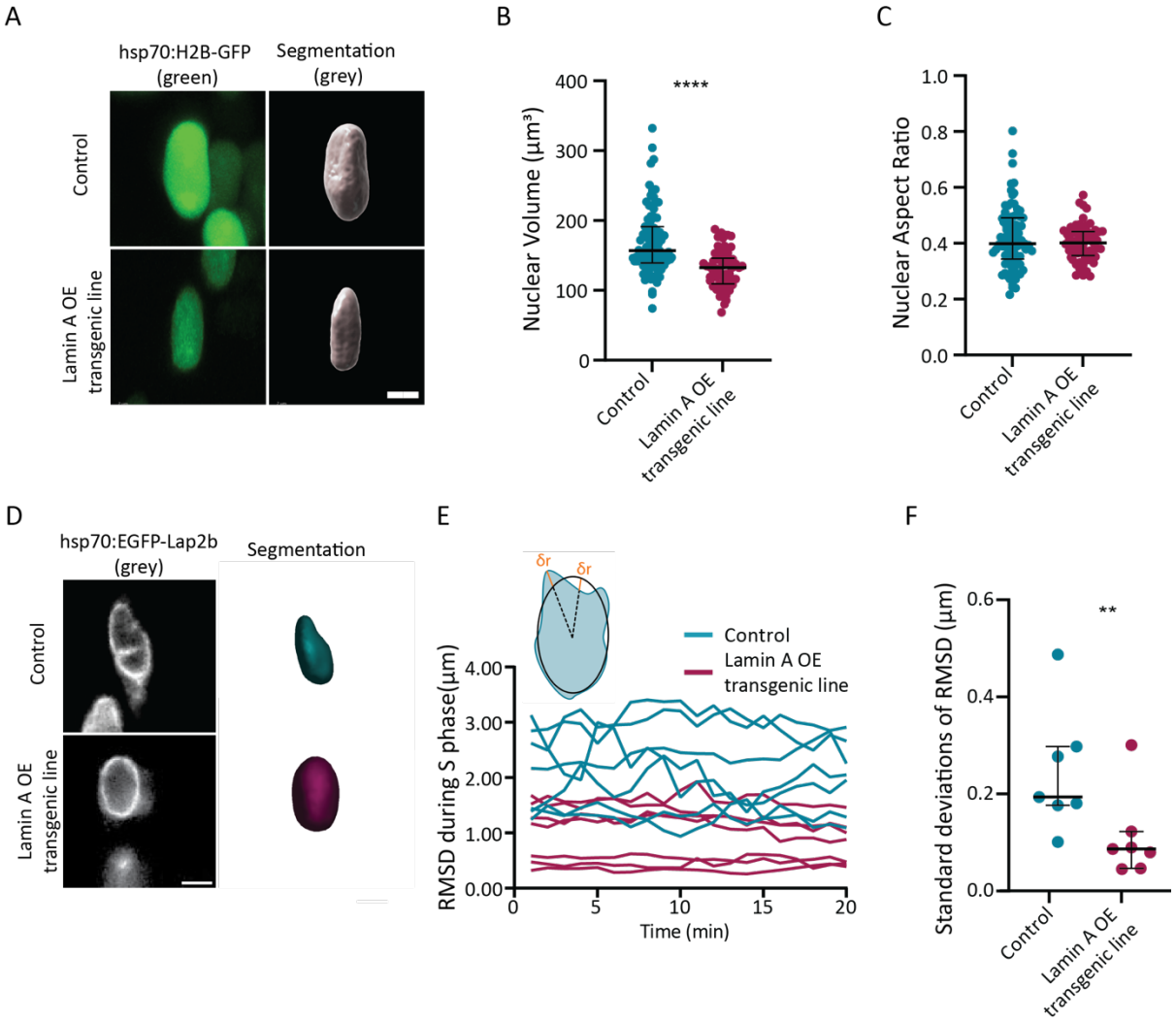

Figure 2. 2 Upon Lamin A overexpression, nuclei become smaller, maintain their aspect ratio, and exhibit reduced surface deformability:

(A) Example of 3D segmentation of nuclei labelled mosaically with H2B-GFP in Tg(hsp70:H2B-RFP) and Tg(hsp70:LMNA-mKate2) retinas. Scale bar: 4 µm. (B) Quantification of nuclear volume (B) and aspect ratio (C) from 3D segmented nuclei (shown in A). Nuclei overexpressing Lamin A are isometrically smaller compared to controls ($p_{Volume} < 0.0001$, $p_{Aspect\ Ratio} = 0.5891$, Mann-Whitney test). The variance in nuclear volume and aspect ratio is smaller in the Lamin A OE transgenic line (variance comparison: $p_{Volume} < 0.0040$, $p_{Aspect\ Ratio} < 0.00119$, Levene's test). Error bars represent the median and interquartile range. (D) Example of 3D segmented nuclei in S-phase, mosaically labelled with Lap2b-GFP in control Tg(hsp70:H2B-RFP) and Lamin A OE Tg(hsp70:LMNA-mKate2) retinas. Scale bar: 5 µm. (E) Root Mean Squared Deviations (RMSD) of nuclear shapes from a perfect ellipsoid at consecutive time points during S-phase. Trajectories over 20 minutes show nuclear shape changes in control (cyan) and Lamin A OE (magenta) cells. A schematic representation of RMSD analysis is shown in the top left corner, illustrating that nuclear deformability was quantified by measuring the deviation (δr) between the actual nuclear surface and its idealised ellipsoid shape. (F) Standard deviations (SDs) of the RMSD of S-phase nuclei at consecutive time points ($p_{SD\_RMSD} = 0.0043$, Mann-Whitney test).

2.3 Lamin A overexpression changes nuclear and tissue stiffness: theory and experiment

(In this section, the mechanical model resulted from a collaboration with Dr. Anna Erzberger and Dr. Roman Belousov. The atomic force microscopy experiments were performed in collaboration with Dr. Elias Barriga and Dr. Jaime Espina)

The 3D-segmented data on nuclear shape during the S phase, described above, was further used to develop a mechanical model and assess whether theoretical predictions support that Lamin A-overexpressing nuclei are less deformable. To theoretically explore the effects of Lamin A overexpression on nuclear deformability, the confined nuclei were modelled as compressible droplets using a simple mechanical framework:

$$F(a,b) = \gamma A(a,b) + k2\,[V(a,b) - V0]2 - \psi\alpha(b)$$

Here, the nuclear surface was approximated as an elongated axisymmetric spheroid, with a as the longest axis and b as the two shorter axes. V(a,b) represents the spheroid's volume, A(a,b) its surface area, and α(b) the area of the nucleus's largest cross-section perpendicular to the apicobasal axis (Figure 2.3 A). The mechanical model assumes that the compressive tension ψ is similar in control and Lamin A OE tissues and predicts the preferred volume (V_o), the surface tension (γ/ψ) and the volume elastic coefficient (k/ψ) from measurements of nuclei ellipsoid axis.

As expected from the previous experimental analyses showing that Lamin A-overexpressing nuclei are smaller than controls (Figure 2.2 B), the model estimated a smaller preferred volume (V_o) for Lamin A-overexpressing nuclei (885.7 ± 182.8 μm^3) compared to controls (1,056 ± 360 μm^3) (Figure 2.3 B). The tension coefficient (γ/ψ) increases from 0.262 ± 0.07 μm^{-4} in controls to 0.519 ± 0.21 μm^{-4} in response to Lamin A overexpression (Figure 2.3 C). The model also predicted that the volume elastic coefficient (k/ψ) increases 2-fold in Lamin A-overexpressing nuclei ((3.2 ± 1.6) × 10^{-5} μm^{-4}) compared to controls ((6.4 ± 3.6) × 10^{-5} μm^{-4})(Figure 2.4 D).

Overall, this theoretical analysis predicts an increase in surface tension and in the volume elastic coefficient, suggesting that the nuclear surface deformations are energetically

more costly in the Lamin A condition and that higher Lamin A expression levels enhance the resistance of stiffer nuclei to compression.

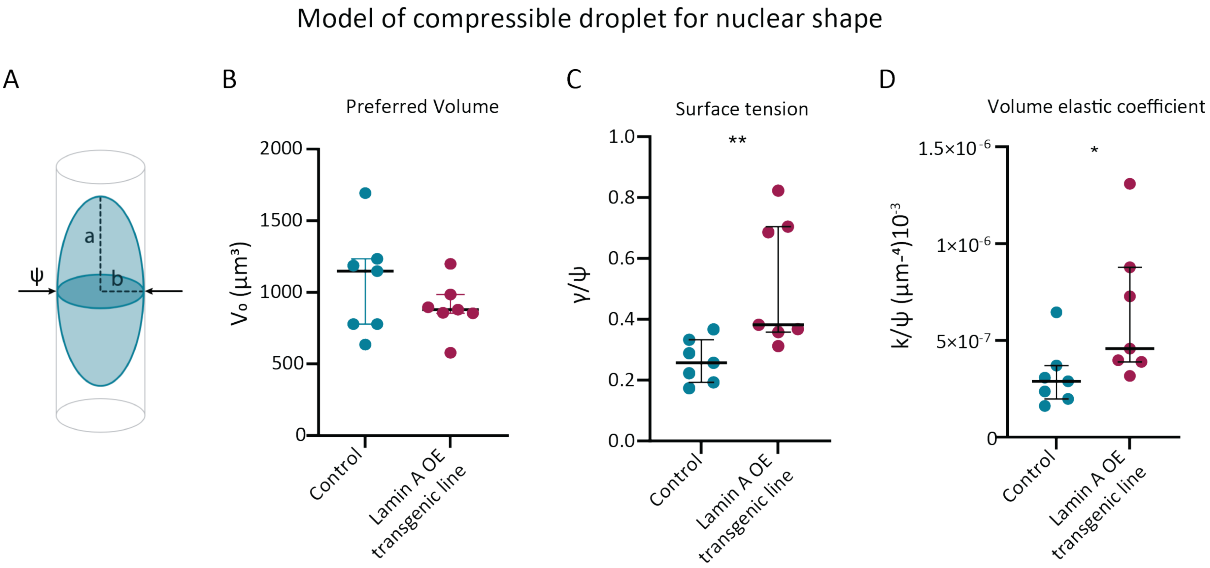

Figure 2. 3 Model of compressible droplets predicts an increase in nuclear stiffness upon Lamin A overexpression:

(A) Schematic representation of the parameters used in the mechanical model. Here, a represents the longest axis, and b represents the two shorter axes. ψ denotes the compressive tension, which is assumed to be similar between control and Lamin A overexpressing conditions. The model predicts a slight decrease in the preferred volume (V_0) (B, p = 0.620) and an increase in surface tension (γ/ψ) (C, p = 0.004) and volume elastic coefficient (k/ψ) (D, p = 0.011) (Mann-Whitney test).

To confirm the above-mentioned theoretical predictions, together with our collaborators Elias Barriga and Jaime Espina, the apparent elastic moduli of control and Lamin A overexpressing retinal tissues was probed using atomic force microscopy (AFM). As nuclei are the largest organelle within retinal cells and occupy most of the cell volume, we expected that changes in nuclear properties would impact tissue-scale stiffness. This idea is aligned with recent data showing that, in Lamin A overexpressing zebrafish retinas, tissue stiffness depends on nuclear stiffness (Kim et al., 2024). To assess this, I dissected zebrafish retinas from both control and Lamin A-overexpressing conditions, removed the retinal pigmented epithelium and the lens, and plated clusters of progenitor cells on a Poly-D-Lysine coated dish (Figure 2.4 A and D), which were then probed with AFM *ex vivo.* The apparent elasticity (Pa) of each cell cluster was measured using a 5 × 5 grid (Figure 2.4 B). Measurement quality was evaluated based on curve shape (Figure 2.4 C), and the median apparent elasticity (Pa) for each cell

cluster was calculated using only high-quality curves, excluding lower-quality ones (Figure 2. 4 E). Therefore, each data point in figure 2.4 E represents the median value calculated from high-quality measurements acquired in a 5×5 grid of a cluster of dissected retinal cells. Analysis of these *ex vivo* indentations revealed that Lamin A-overexpressing tissues (462.2 ± 161.3 Pa) exhibited an almost 2-fold increase in the apparent elastic moduli comparing to controls (251.2 ± 125.3 Pa) (Figure 2.4 E).

Overall, both theoretical modelling and experimental analysis confirm that Lamin A overexpression increases nuclear stiffness, resulting in less deformable nuclei. This conclusion aligns with recent findings from another laboratory, which used magnetically responsive oil microdroplets to demonstrate a 2-fold increase in nuclear stiffness in Lamin A-overexpressing zebrafish retinas (Kim et al., 2024).

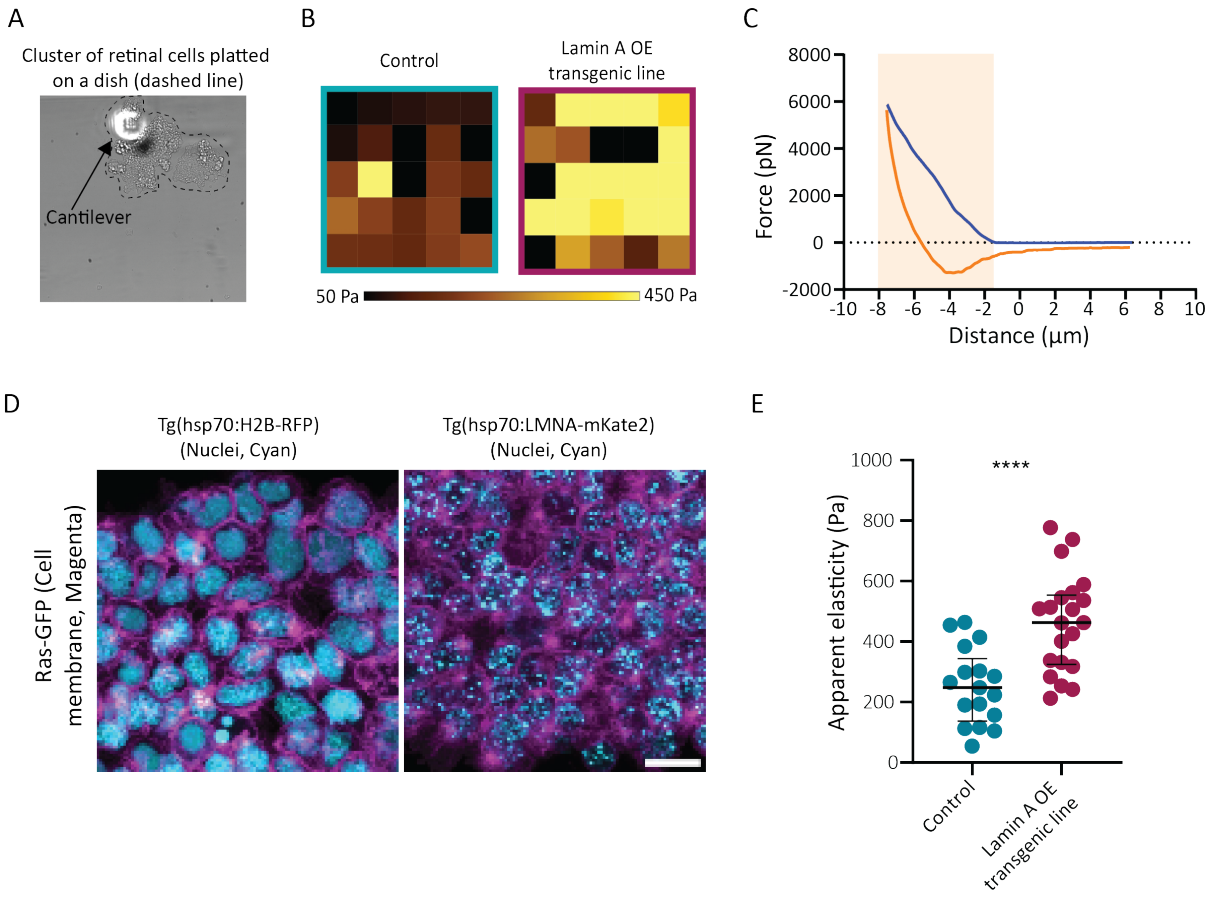

Figure 2. 4 Apparent elasticity (Pa) increases upon Lamin A overexpression, as measured by Atomic Force Microscopy (AFM):

(A) Image showing the position of the AFM cantilever relative to dissected retinal cells plated on a dish. (B) Heat map of control (cyan) and Lamin A overexpressing (OE) transgenic retinal cells (magenta), displaying measurements acquired in a 5x5 grid with a 50 µm x/y resolution. This grid illustrates the distribution of data within the tissue, where darker and lighter colours respectively correspond to lower and higher measured values (Pa). All measurements were performed using a cantilever with a 2.25 µm diameter bead as the tip. (C) Representative force-distance curve obtained with cantilevers coated with 2.25 µm beads. Approach curves are shown in blue, and withdraw curves in orange. The indentation at the contact point is highlighted by a light orange rectangle. (D) Retinal cells were dissected and plated on a glass-bottom dish. Tg(hsp70:H2B-RFP) labels the nuclei (cyan) in control cells, while Tg(hsp70:LMNA-mKate2) labels the nuclei (magenta) in Lamin A overexpressing cells. RAS-GFP labels the plasma membrane (magenta). Note that the control and Lamin A overexpressing nuclei are marked with different nuclear labels, H2B-RFP and LMNA-mKate2, respectively. Scale bar: 10 µm. (E) AFM measurements of plated retinal cells show a significant increase in elasticity upon Lamin A overexpression ($p < 0.0001$, t-test). Each data point **E** represents the median value calculated from the 5x5 grid measurements of a cluster of dissected retinal cells. Error bars represent the median and interquartile range.

2.4 Overexpression of Lamin A lengthens the G2 phase but not the overall cell cycle

Having established that Lamin A overexpression increases nuclear stiffness, we next investigated whether and how this affects retinal development. Given that Lamin A–mKate2 levels are higher during the retina's proliferative phase (Figure 2.1 A), we explored whether its overexpression influences proliferative dynamics, including overall cell cycle progression and the associated apico-basal nuclear movements.

One indicator of potential cell cycle abnormalities can be the presence of DNA damage. To determine whether Lamin A overexpression induces DNA damage, I performed immunostaining for γ-H2AX, a marker of H2AX phosphorylation that signals the early cellular response to DNA double-strand breaks. As expected, γ-H2AX foci were observed in the positive control, where DNA damage was chemically induced using Hydroxyurea and Aphidicolin (HU + A) treatment (Figure 2.5 A). These compounds inhibit DNA replication by blocking ribonucleotide reductase and DNA polymerase activity, respectively, leading to S-phase arrest, replication stress, and subsequent DNA damage. However, no γ-H2AX foci were detected in either control or Lamin A-overexpressing retinas (Figure 2.5 A), suggesting that Lamin A overexpression does not induce DNA damage or disrupt DNA replication processes.

Another way to assess whether cell cycle progression is affected is by measuring the duration of the cell cycle. The cell cycle includes several checkpoints that halt progression when DNA replication issues are detected, providing time for error correction. Therefore, if Lamin A overexpression were to interfere with DNA replication, we would expect to observe an elongation in the cell cycle duration.

To address this question, I imaged control and Lamin A-overexpressing zebrafish retinas during the proliferative phase and quantified cell cycle duration. I used light-sheet microscopy, which reduces phototoxicity compared to confocal microscopy, enabling high-temporal-resolution live imaging while maintaining the necessary cell and nuclear resolution (Icha et al., 2016b, 2017). To identify the different phases of the cell cycle, I mosaically labeled zebrafish retinas with proliferating cell nuclear antigen (PCNA), with replication foci marking S phase and G1 corresponding to the post-division phase (Figure 2.5 B) (Leung et al., 2011). This is important because different cell cycle phases are associated with distinct events, including various checkpoints and specific nuclear movements (Leung et al., 2011). By comparing the phases individually, we can gain greater resolution in understanding how Lamin A overexpression might affect nuclear dynamics during cell cycle progression, rather than just assessing the overall cell cycle.

Control cells required about 6 hours to complete a full cell cycle, consistent with previous studies on 36-hour post-fertilisation zebrafish retinas (Matejčić et al., 2018). Lamin A-overexpressing cells cycled slightly faster, taking 5 hours and 37 minutes (Figure 2.5 C). This small difference does not suggest any disruption in cell cycle progression, as there is no significant elongation.

By examining the duration of each cell cycle phase using PCNA labelling, I found that the overall decrease in cell cycle duration was primarily due to a slightly shorter S phase in Lamin A-overexpressing cells (3 hours and 45 minutes) compared to controls (4 hours and 6 minutes) (Figure 2.5 D). However, this difference is unlikely to have biological significance, as only an elongation of the cell cycle would indicate issues with cell cycle progression. The G1 phase lasted approximately 1 hour and 30 minutes on average in both control and Lamin A cells (Figure 2.5 E).

While control cells spent an average of 29 minutes in the G2 phase, Lamin A-overexpressing cells spent 43 minutes, with more variability in duration (Figure 2.5 F). However, despite this 15-minute elongation, representing a 51% increase in G2 duration, the overall cell cycle duration was not significantly affected. This is because G2 phase constitutes only a small portion of the total cell cycle (about 30 minutes in a 6-hour cycle), meaning that even a large elongation in G2 duration does not substantially impact the overall cell cycle time.

To test if the G2 elongation effect in Lamin A-overexpressing cells is cell-autonomous, I overexpressed Lamin A in individual nuclei by injecting a DNA plasmid into one-cell-stage

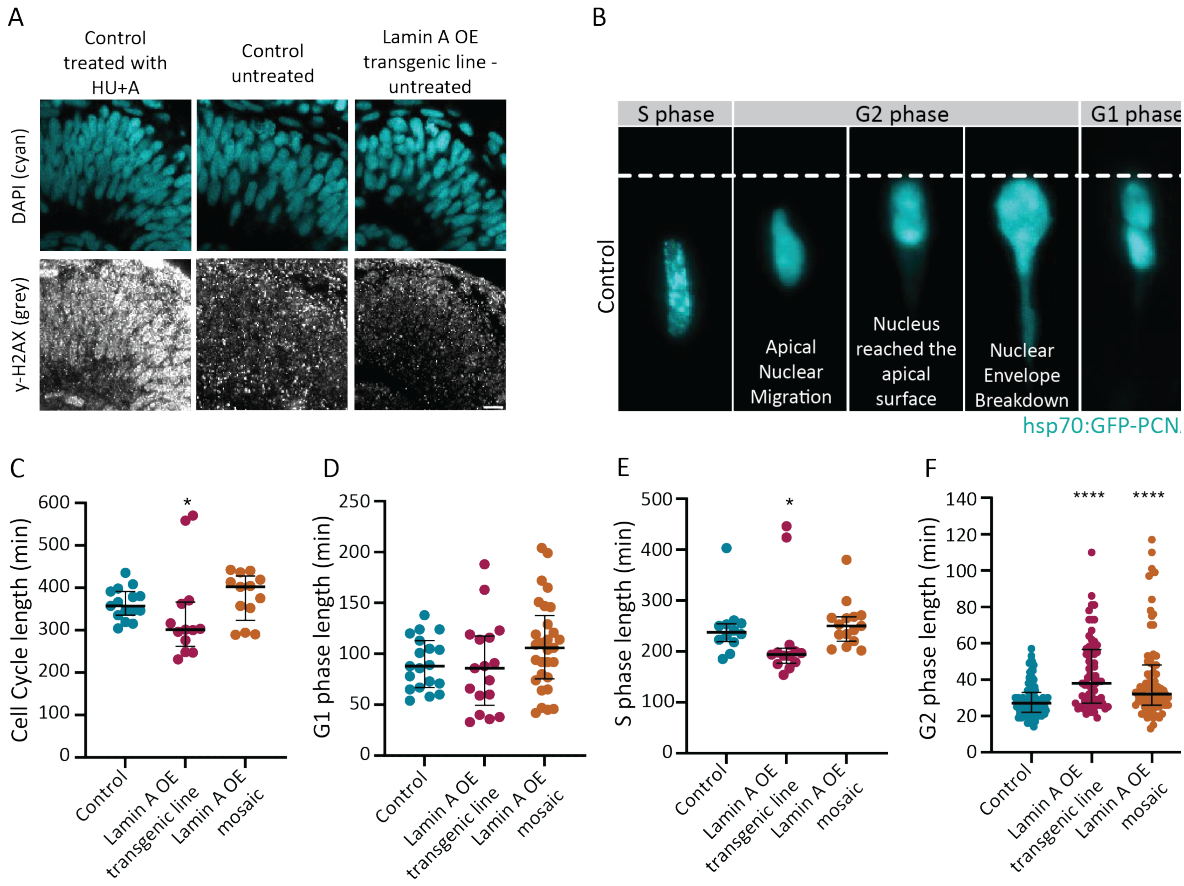

Figure 2. 5 Overexpression of Lamin A does not induce DNA damage or overall cell cycle alterations. However, nuclei with Lamin A overexpression exhibit a slower G2 phase:

(A) Immunostaining of γh2ax revealing no obvious DNA damage in control (center) and Lamin A OE transgenic line retinal neuroepithelia (right). Left: Control retinas were treated with 150µM aphidicolin + 20 mM hydroxyurea for 6 hours to induce DNA damage (left). Scale bar: 10µm. (B) Panel showing the nuclear hsp70:GFP-PCNA marker in the different cell cycle phases. Dotted appearance marks S-phase that shows even nuclear distribution when moving into G2-phase. Scale bar: 10 µm. (C-F) Duration (in minutes) of cell cycle and its phases (C), G1 (D), S (E), and G2 (F) phases in control, lamin A OE line, and lamin A OE mosaic retinal neuroepithelial cells. Imaged at 1 min time intervals. Cell cycle length: $p_{\text{Lamin A OE transgenic line}} = 0.0245$, $p_{\text{Lamin A OE mosaic}} = 0.3701$, Mann-Whitney test and t test, respectively; G1: $p_{\text{Lamin A OE transgenic line}} = 0.8337$, $p_{\text{Lamin A OE mosaic}} = 0.1302$, t test; S phase: $p_{\text{Lamin A OE transgenic line}} = 0.0188$, $p_{\text{Lamin A OE mosaic}} = 0.3792$, Mann-Whitney test; G2: $p_{\text{Lamin A OE transgenic line}} < 0.0001$, $p_{\text{Lamin A OE mosaic}} < 0.0001$, Mann-Whitney test.

embryos. If the effect is cell-autonomous, it should occur even in cells overexpressing Lamin A that are surrounded by control cells. In this Lamin A OE mosaic condition, only some nuclei overexpress Lamin A, while the rest of the tissue remains control. This contrasts with the Lamin A OE line, where Lamin A is overexpressed tissue-wide using heat shock in the Tg(hsp70:LMNA-mKate2) transgenic line.

In the mosaic condition, the overall cell cycle length, as well as the duration of G1 and S phases, remain comparable to controls (Figure 2.5 C, D and E respectively). However, similar

to observations in the Lamin A OE line, the G2 phase is extended by 12 minutes, representing a 40% increase, with an approximately total duration of 40 minutes in the mosaic condition (Figure 2.5 F).

These results show that Lamin A overexpression specifically elongates the duration of the G2 phase, without altering the overall cell cycle dynamics nor inducing DNA damage. Together, this indicates that tissue integrity is not compromised upon Lamin A overexpression but suggests that Lamin A may modulate specific aspects of the G2 phase, without affecting the broader cell cycle progression or inducing stress responses.

2.5 Lamin A-overexpression does not delay retinal neurogenesis onset and lamination

(The work presented in this section is part of Maria Gorjão's master thesis. I co-supervised Maria's thesis and collaborated with her on performing the injection and imaging experiments.)

To confirm that Lamin A overexpression does not impact organ development, I asked whether progenitor cells overexpressing Lamin A can successfully differentiate into neurons. It is important to note that, as observed in the Western blot analysis (Figure 2.1A), Lamin A levels begin to decrease around 10 hours after heat shock. This suggests that any potential alterations during neurogenesis are more likely to result from an earlier disruption in proliferation rather than a direct effect of Lamin A overexpression on the differentiation programme. We therefore assessed the onset of neurogenesis and the consequent neuronal lamination in zebrafish retinas upon Lamin A overexpression.

To this end, we injected an Ath5:GFP-CAAX-expressing plasmid into one-cell stage control and Lamin A OE transgenic embryos. The transcription factor Ath5 is expressed by the first neurogenic progenitors, which give rise to retinal ganglion cells, photoreceptors, amacrine cells, and horizontal cells (Nerli et al., 2023, 2020). Confocal imaging at 56 hours post-fertilisation (hpf), when neurogenesis is ongoing, revealed no differences in the distribution of Ath5-positive cells between control (Figure 2.6 A) and Lamin A-overexpressing retinas (Figure 2.6 B).

To determine whether retinal layering was affected, DAPI staining was performed to assess nuclear organization and tissue integrity, and whole retinas were imaged at 72 hpf. Image analysis showed that the nuclei within the retinal layers were properly organized in both

control (Figure 2.6 C) and Lamin A OE retinas (Figure 2.6 D), suggesting that the overall tissue architecture, including the neuronal and plexiform layers, was preserved.

These results indicate that, despite the G2 elongation during the proliferative phase, Lamin A overexpressing progenitor cells successfully differentiate into neurons and laminate correctly in their corresponding neuronal layer. Despite the high robustness of the developmental process, which could mask some defects, all results so far indicate that the tissue integrity is maintained upon Lamin A overexpression.

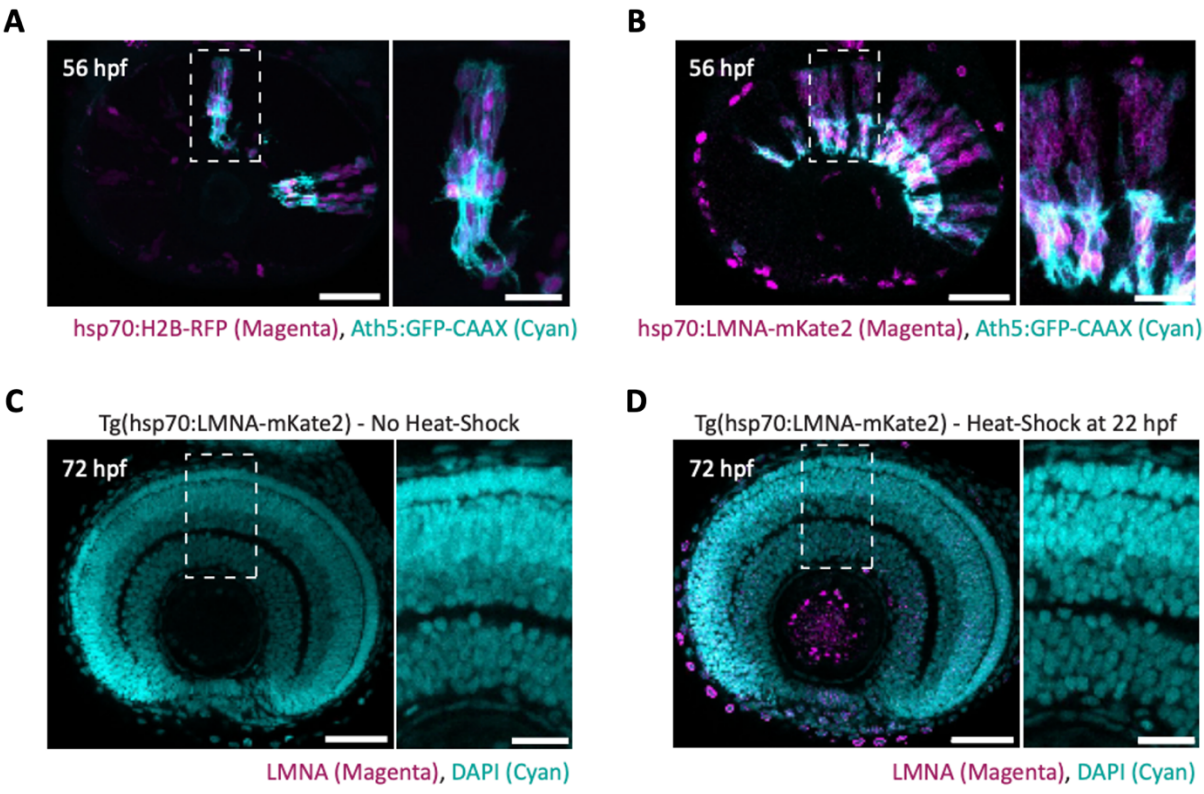

Figure 2. 6 Lamin A overexpression does not influence neurogenesis or lamination:

(A-B) Ath5:GFP-CAAX expression (cyan) in control (A) and Lamin A OE mosaic (B) retinas at 56 hpf, demonstrating comparable expression of the early neurogenic marker Ath5. Nuclei are shown in magenta. Scale bars: 50 µm and 20 µm. (C-D) Retinal lamination at 72 hpf in Tg(hsp70:LMNA-mKate2) retinas without heat shock (C) and following heat shock at 22 hpf (D). DAPI staining reveals proper retinal layer formation in both conditions. Scale bars: 50 µm and 20 µm.

2.6 Nuclei can reach the apical surface prior to mitosis despite increased Lamin A expression

The specific delay in the G2 phase, the only phase where nuclei move actively (Leung et al., 2011; Norden et al., 2009), led me to hypothesize that Lamin A overexpression may interfere with the ability of nuclei to move over time. In the G2 phase, where nuclear movement is particularly prominent, any interference with the flexibility or dynamics of the nuclear envelope could impair apical nuclear migration. Therefore, Lamin A overexpression, by increasing nuclear stiffness and reducing the nucleus's ability to deform, may reduce nuclei capacity to move effectively through confined spaces.

To investigate whether Lamin A overexpression affects apical nuclear positioning prior to mitosis, I performed immunostaining for phospho-H3 (pH3), a nuclear marker of mitotic chromatin condensation, and compared the division position of control and Lamin A-overexpressing nuclei relative to the retinal surface (Figure 2.7 A and B). Using 3D analysis, I manually segmented the apical surface of multiple zebrafish retinas from both conditions (Figure 2.7 A) and measured the distance of the pH3 signal from the apical surface. Results

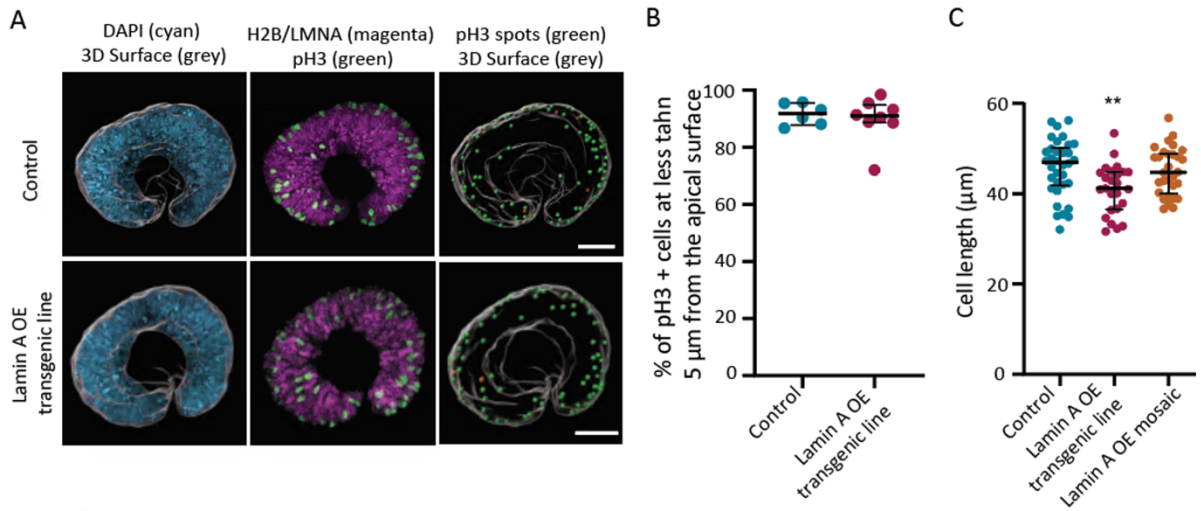

Figure 2. 7 Nuclei overexpressing Lamin A divide apically:

(A) pH3 staining (green) showing mitotic cells in the neuroepithelium of controls and Lamin A OE transgenic line (nuclei in magenta) (centre). 3D surface (grey) created from DAPI staining (left). pH3 spots (green/orange) (right) were classified according to their distance to the 3D surface. Green: pH3 spots within ≤ 5µm from the apical surface. Orange: pH3 spots > 5µm from the apical surface (right). Scale bar: 50µm. (B) Quantification of the % of pH3 spots within %5 mm (green) from the apical surface. (p% pH3 spots > 0.9999, Mann-Whitney test). (C) Quantification of cell length (in µm) in controls, Lamin A OE transgenic line and Lamin A OE mosaic condition (p Lamin A OE transgenic line = 0.0043, p Lamin A OE mosaic < 0.6364, Mann-Whitney test) showing that in the Lamin A OE line condition cells are smaller. Error bars: median with interquartile range.

show that, regardless of Lamin A expression levels, more than 90% of nuclei divide within 5 µm of the apical side (Figure 2.7 B), suggesting that Lamin A-overexpressing nuclei can successfully reach the apical surface before mitosis—an essential hallmark of pseudostratified epithelium maturation. In addition, we noticed that in the Lamin A overexpressing line (40.99 ± 5.489 µm), cells are smaller than in controls (45.69 ± 6.354 µm) and in the mosaic condition (44.99 ± 5.265 µm) (Figure 2.7 C).

2.7 Nuclear stochastic movements associated with S and G1 phases are not altered by Lamin A overexpression

I next investigated whether increased Lamin A expression affects nuclear positioning throughout the cell cycle. As nuclear movements in the neuroepithelium vary according to the cell cycle phase, analysing nuclear positioning at different phases allows us to explore the effect of Lamin A on interkinetic nuclear migration. While nuclear movement is persistent and directed towards the apical surface during G2, nuclei fluctuate stochastically along the apico-basal axis during S and G1 phases, with a slight basal drift following apical mitosis (Leung et al., 2011).

To investigate this, I tracked nuclei during the S and G1 phases and examined whether stochastic nuclear positioning is affected by Lamin A overexpression (Leung et al., 2011). Nuclei were mosaically labelled with PCNA to distinguish cell cycle phases, (Figure 2.5 B). Using lightsheet microscopy, I imaged control, Lamin A OE line, and Lamin A OE mosaic retinas in vivo and compared nuclear behaviour across these conditions (Figure 2.8 A–H).

From these live imaging movies, I quantified the nuclear distance to the apical surface and plotted trajectories during S phase, where t = 200 min represents the last time point before nuclei entered G2. This allowed me to analyse the maximum number of time-points during their passive movement (Figure 2.8 A–C). I also tracked nuclear movement during G1 phase, where t = 0 min corresponds to the moment the two daughter cells were born (Figure 2.8 E–G). To characterise nuclear movements, I quantified the mean square displacement (MSD) of nuclear positions over time. MSD assesses the area explored by nuclei and distinguishes stochastic (back-and-forth) from active, directed movement. As previously described (Leung et al., 2011), control nuclei in S and G1 phases exhibited purely stochastic motion. Similarly, Lamin A-overexpressing nuclei in both conditions followed a stochastic pattern during S and G1, with

A-D) Nuclei in S phase

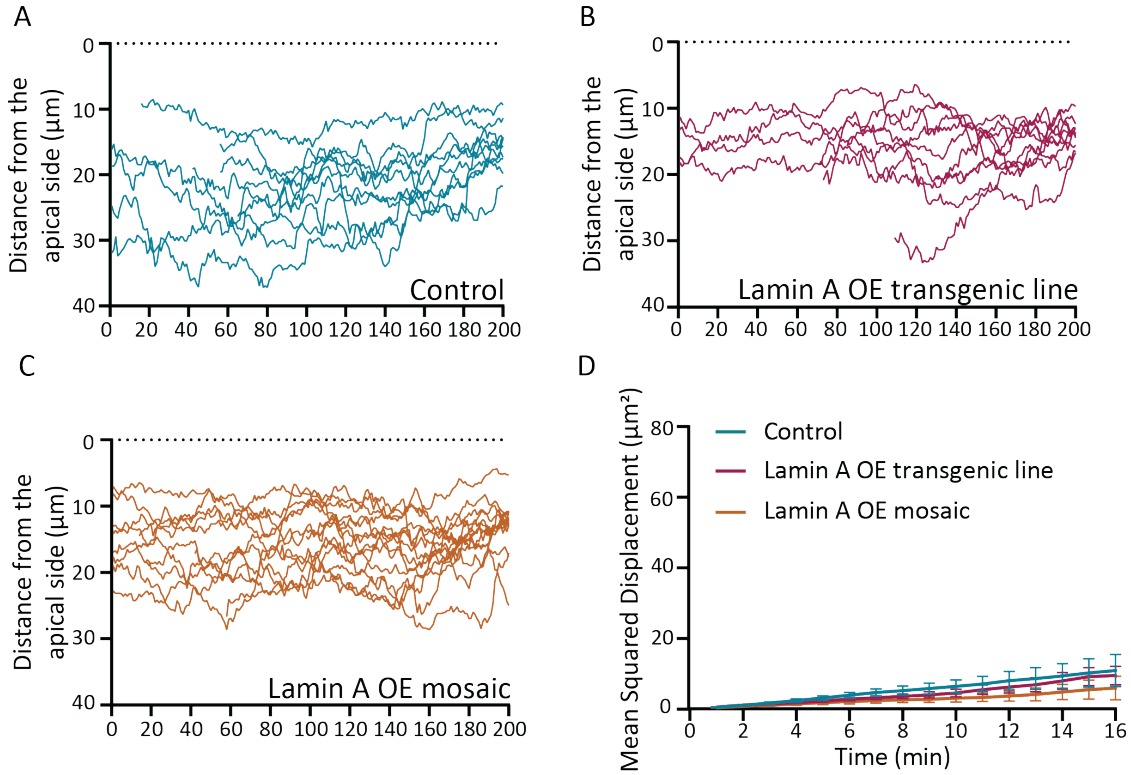

E-H) Nuclei in G1 phase

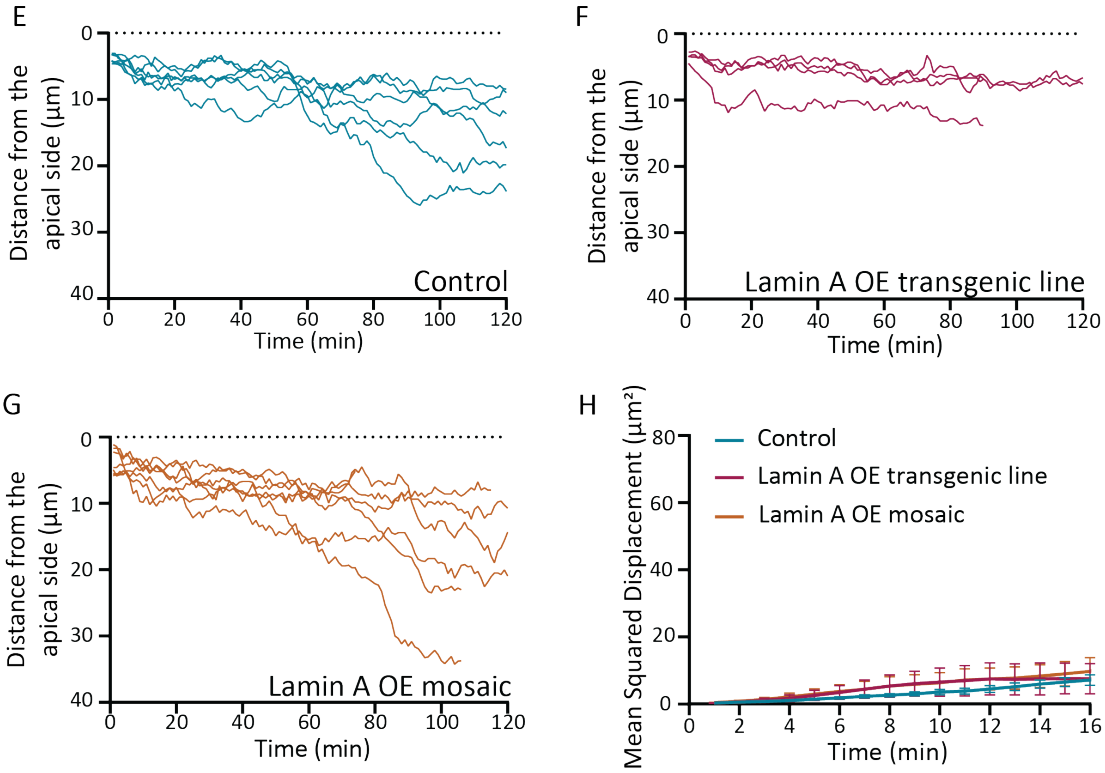

Figure 2. 8 Trajectories of Lamin A overexpressing nuclei during S- and G1-phases are similar to controls:

(A-C) S-phase nuclear trajectories in control (A), Lamin A OE transgenic line (B), and Lamin A OE mosaic condition (C). t200 (min) marks the final time point of S-phase, indicating the transition to G2-phase. (D) **Mean squared displacement (MSD) analysis** of nuclear movements during S-phase, comparing controls (cyan) with Lamin A OE transgenic line (magenta) and mosaic condition (orange). MSD curves largely overlap. (E-G) **G1-phase nuclear trajectories** in control (E), Lamin A OE transgenic line (F), and Lamin A OE mosaic condition (G). t1 (min) denotes the post-division time point marking entry into G1-phase. (H) **MSD analysis** of nuclear movements in G1-phase, comparing control (cyan) with Lamin A OE transgenic line (magenta) and mosaic condition (orange). Error bars: standard deviation. Images acquired at 1-minute intervals.

MSD curves comparable to controls (Figure 2.8 A and 2.8 H, respectively). These findings suggest that when movement is purely stochastic, nuclear positioning remains unaffected by Lamin A overexpression.

2.8 Lamin A-overexpression slows apical nuclear migration by 50% and disrupts directionality before mitosis

Following, I quantified the duration of apical migration from the onset of G2 (marked by the disappearance of PCNA foci) to the moment nuclei reach the apical surface (Figure 2.9 A-F). The apical surface was identified by the labelling of the cell membrane, using utrophin, a cytoskeleton protein present at the cell membrane, as a marker. I found that on average, Lamin A OE nuclei took 30.62 ± 17.46 min in the line condition and 36.95 ± 23.38 min in the mosaic condition, compared to 20.32 ± 8.39 min in controls (Figure 2.10 A). This represents a 50–80% increase in migration time. Importantly, the observed delay occurs specifically during periods of active nuclear migration, when movement relies on cytoskeletal forces. No comparable delay was detected during phases of passive nuclear movement. This strongly supports the idea that Lamin A overexpression interferes with active nuclear migration, likely by reducing nuclear deformability.

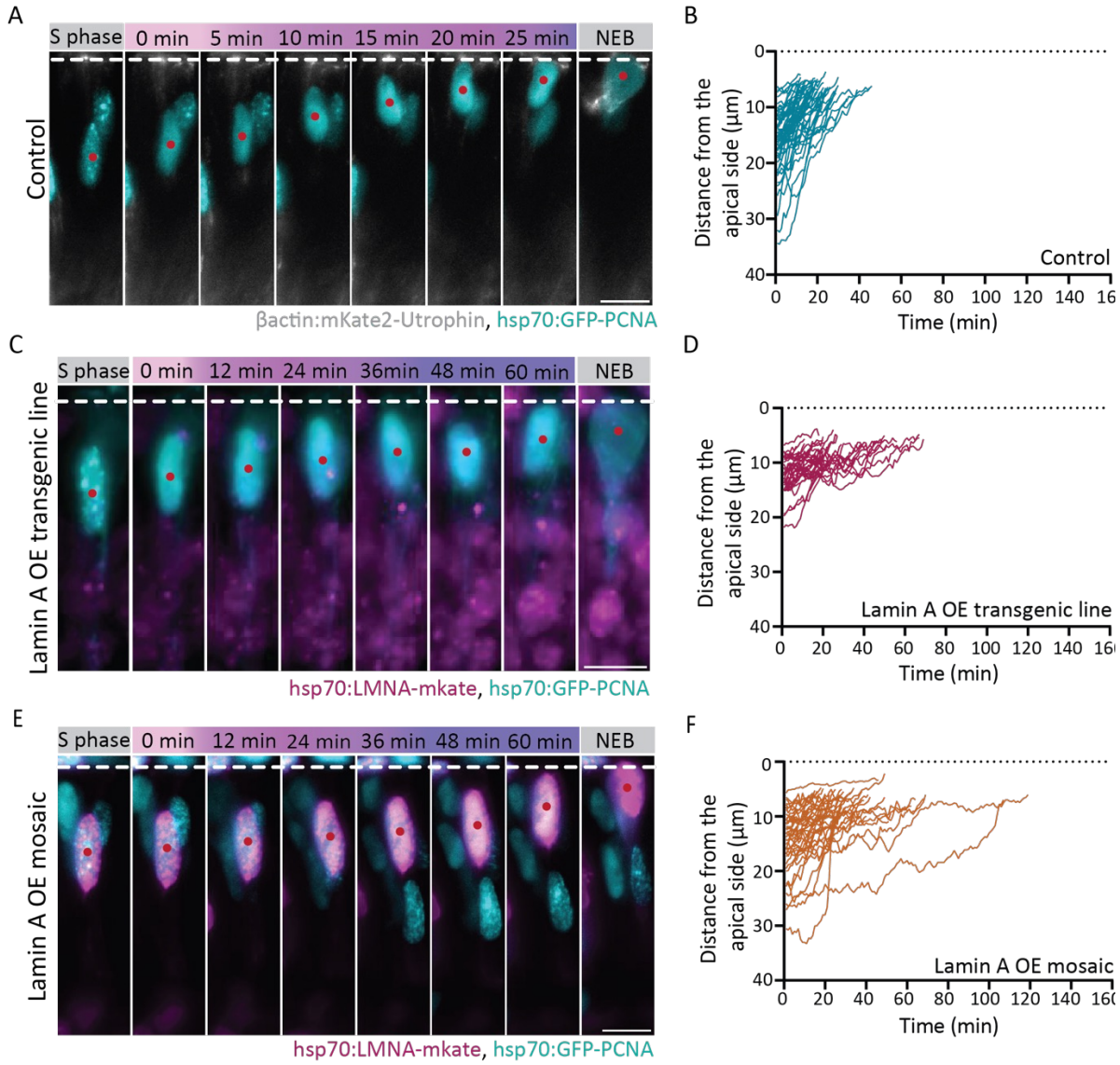

Figure 2. 9 Time-lapse images showing that nuclear trajectories to the apical surface are influenced by Lamin A overexpression:

(A, C, E) Representative montages of apical nuclear movements in control (A), Lamin A OE transgenic line (C), and Lamin A OE mosaic (E) retinal neuroepithelia. Red dots indicate the tracked nucleus, and the dashed line marks the apical surface. The gradient bar (pink to purple) represents the duration of apical nuclear migration, with darker shades indicating longer time spans. hsp70:PCNA-GFP labels nuclei according to cell cycle stage (cyan), and hsp70:LmnA-mKate2 labels Lamin A-overexpressing nuclei (magenta). NEB, nuclear envelope breakdown. Scale bar: 10 µm. (B, D, F) Apical migration trajectories for control nuclei (B, cyan), Lamin A OE transgenic line (D, magenta), and Lamin A OE mosaic (F, orange). Dashed line represents the apical surface.

To investigate how Lamin A overexpression interferes with apical nuclear migration, we first asked whether the prolonged migration time could result from nuclei initiating migration from more basal positions, thereby having to travel longer distances to reach the apical surface. However, when comparing the initial positions of nuclei before apical migration, we

found that control nuclei migrated an average distance of 16.04 ± 5.80 µm, while Lamin A OE nuclei migrated 12.52 ± 3.60 µm in the line condition and 14.64 ± 5.96 µm in the mosaic condition (Figure 2.10 C). These results indicate that Lamin A-overexpressing nuclei travel similar, or even slightly shorter, distances than controls, ruling out migration distance as the cause of the observed delay. The reduced migration distance in Lamin A-overexpressing nuclei may reflect a decrease in overall cell height (Figure 2.6 C).

After establishing that the distance between the starting and division positions (d) was not increased (Figure 2.10 C), I investigated whether the delay in apical migration could be due to a reduced ability of nuclei to move in a directed fashion. To access this, I quantified the surplus of travelled distance—defined as the difference between the total path covered (T, Figure 2.10 B) and the direct distance between the starting and division positions (d, Figure 2.10 C) (Figure 2.10 D). When T and d are similar, nuclear movement is directed, whereas a larger T relative to d indicates more frequent back-and-forth (apical-and-basal) movements, suggesting less efficient migration.

Results show that the surplus distance travelled is, on average, 3.79 ± 3.29 µm in controls, compared to 10.75 ± 10.43 µm in the transgenic Lamin A OE line and 11.02 ± 8.18 µm in the Lamin A OE mosaic condition (Figure 2.10 D), indicating that nuclear apical migration becomes less directed upon Lamin A overexpression. This conclusion was further supported by Mean Squared Displacement (MSD) analysis, a quantitative method used to assess how far a particle (in this case, a nucleus) moves over time. MSD curves that increase linearly over time indicate directed movement, while supralinear curves (with a steeper slope) suggest active and persistent motion. In contrast, sublinear curves reflect hindered or constrained movement. The MSD curves of Lamin A OE nuclei during apical migration showed a reduced amplitude compared to controls, reinforcing the idea that their movement is less efficient and potentially impaired (Figure 2.10 E).

In addition to being less directed, nuclear movement is also slower. When comparing instantaneous velocity, Lamin A OE nuclei in the line (0.19 ± 0.66 µm/min) and mosaic (0.22 ± 0.68 µm/min) conditions move at approximately half the speed of control nuclei (0.48 ± 0.72 µm/min) (Figure 2.10 F). Together, these results demonstrate that Lamin A overexpression prolongs apical nuclear migration by reducing both the speed and directionality of nuclear movement.

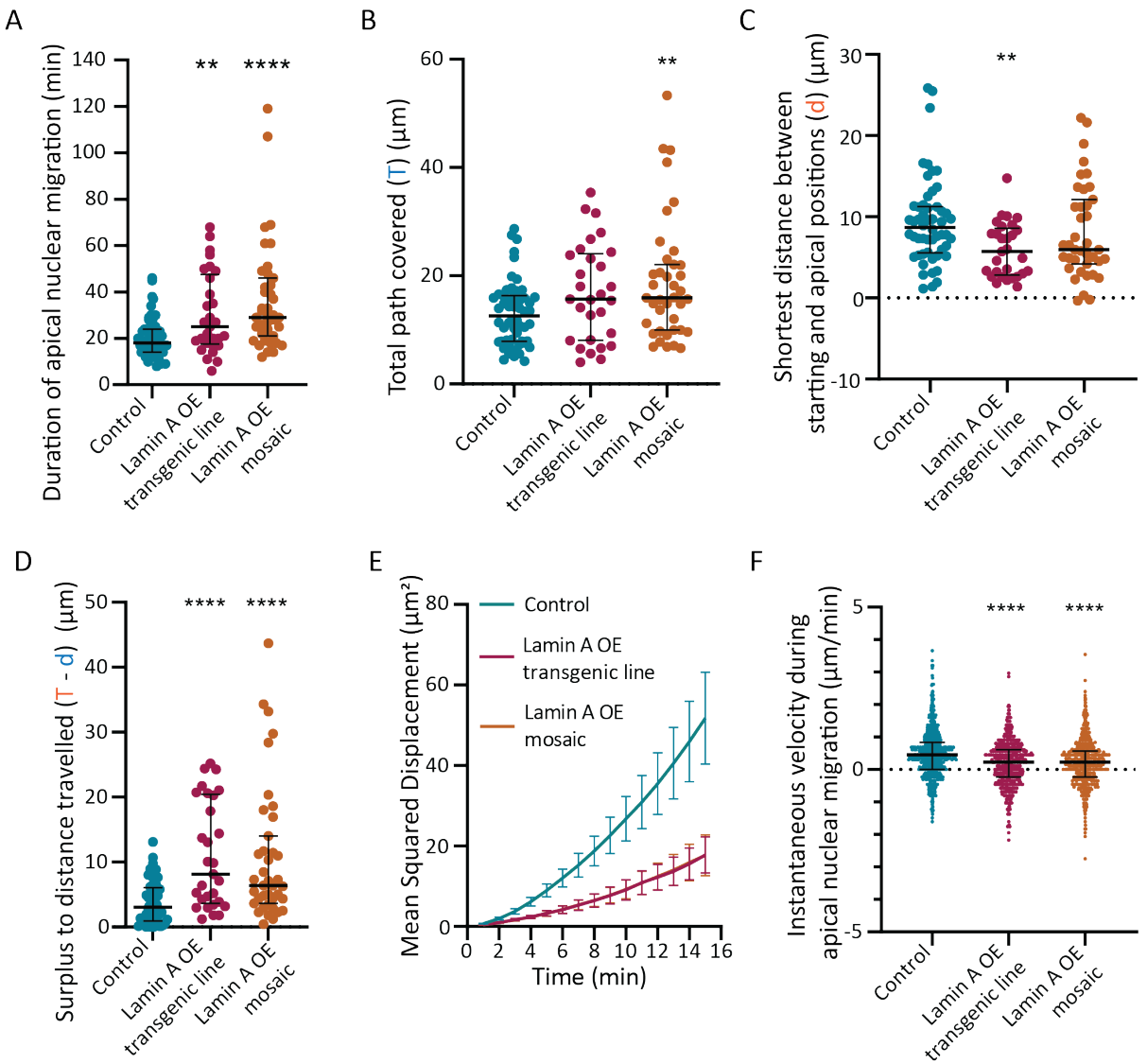

Figure 2. 10 Quantifications of apical nuclear migration showing the Lamin A overexpressing nuclei are less directly and slower:

(A) Duration (in minutes) of apical nuclear migration, defined as the time between G2 onset and the time nuclei reach the apical side ($p_{\text{Lamin A OE transgenic line}} = 0.008$, $p_{\text{Lamin A OE mosaic}} < 0.001$, Mann-Whitney test). Error bars: median with interquartile range. (B) Total path covered during apical nuclear migration (T). (T: $p_{\text{Lamin A OE transgenic line}} = 0.0720$, $p_{\text{Lamin A OE mosaic}} = 0.0096$, Mann-Whitney test). (C) Shortest distance between starting and division positions (d). (d: $p_{\text{Lamin A OE transgenic line}} = 0.0020$, $p_{\text{Lamin A OE mosaic}} = 0.1566$, Mann-Whitney test). (D) Surplus traveled distance corresponding to the difference between the total path covered (T) and the shortest distance between starting point and apical position (d). ($p_{\text{Lamin A OE transgenic line}} < 0.001$, $p_{\text{Lamin A OE mosaic}} < 0.001$, Mann-Whitney test). Error bars: median with interquartile range. (E) Mean squared displacement (MSD) analysis in control (cyan), lamin A OE in the transgenic line (magenta), and lamin A in the mosaic condition (orange). Note that MSD curves for lamin A OE transgenic line and lamin A OE mosaic condition mainly overlap. Error bars: mean and SEM. (F) Instantaneous velocities during apical nuclear migration. (Instantaneous velocities: $p_{\text{Lamin A OE transgenic line}} < 0.0001$, $p_{\text{Lamin A OE mosaic}} < 0.0001$, Mann-Whitney test). Error bars: Median with interquartile range.

2.9 Lamin A-overexpressing does not interfere with cytoskeleton arrangements

(The work presented in this section is part of Maria Gorjão's master thesis. I co-supervised Maria's thesis and collaborated with her on performing the injection and imaging experiments.)

The findings of this study suggest that Lamin A overexpression specifically interferes with nuclear positioning during active migration. In contrast, passive and random nuclear movements along the apical-basal axis are not affected by Lamin A overexpression.

Nuclear active movement and positioning rely on the transmission of forces between the cytoskeleton and the nucleus. LMNA mutations have been linked to disruptions in the organization of cytoskeletal components, including microtubules and actin, particularly in mechanically active tissues like cardiac muscle. In the zebrafish retina, while nuclei are surrounded by a microtubule network, actomyosin is the primary driver of nuclear apical migration through a formin-dependent pushing mechanism. Given these connections, I aimed to investigate whether Lamin A overexpression disrupts the organization of the cytoskeleton, potentially impairing the transmission of forces necessary for nuclear movement and positioning.

To investigate whether the observed migration defects were associated with cytoskeletal rearrangements, I labeled microtubules using the βactin:EGFP-DCX DNA construct, which labels doublecortin (DCX), a microtubule-associated protein. I then analyzed the distribution of microtubules in control and Lamin A OE mosaic cells. Confocal imaging revealed that microtubules were evenly distributed along the entire apico-basal axis, forming a cage-like structure around the nucleus (Norden et al., 2009) in both conditions, regardless of nuclear positioning (Figure 2.11 A and B). This indicates that Lamin A overexpression does not alter microtubule organisation.

We then examined whether actin structures were affected by Lamin A overexpression. Previous studies have shown that an actin "cloud" forms beneath nuclei migrating apically, generating a formin-dependent pushing force essential for nuclear movement (Yanakieva et al., 2019). To visualise this structure, we used an actin-chromobody under a β-actin constitutive promoter in control and Lamin A OE mosaic cells. Lightsheet microscopy time-lapse images revealed the presence of an active actin cloud beneath apically migrating nuclei

in both conditions (Figure 2.11 C and D). These findings demonstrate that Lamin A overexpression does not disrupt the primary actin-driven mechanism responsible for apical nuclear migration.

Overall, the similar organisation of microtubule and actin structures between control and Lamin A-overexpressing cells suggests that cytoskeletal arrangements do not account for the differences observed in nuclear migration.

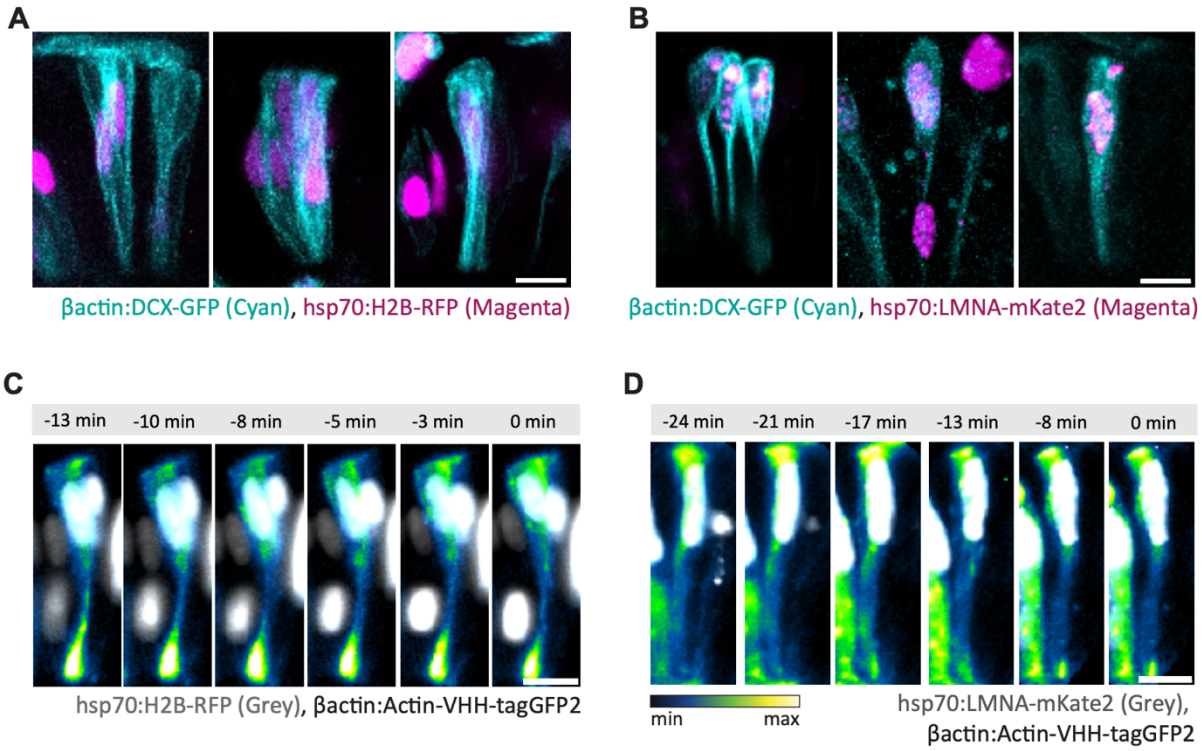

Figure 2. 11 Lamin A overexpression does not interfere with cytoskeletal organization:

(A-B) Microtubule distribution in control and Lamin A OE mosaic cells. βactin:DCX-GFP labels microtubules (cyan), which extend along the entire apico-basal axis in both control (A) and Lamin A OE mosaic (B) cells. Control (hsp70:H2B-GFP) and Lamin A OE mosaic nuclei are shown in magenta. Scale bar: 10 µm. (C-D) Actin dynamics during apical nuclear migration. βactin:Actin-VHH-tagGFP2 labels actin organization during nuclear movements before nuclei reach the apical surface, at t = 0 min. Time-lapse images show actin accumulation beneath nuclei in both control (C) and Lamin A OE mosaic (D) cells. The lookup table represents the minimum and maximum actin expression intensities. Control (hsp70:H2B-GFP) and Lamin A OE mosaic nuclei are shown in gray. Scale bar: 10 µm.

2.10 Reduced nuclear deformability is associated with defects in apical nuclear migration in Lamin A-overexpressing nuclei

(The work presented in this section is part of Maria Gorjão's master thesis. I co-supervised Maria's thesis and collaborated with her on performing the injection and imaging experiments. 3D analysis was done in collaboration with Dr. Anna Erzberger and Dr. Roman Belousov.)

Another possible explanation for the defects in apical nuclear migration is the increased nuclear stiffness caused by Lamin A overexpression. In the densely packed environment of the neuroepithelium, where nuclei frequently undergo deformation, we hypothesized that nuclear deformability may be important for efficient migration through these confined spaces.

To investigate a potential link between nuclear deformability and apical migration, individual nuclei—either control or Lamin A OE line—were labeled using the nuclear envelope marker EGFP-Lap2b. 3D nuclear segmentations were then performed to measure changes in nuclear surface during apical migration. As previously described in figure 2.2 E and F for S phase, the root mean squared deviations (RMSD) of nuclei's surface was calculated from a perfect ellipsoid, as a proxy for nuclear deformability (scheme in figure 2.12 A).

Control nuclei undergo the most pronounced shape changes during apical nuclear migration, as reflected by the increase in RMSD standard deviations from S phase (0.21 ± 0.07 µm) to G2 phase (0.35 ± 0.03 µm) (Figure 2.12 B and C). This suggests that nuclear deformations in control cells facilitate apical migration. If this was the case, Lamin A OE nuclei—for which migration is impaired—would be expected to exhibit reduced nuclear deformations compared to controls. Indeed, in the Lamin A OE condition, nuclear deformations during G2 (0.15 ± 0.09 µm) do not significantly increase compared to S phase (0.08 ± 0.03 µm) and remain consistently lower than those observed in control nuclei (0.21 ± 0.07 µm in S phase; 0.35 ± 0.03 µm in G2 phase) (Figure 2.12 C).

This result correlates defects in apical migration to increased nuclear stiffness and reduced nuclear deformability, strongly suggesting that altered nuclear properties impair apical nuclear migration in the zebrafish retina.

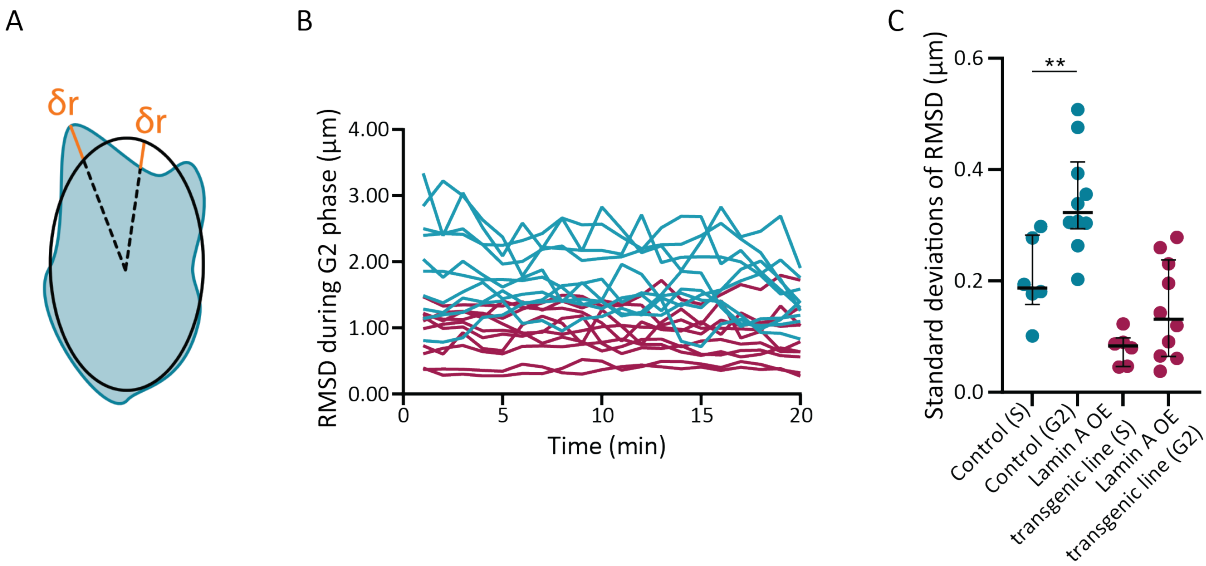

Figure 2. 12 Quantification of nuclear deformability showing reduced nuclear deformations when apical migration is impaired:

(A) Schematic representation of Root Mean Squared Deviations (RMSD) analysis, illustrating that nuclear deformability was quantified by measuring the deviation (δr) between the actual nuclear surface and its idealized ellipsoid shape. (B) Trajectories of Root Mean Squared Displacement (RMSD) for individual nuclei during apical nuclear migration in control (cyan) and Lamin A OE transgenic (magenta) conditions. (C) Comparison of the standard deviations of RMSD trajectories during G2 phase relative to S phase ($p_{control}$ = 0.003, $p_{Lamin\ A\ OE\ line}$ = 0.147, Mann-Whitney test). Error bars represent the median with interquartile range.

2.11 Effects of Lamin A overexpression are less pronounced in the looser packed hindbrain

(In this section, DNA plasmid injection and the live imaging experiments were done together with Juliette Gouhier, under the scope of her master's internship)

Thus far, we have shown that apical nuclear migration in the zebrafish retina is slower and less efficient when the migrating nucleus overexpresses Lamin A. Our findings suggest that this defect is linked to impaired nuclear deformability, indicating that nuclear deformations play a key role in facilitating nuclear positioning within the densely packed retinal tissue. We hypothesize that such deformations are necessary for nuclei to squeeze through narrow spaces and navigate past neighbouring nuclei. In contrast, in more loosely packed epithelia, nuclei are likely to encounter fewer obstacles during migration and may therefore rely less on deformation to reach the apical surface. The hindbrain, a pseudostratified cuboidal

neuroepithelium located between the retinas, has recently been characterized as less densely

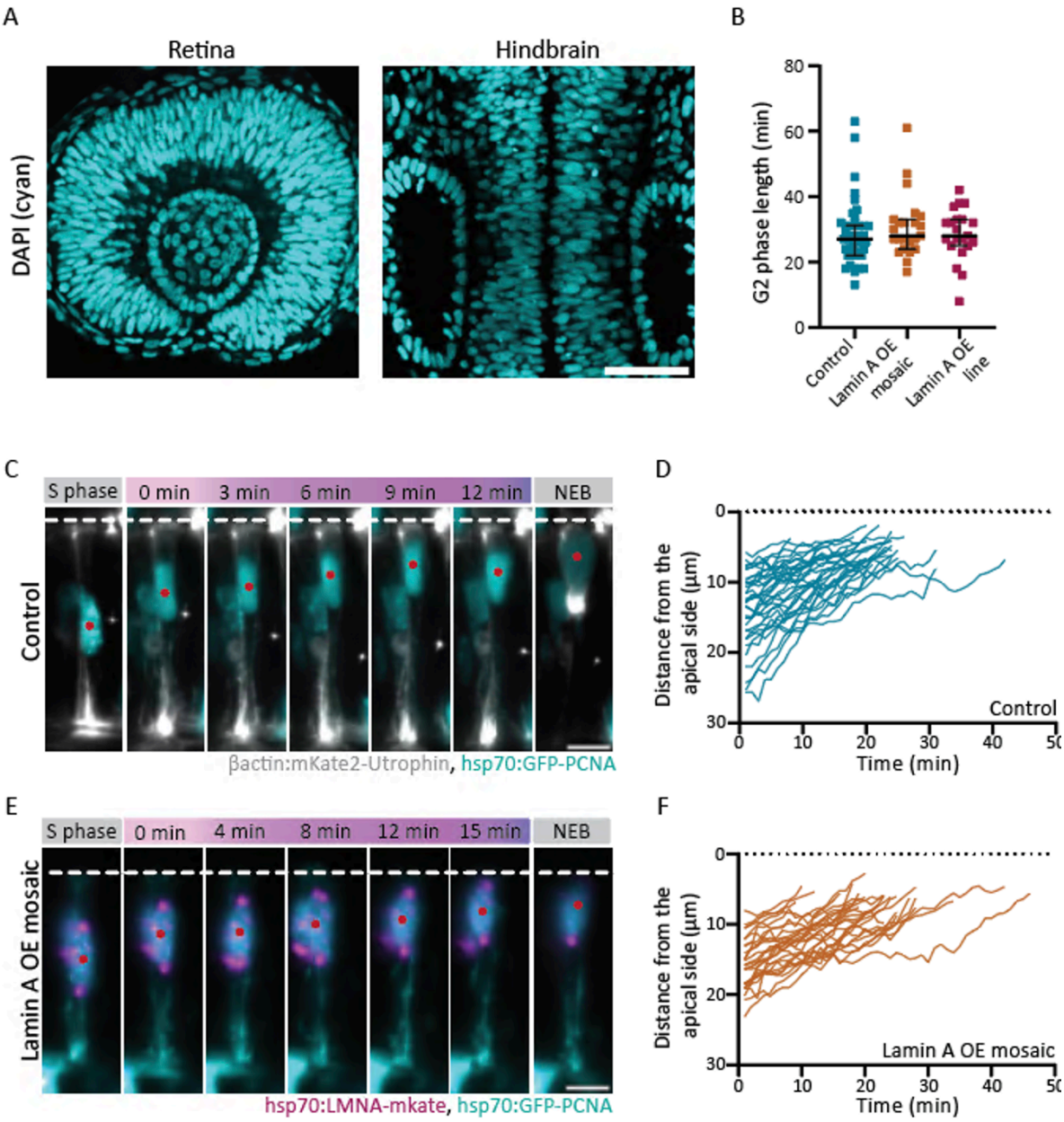

Figure 2. 13 G2 phase length and nuclear apical migration in the less packed hindbrain:

(A) DAPI staining of a retina (left image) and a hindbrain (right image) showing that retinal nuclei are more densely packed. Scale bar: 50µm. (B) G2 phase length in minutes *($p_{Lamin\ A\ OE\ mosaic} = 0.2633$, $p_{Lamin\ A\ OE\ line} = 0.4144$, Mann-Whitney test)* (C and E) Example montages of apical nuclear movements in control (C) and lamin A OE mosaic (E) hindbrain neuroepithelia. Red dots indicate the nucleus followed. Dashed line corresponds to the apical surface. Gradient bar from pink to purple indicates the time of apical nuclear migration, where darker colors represent longer time spans. hsp70:PCNA-GFP labels nuclei depending on cell cycle stage (cyan), hsp70:LmnA-mKate2 labels nuclei overexpressing lamin A (magenta). NEB, nuclear envelope breakdown. Scale bar: 10 mm. (D and F) Apical migration trajectories for control nuclei (D, cyan) and Lamin A OE mosaic (F, orange). Dashed line corresponds to the apical surface.

packed, with fewer nuclei per unit volume (Ferme et al., 2024; Kim et al., 2024), making it a suitable model to test this hypothesis.

Thus, we overexpressed Lamin A in the less densely packed hindbrain (Ferme et al., 2024; Kim et al., 2024) (Figure 2.13 A) and analysed cell cycle dynamics, nuclear migration and deformation as previously done in the retina (Figures 2.9, 2.10, and 2.12). We imaged hindbrains during a time window in which little neurogenesis occurs and the tissue is predominantly proliferative—between 18 and 22 hours post-fertilisation (hpf).

We first asked whether Lamin A overexpression influences cell cycle dynamics in the hindbrain. We focused specifically on the duration of G2 phase, as this phase was previously found to elongate by approximately 40–50% when Lamin A was overexpressed in the retina (Figure 2.5 F). In control hindbrain cells, G2 lasted an average of 28.50 ± 9.93 minutes. Nuclei overexpressing Lamin A showed similar durations—28.43 ± 9.97 minutes in the line condition and 30.61 ± 9.52 minutes in the mosaic condition (Figure 2.13 B). These results indicate that, unlike in the retina (Figure 2.5 F), Lamin A overexpression does not affect G2 duration in the hindbrain. This supports the idea that the impact of Lamin A on G2 progression is tissue-dependent.

Light-sheet microscopy movies showed that nuclei in the hindbrain moved in a similar way in both control cells (Figure 2.13 A and B) and Lamin A-overexpressing mosaic cells (Figure 2.13 C and D). Quantification of nuclear positioning during apical nuclear migration—from the onset of G2 until nuclei reached the apical surface—showed that control nuclei took an average of 20.29 ± 6.819 min, while Lamin A-overexpressing mosaic nuclei took 22.04 ± 5.788 min (Figure 2.14 A). The surplus travel distance was approximately 4 µm in both conditions (Figure 2.14 A), and the mean squared displacement (MSD) curves largely overlapped (Figure 2.14 B). This suggests that nuclei migrate in a directed manner towards the apical surface, independent of Lamin A expression levels.

Furthermore, root mean squared displacement (RMSD) analysis showed no statistically significant differences between S and G2 phases in control hindbrain nuclei (Figure 2.14 D – F), suggesting that nuclear deformability is less critical for active nuclear positioning in this less packed environment. The RMSD values were also similar between S and G2 phases for the Lamin A OE mosaic condition (Figure 2.14 D).

Together, these results suggest that it is not Lamin A overexpression per se, but the resulting change in nuclear material properties, that influences nuclear movement, with

nuclear deformability playing a key role in apical nuclear migration depending on the packing density in the neuroepithelium.

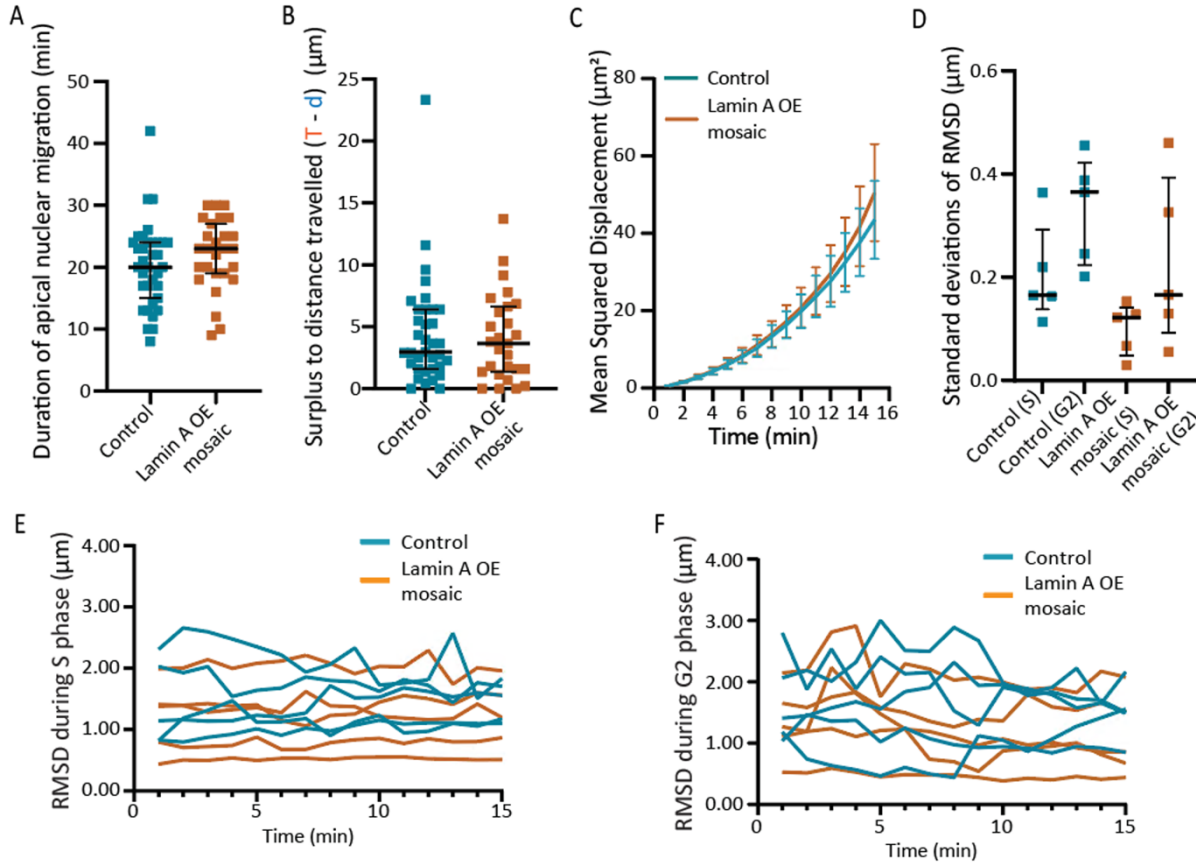

Figure 2. 14 Lamin A overexpression shows less pronounced effects on apical nuclear migration in the hindbrain neuroepithelium:

(A) Duration (in minutes) of apical nuclear migration, defined as the time between G2 onset and the time nuclei reach the apical side (p Lamin A OE mosaic = 0.1859, Mann-Whitney test). Error bars: median with interquartile range. (B) Surplus traveled distance corresponding to the difference between the total path covered (T) and the shortest distance between starting point and apical position (d) (p Lamin A OE mosaic = 0.8740, Mann-Whitney test). Error bars: median with interquartile range. (C) MSD analysis in control (cyan) and lamin A in the mosaic condition (orange). Error bars: mean and SEM. (D) Plot of the Standard Deviations (SDs) of the RMSD trajectories during G2 phase compared with S phase (pcontrol = 0.0556, pLamin A OE mosaic = 0.1508, Mann-Whitney test). (E,F) Control (cyan) and Lamin A OE mosaic (orange) trajectories of the Root Mean Squared Displacement (RMSD) for each nucleus followed during S-phase (E) and apical nuclear migration (F). Error bars: median with interquartile range.

2.12 Increased nuclear stiffness impairs apical nuclear migration in a non-cell autonomous manner

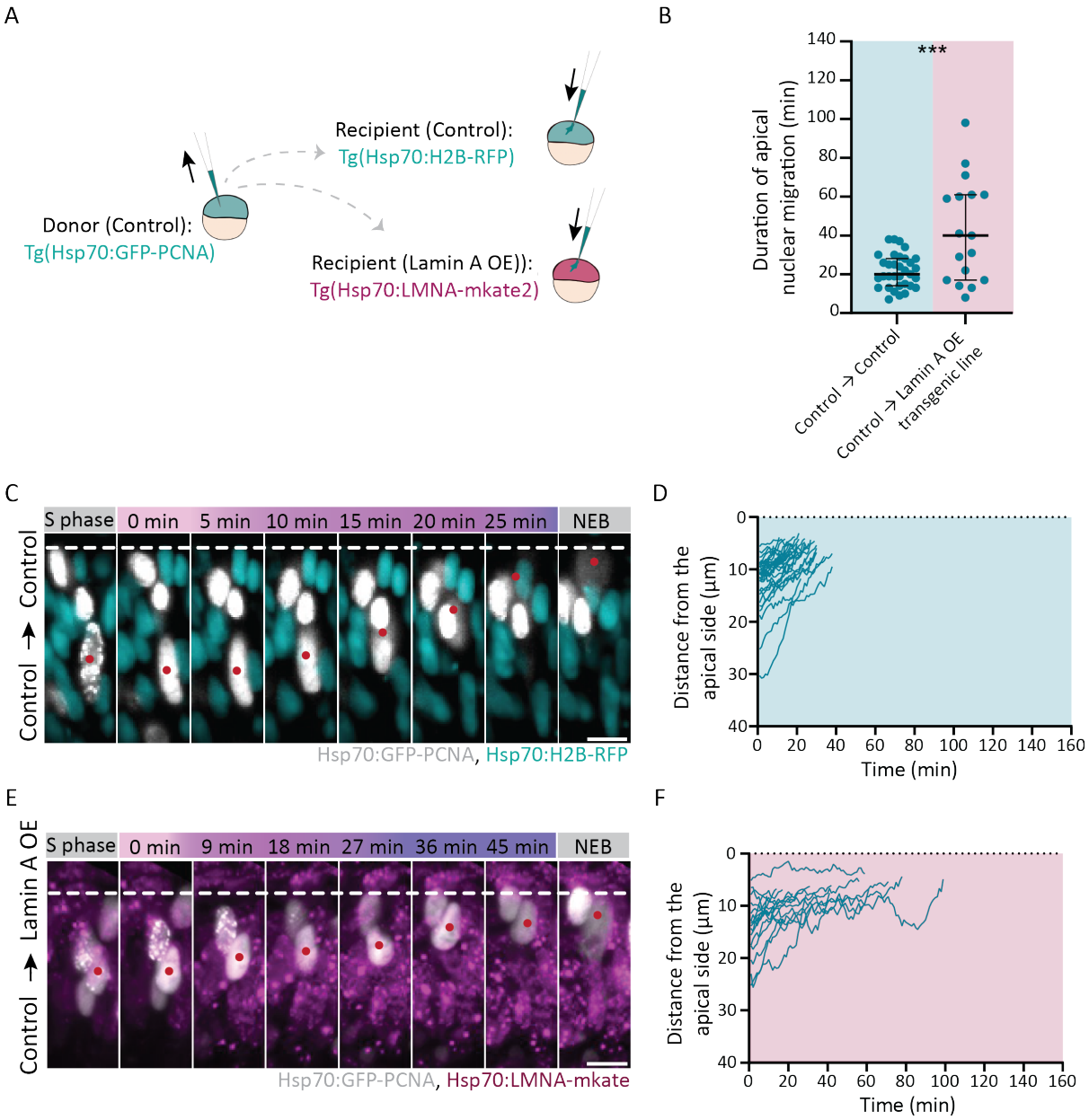

Figure 2. 15 Lamin A overexpression in the environment affects apical nuclear migration of control nuclei:

(A) Schematic of the transplantation experiment: cells from control Tg(ß-actin:PCNA-GFP) blastulas were transplanted into either control Tg(hsp70:H2B-RFP) or Lamin A OE Tg(hsp70:LMNA-mKate2) blastulas. (B) Quantification of apical nuclear migration duration (min), measured as the time from G2 onset to nuclear arrival at the apical surface p $_{Duration\ of\ Apical\ Migration}$ = 0.003, Mann-Whitney test). Error bars represent medians with interquartile range. (C, E) Representative time-lapse montages of apical nuclear migration in control cells transplanted into either control (C) or Lamin A OE transgenic (E) blastulas. The tracked nucleus is marked with a red dot. The dashed line indicates the apical surface. A gradient bar from pink to purple represents the duration of apical nuclear migration, with

darker shades indicating longer times. Transplanted nuclei are labeled with β-actin:PCNA-GFP (gray), while surrounding nuclei are labeled with hsp70:H2B-RFP (cyan) and hsp70:LmnA-mKate2 (magenta). NEB, nuclear envelope breakdown. Scale bar: 10 µm. (D, F) Apical nuclear migration trajectories for control cells transplanted into either control (D) or Lamin A OE transgenic (F) environments. The dashed line marks the apical surface.

The milder effect of Lamin A overexpression in the less densely packed hindbrain suggests that nuclear deformability becomes less essential when physical constraints are reduced. In a looser environment with fewer nuclei per volume, there is more space available, and nuclei may migrate without needing to deform extensively. This observation led me to hypothesize that, in densely packed tissues like the retina, the mechanical properties of neighboring nuclei contribute to nuclear movement by shaping the surrounding physical environment. Therefore, I next tested whether nuclear migration in the densely packed retina is influenced not only by the deformability of the migrating nucleus but also by the mechanical properties of surrounding cells—highlighting a potential non-cell-autonomous component of this process.

To address this question, I investigated whether the stiffness of the surrounding retinal neuroepithelium influences the apical nuclear migration of control cells. To this end, I transplanted donor cells from a control blastula into either a control or a Lamin A-overexpressing recipient blastula (Figure 2.15 A). Using the same in vivo nuclear tracking protocol described previously (Figure 2.9, Figure 2.13, and Materials and Methods), I performed light-sheet imaging of zebrafish retinas generated through blastula cell transplantations. I then analysed the positioning of control nuclei within both control (Figure 2.15 C and D) and Lamin A-overexpressing (Figure 2.15 E and F) tissue environments. This experimental setup enabled me to explore the non-cell-autonomous effects of nuclear deformability on apical nuclear migration.

In a control neuroepithelium, nuclei of control cells migrated directly to the apical side, taking an average of 21.64 ± 8.536 min (Figure 2.15 B), consistent with the control condition in Figure 2.10 A (20.32 ± 8.386 min). This confirmed that the transplantation procedure itself does not affect apical nuclear migration. In contrast, control nuclei in a Lamin A-overexpressing environment took, on average, 42.29 ± 26.53 min to reach the apical side (Figure 2.15 B) — representing a ~95% increase in migration time. Analysis of the surplus travel distance showed that control nuclei migrated an additional 10 µm in a Lamin A-overexpressing tissue compared to controls in a normal environment (Figure 2.16 A-C). This corresponds to roughly a 200% increase in apical-basal back-and-forth movement, indicating that migration is less directed.

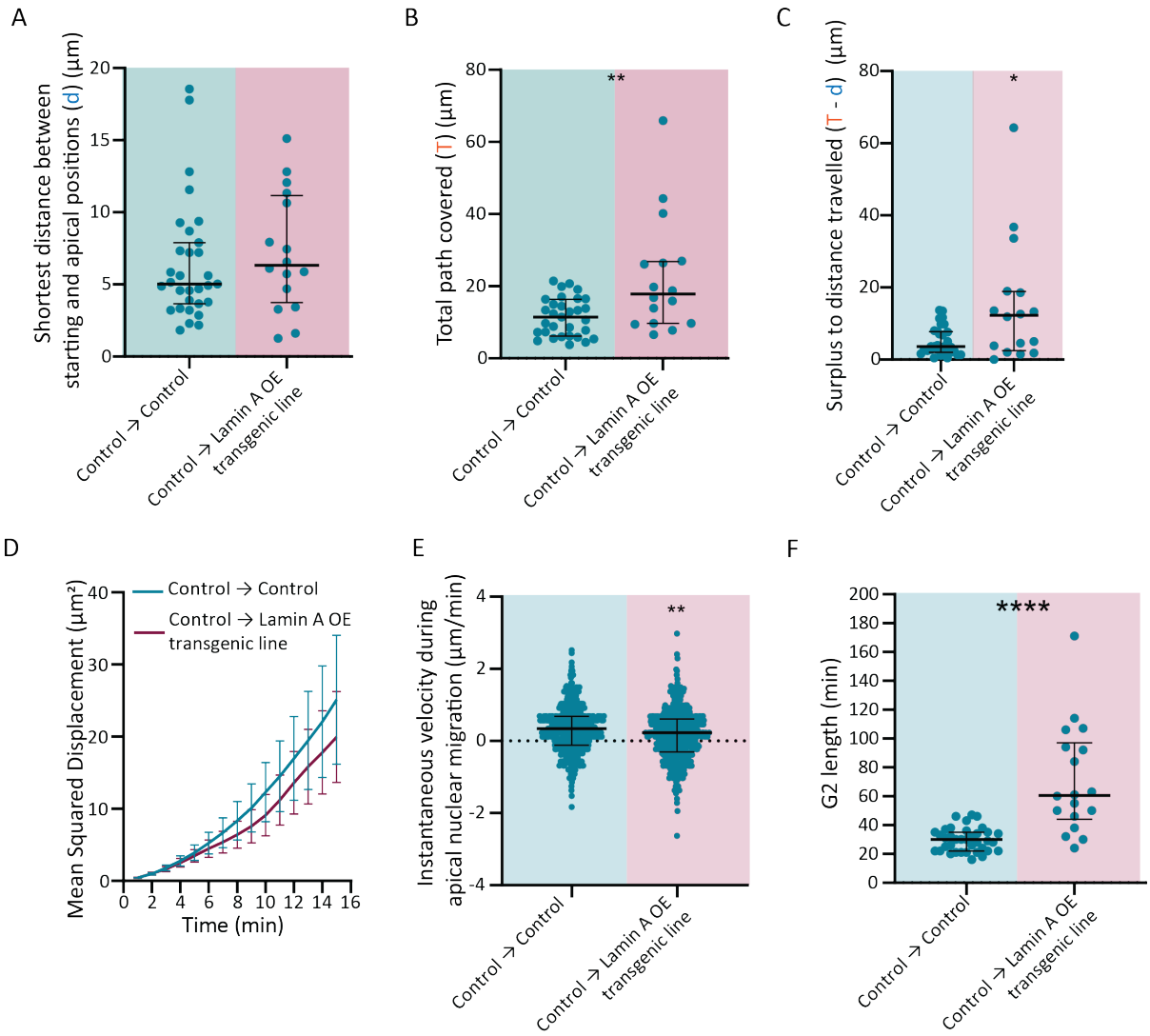

Figure 2. 16 Quantitative Analysis of Apical Migration in a Lamin A overexpressing environment:

(A) ***Shortest Distance (d):*** *The minimal linear distance between the starting position and the division site. Statistical significance:* ***p*** *= 0.3409 (Mann-Whitney test). (B)* ***Total Path (T):*** *The total trajectory covered by the nucleus during apical migration. Statistical significance:* ***p*** *= 0.0059 (Mann-Whitney test). (C)* ***Surplus Traveled Distance:*** *The excess distance traveled by the nucleus, calculated as the difference between the total path covered (T) and the shortest linear distance (d). Statistical significance (control → Lamin A OE transgenic line):* ***p*** *= 0.025 (Mann-Whitney test). Error bars represent the median with interquartile range. (D)* ***Mean Squared Displacement (MSD) Analysis:*** *MSD comparison of control cells transplanted into control environments (cyan) versus control cells transplanted into a Lamin A OE transgenic environment (magenta). Error bars represent the mean ± SEM. (E)* ***Instantaneous Velocities:*** *Measurement of nuclear migration speeds at different time points. Statistical significance:* ***p*** *= 0.0015 (Mann-Whitney test). (F)* ***G2-Phase Duration:*** *Quantification of G2-phase length (in minutes) for control nuclei transplanted into either a control or a Lamin A OE environment. Statistical significance:* ***p*** *< 0.001 (Mann-Whitney test). Error bars represent the median with interquartile range.*

This interpretation is further supported by the flatter slope of the MSD curve (Figure 2.16 D). In this stiffer environment, control nuclei migrate more slowly, showing average instantaneous velocities of 0.3071 ± 0.6236 µm/min in a control environment and 0.1801 ± 0.6792 µm/min in a Lamin A-overexpressing environment (Figure 2.16 E). Consistent with this delayed apical migration, I found that G2 phase—the period during which nuclei actively move toward the apical surface—lasts 70.94 ± 37.62 minutes in a Lamin A-overexpressing environment (Figure 2.16 F). Compared to a control environment, this represents a 40-minute extension, corresponding to a 133% increase in G2 duration.

Overall, these results demonstrate that the movement of control nuclei is impaired by increased nuclear stiffness in the surrounding tissue. This suggests that nuclear mechanical properties, at the tissue level, can influence nuclear behaviour in a non-cell-autonomous manner.

2.13 Increased nuclear, and therefore tissue, stiffness delays nuclear envelope breakdown and mitotic rounding

A 95% delay in apical nuclear migration alone is not sufficient to account for the 133% increase in G2 phase duration observed in control nuclei within a stiffer environment, compared to those in a control environment (Figure 2.15 C). It is possible that increased environmental stiffness affects not only nuclear migration but also other morphogenetic processes occurring during this phase that require space.

One such cellular event is mitotic rounding, which requires sufficient space to ensure proper spindle formation. Previous studies have shown that in isolated HeLa cells, confinement conditions can impair mitotic rounding, leading to delayed mitotic progression. Specifically, when cells are forced to deform in a stiffer hydrogel in order to round, mitotic rounding is delayed (Lancaster et al., 2013). Given that the zebrafish retina is a highly confined environment and Lamin A overexpression increases nuclear stiffness across the tissue, I hypothesised that this elevated stiffness could impair mitotic rounding.

To test this hypothesis in the zebrafish retina, I quantified the time nuclei spent at the apical side before undergoing nuclear envelope breakdown (NEB) (Figure 2.17 A and B). First, I observed that when Lamin A was overexpressed in the migrating nuclei themselves, NEB timing remained similar to control conditions (7.947 ± 5.935 min in controls and 9.513 ± 14.30 min in

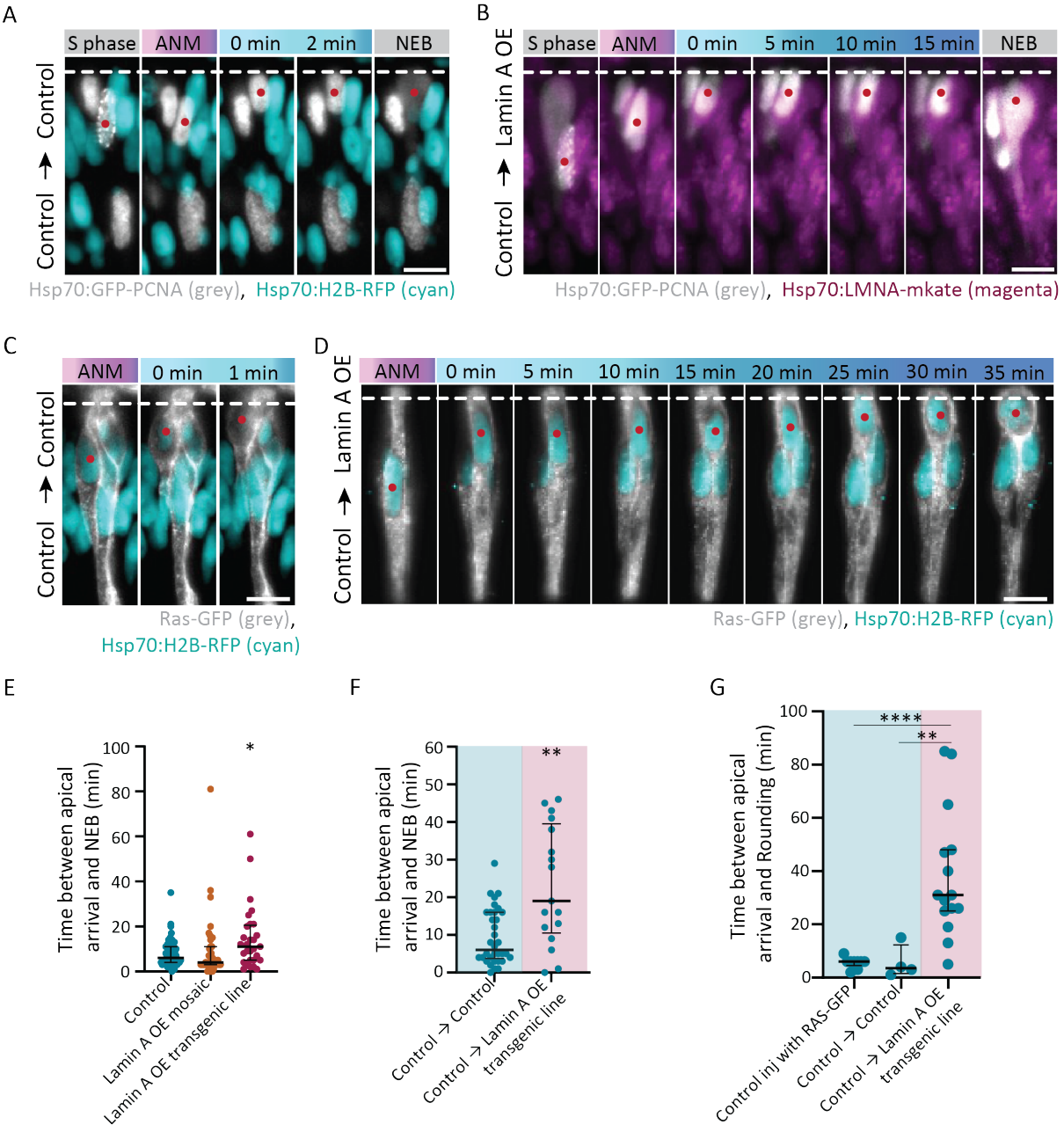

Figure 2. 17 Lamin A Overexpression in the Environment Affects NEB Timing and Mitotic Rounding:

(A, B) Time-lapse montages showing NEB in control cells transplanted into either a control (A) or Lamin A OE (B) environment. Red dots indicate the tracked nucleus, with time 0 min marking its arrival at the apical surface. The blue bar represents the duration nuclei remain at the apical surface before undergoing NEB, with darker shades indicating longer durations. The dashed line marks the apical surface. Transplanted nuclei are labeled with β-actin:PCNA-GFP (gray), while surrounding nuclei are labeled with hsp70:H2B-RFP (cyan) and hsp70:LMNA-mKate2 (magenta). NEB, nuclear envelope breakdown; ANM, apical nuclear migration. Scale bar: 10 µm. (C, D) Time-lapse montages showing mitotic rounding in control cells transplanted into either a control (C) or Lamin A OE (D) environment. Red dots track the nucleus upon reaching the apical surface. The dashed line marks the apical surface. Transplanted nuclei and plasma membranes are labeled with hsp70:H2B-RFP (cyan) and RAS-GFP (gray), respectively. In Lamin A OE conditions, surrounding nuclei are labeled with hsp70:LMNA-mKate2, though this labeling is not visible in the montage. Scale bar: 10 µm. (E, F)

Quantification of the time (in minutes) from apical arrival to NEB in control, Lamin A OE mosaic, and Lamin A OE transgenic conditions (E), as well as in control cells transplanted into either a control or Lamin A OE environment (F). Statistical significance: p (Lamin A OE mosaic) = 0.2386, p (Lamin A OE transgenic line) = 0.0282, p (control → Lamin A OE line) = 0.0027 (Mann-Whitney test). (G) Quantification of the time (in minutes) from apical arrival to mitotic rounding onset. Statistical significance: p (control → Lamin A OE line) < 0.0001, p (control → control) = 0.0021 (Mann-Whitney test). Error bars represent the median with interquartile range.

the Lamin A OE mosaic condition) (Figure 2.17 E), suggesting that Lamin A overexpression per se does not directly affect NEB. Interestingly, in the Lamin A OE transgenic line, where stiffness increased tissue-wide, nuclei took slightly longer than controls to undergo NEB (14.55 ± 14.02 min) (Figure 2.17 E). These results indicate that while Lamin A does not directly affect NEB in a cell-autonomous manner, it may exert a non-cell-autonomous influence.

To explore this non-cell autonomous effect, I quantified the time nuclei spent apically before NEB in the transplantation experiments described in Figure 2.15. I observed that in a control environment, control nuclei took an average of 9.412 ± 7.370 min to undergo NEB (Figure 2.17 A and F). In contrast, in a Lamin A-overexpressing environment, control nuclei remained at the apical side for an average of 23.24 ± 15.71 min before NEB (Figure 2.16 B and F). This corresponds to an approximately 150% increase in time that control nuclei spent at the apical surface before NEB when surrounded by less deformable Lamin A-overexpressing nuclei (Figure 2.17 F).

Next, I sought to confirm whether the delay in NEB corresponded to a delayed mitotic rounding, as initially hypothesised. To this end, I transplanted donor cells from a Tg(ßactin:HRAS-EGFP) zebrafish blastula into either control (Figure 2.17 C) or Tg(hsp70l:lmna-mKate2) (Figure 2.17 D) recipient blastulas. The HRAS-EGFP labelling enabled visualisation of the plasma membrane which allows the visualisation of the cell rounding. Additionally, as a control, I used microinjection of RAS-GFP mRNA at the one-cell stage.

Live imaging and following analysis of the cell membrane showed that control cells required, on average, 33 minutes longer to undergo mitotic rounding in a stiffer environment. While control cells in a control environment rounded in 5.75 ± 6.29 minutes, those in the Lamin A OE line took 38.27 ± 23.83 minutes (Figure 2.17 G), representing a 665% delay in mitotic progression. These findings in the developing retinal neuroepithelium suggest that nuclear mechanics—and, by extension, tissue mechanical properties—can influence key cellular and developmental processes, such as nuclear envelope breakdown and mitotic rounding.

Together, the results of this study demonstrate that nuclear deformability—modulated by Lamin A expression—shapes key biological processes during organ development. By directly influencing nuclear migration and mitotic progression, nuclear mechanics emerge as a central force driving successful organogenesis.

3. Discussion

This study reveals that nuclear stiffness—modulated by Lamin A/C expression—can hinder efficient apical nuclear migration through the crowded zebrafish retina. These migration defects were reduced in the less densely packed hindbrain, highlighting the importance of tissue context, such as nuclear packing density, in shaping nuclear behaviour. Remarkably, increasing nuclear stiffness tissue-wide was sufficient to impair nuclear positioning and mitotic entry in control cells, revealing a non-cell-autonomous role for nuclear material properties in driving epithelial dynamics. Together, these findings underscore nuclear deformability as a key material property essential for successful organogenesis (Figure 3.1).

Figure 3. 1 Nuclear deformability facilitates apical nuclear migration in the zebrafish retina:

Apical mitosis is the ultimate goal of apical nuclear migration. In the densely packed retinal epithelium, nuclei overexpressing Lamin A are less deformable and struggle to navigate through the confined space, whereas more deformable control nuclei migrate efficiently and directly to the apical side. (This graphical abstract was designed by Maria Gorjão under the scope of her master thesis.) ***(Adapted from Maia-Gil et al., 2024).***

3.1 Linking nuclear material properties and migration within the context of a developing tissue

3.1.1 The relevance of nuclear deformability for nuclear positioning depends on the tissue context

My experiments revealed a link between nuclear deformability, regulated by Lamin A expression, and nuclear positioning in the densely packed zebrafish retinal neuroepithelium. Nuclei overexpressing Lamin A were less deformable (Figure 2.2 D-F and Figure 2.4 E) and showed impaired positioning in this highly confined tissue environment (Figure 2.9 A-F. and 2.10 A-F). These findings are in line with previous studies showing that high Lamin A/C expression correlates with reduced migratory efficiency in cells navigating confined environments, such as narrow microchannels (Bell et al., 2022; Davidson et al., 2014; Harada et al., 2014; Lomakin et al., 2020; McGregor et al., 2016). This relationship has gained attention particularly in cancer biology, where low Lamin A/C levels are associated with enhanced metastatic capacity (Urciuoli et al., 2021). in understanding cell migration came with the transition from 2D to 3D in vitro models, which more accurately capture the physically constraints encountered in vivo. These studies demonstrated that 3D confinement can modulate the forces acting on migrating cells and their nuclei (Calero-Cuenca et al., 2018; Friedl et al., 2011; Yamada and Sixt, 2019). While these systems highlight the importance of the 3D physical context, much remains to be explored about how nuclear mechanics influence cellular behaviour in the dynamic and spatially complex environment of a developing tissue.

Evidence bridging this gap came from studies of myofiber development, where Lamin A overexpression increased nuclear stiffness and disrupted nuclear migration to the periphery of the muscle fibre—a process that normally relies on guidance by myofibril-generated forces within a confined cytoplasmic space (Roman et al., 2017). This study demonstrated that, in a

developing tissue, nuclear stiffness can act as a barrier to efficient positioning. My findings in the zebrafish retina support this concept: Lamin A overexpression impaired apical nuclear migration specifically in the densely packed retinal tissue—where spatial constraints are more severe—while having only a minor effect in the more loosely packed hindbrain. By quantifying nuclear deformations, we established a link between nuclear deformability and efficient nuclear movement within densely packed epithelia. Nuclei in the retinal neuroepithelium exhibited more pronounced deformations during apical migration compared to stochastic movements along the apical-basal axis, whereas this increase in deformation was not observed in the more loosely packed hindbrain. This suggests that nuclei must squeeze through limited intercellular space in order to move within densely packed epithelia. It is therefore possible that enhanced nuclear deformability represents an adaptation that ensures efficient nuclear movement as tissues become increasingly crowded during development.

Importantly, these results indicate that the influence of nuclear material properties on positioning is not solely intrinsic to the nucleus, but also emerges from its physical context within the tissue. Unlike static 3D in vitro microchannels (Bell et al., 2022; Davidson et al., 2014; Lammerding et al., 2006; McGregor et al., 2016), developing tissues are dynamic, with physical properties such as nuclear density and intercellular space changing over time (Matejčić et al., 2018; Norden, 2017; Strzyz et al., 2016). Our data suggest that the extent of nuclear packing determines whether nuclear stiffness becomes a limiting factor for nuclear positioning. As neuroepithelia mature and become more crowded, nuclear deformability likely becomes increasingly critical for timely and efficient positioning. In this context, it is conceivable that later in development, as for example during neuronal lamination when nuclear packing approaches its theoretical limit, soma translocation and neuronal migration to their final positions rely, at least in part, on nuclear deformability. Yet, the role of nuclear material properties in neuronal lamination has thus far been only modestly investigated (Amini et al., 2022a).

3.1.2 Nuclear deformability tissue-wide facilitate nuclear positioning and mitotic entry

Our results, showing that Lamin A overexpression hinders apical nuclear migration depending on tissue confinement, raise the possibility that other tissue properties may also influence the effect of Lamin A on nuclear positioning.

In vitro studies have shown that substrate stiffness can impair mitotic rounding. To round up, cells must deform their surroundings to create sufficient space. In softer gels, this is achieved more easily as the environment yields; in contrast, stiffer gels resist deformation, making rounding more difficult (Lancaster et al., 2013). These observations suggest that the ability to deform the surrounding environment is a prerequisite for efficient mitotic rounding. Consistent with this, our data from the zebrafish retina show that mitotic rounding of control cells was delayed in a tissue-wide stiffer environment. This indicates that the increased resistance of a stiffer tissue may hinder mitotic entry by limiting the space needed for cell rounding. Interestingly, in the Lamin A-overexpressing line, where intrinsically stiff nuclei are surrounded by similarly stiff neighbouring nuclei, this delay in mitotic rounding was less pronounced. This suggests that increased nuclear stiffness may facilitate mitotic rounding in a stiffer environment, pointing to a potential interplay between nuclear and tissue mechanical properties. It is therefore possible that the forces driving mitotic rounding are modulated, at least in part, by the intrinsic material properties of the nucleus. How this communication between nuclear stiffness and cell rounding is mechanistically coordinated remains unknown.

As overall tissue stiffness limits the space needed for cellular rounding, it may also constrain other space-dependent processes, such as nuclear positioning within densely packed epithelia. Our results show that apical nuclear migration in control cells is disrupted when Lamin A is overexpressed tissue-wide in the zebrafish retina, leading to an overall stiffer tissue environment. This suggests that even deformable nuclei may struggle to migrate apically if the surrounding tissue resists deformation, highlighting the importance of a permissive mechanical environment for efficient nuclear positioning.

In contrast to the less pronounced delay in mitotic rounding observed in the Lamin A overexpression (OE) line, where stiff nuclei migrate within a stiffer environment, apical nuclear migration is brutally impaired. One possible explanation is that nuclear deformability, while not essential for mitotic rounding in a cell-autonomous manner (as cells round and nuclear envelope breakdown) with similar timing regardless of Lamin A levels), is more critical for apical migration. As discussed above, deformability enables nuclei to squeeze through densely packed tissue. In the Lamin A OE line, although stiffer nuclei may generate greater force to

deform their surroundings, their limited ability to deform themselves restricts their movement through confined spaces. As a result, we do not observe a reduced migration delay, despite their increased potential to deform neighbouring nuclei. This suggests that effective nuclear migration relies on a balance between the deformability of the migrating nucleus and that of the surrounding tissue.

If nuclear deformability facilitates apical migration both by enabling the nucleus to squeeze through tight spaces and by allowing it to deform neighbouring nuclei to create space, one would expect that impairing both (by increasing stiffness in both migrating and surrounding nuclei, as in the OE line) would produce a stronger migration defect than in the mosaic condition, where only the migrating nucleus is stiff. Surprisingly, however, apical migration is similarly delayed in both conditions. This lack of an additive effect suggests that nuclear positioning is not governed by a simple sum of cell-autonomous and non-cell-autonomous mechanical properties. Instead, it points to a more complex interplay where 'the whole is more than the sum of its parts' and highlights that much remains to be understood about how nuclear and tissue material properties are integrated during nuclear positioning and organ development.

3.1.3 Nuclear deformability can influence the material properties of pseudostratified epithelia

Our results showing that tissue-wide Lamin A overexpression in the pseudostratified retina increases overall tissue stiffness suggest that the material properties of a pseudostratified epithelium can, at least in part, be influenced by the material properties of its nuclei. It would therefore be interesting to investigate whether this relationship also applies to other pseudostratified epithelia, such as the zebrafish hindbrain or Drosophila imaginal discs. One hypothesis is that in tissues where nuclei occupy a large fraction of the cell volume, nuclear stiffness may substantially contribute to overall tissue stiffness. To test this, it will be important to examine how nuclear and tissue stiffness correlate across epithelia with distinct spatial organizations and varying nucleus-to-cytoplasm ratios.

Our work not only expands our understanding of nuclear deformability in vivo but also establishes a model system to study how nuclear properties influence broader biological

properties and processes. It introduces a novel method to quantify nuclear shape changes in 3D directly from imaging data—an advancement that enables a more precise assessment of nuclear material properties in complex, dynamic environments (Figure X). This approach can serve as a powerful tool to investigate nuclear deformability across different tissue types.

Overall, our study suggests that the levels of Lamin A/C expression, which determine nuclear deformability in pseudostratified epithelia, play a crucial role in regulating key processes of morphogenesis. However, it is also possible that Lamin A/C may influence cell behaviour and nuclear positioning through mechanisms beyond nuclear mechanics, such as gene regulation.

3.2 Lamin A overexpression: affects nuclear mechanics rather than gene regulation

Lamin A overexpression could influence cellular processes beyond nuclear stiffness. Previous studies have shown that Lamin A interacts with chromatin, impacting DNA replication and gene transcription (Dechat et al., 2008; Gruenbaum and Foisner, 2015; Herrera et al., 2023; Zheng et al., 2022). This has led to a long-standing debate about whether the primary functional role of Lamin A lies in gene regulation, nuclear mechanics, or a combination of both (Lammerding et al., 2006). In our experiments, we observed that the majority of overexpressed Lamin A integrates into the nuclear lamina, although a small pool of intranuclear Lamin A puncta was also detected (Figure 2.1 C). These intranuclear puncta may interact with chromatin, raising the possibility of additional effects on gene regulation. Indeed, Lamin A within the nucleoplasm has been proposed to modulate gene expression at both transcriptional and post-transcriptional levels through interactions with splicing factors (Hutchison and Worman, 2004). If this occurs in our model system, it is conceivable that the observed phenotypes could, at least in part, reflect gene expression dysregulation rather than altered nuclear mechanics.

My results argue against a major role for Lamin A overexpression in altering gene regulation in this context. It is well established that disruptions in DNA synthesis typically lead to prolonged cell cycle phases and increased DNA damage. For example, treatment of zebrafish retinas with hydroxyurea and aphidicolin, which block DNA replication, causes both effects. These parameters therefore serve as useful indicators of compromised cell cycle function. In contrast, Lamin A overexpression does not affect overall cell cycle timing or induce detectable

DNA damage (Figure 2.5 C), indicating that it does not disrupt cell cycle regulation or DNA replication.

Interestingly, G2 phase is specifically prolonged in the densely packed retina, but not in the more loosely packed hindbrain (Figure 2.9, 2.10, 2.12 and 2.14). If this delay were driven by changes in gene expression, one would expect it to occur consistently across tissues. Its tissue-specific nature instead points to mechanical constraints, such as nuclear packing, as the primary cause. These findings support the conclusion that Lamin A overexpression predominantly influences nuclear mechanics rather than gene regulatory processes. However, we cannot entirely exclude the possibility that Lamin A overexpression has minor effects on gene regulation that were not detectable within the scope of this study.

This emphasizes the importance of mechanical context in shaping how nuclear properties influence cell behavior, particularly in confined environments like pseudostratified epithelia. Together, these observations suggest that the delays in nuclear movement are not due to gene regulation defects but rather to mechanical changes in the nucleus itself, leading to the next key question: could Lamin A overexpression impair nuclear movement by disrupting the cytoskeleton or its interactions with the nucleus? Given the cytoskeleton's known role in nuclear positioning, it is important to explore whether mechanical changes in the nucleus are the primary driver, or whether cytoskeletal defects might also contribute.

3.2.1 Ruling out alternative explanations: Cytoskeleton and Nuclear Envelope

Beyond regulating nuclear stiffness, the nuclear envelope plays a crucial role in nuclear movement by serving as the interface for force transmission between the cytoskeleton and the nucleus. Whether through anchoring or through indirect contact, such as pushing forces, the cytoskeleton relies on the nuclear envelope to transmit mechanical cues (Deshpande and Telley, 2021; Lee and Norden, 2013). Lamin A overexpression could, in principle, disrupt these interactions by altering the composition of the nuclear lamina. However, my results do not support this: microtubule distribution remains comparable between Lamin A-overexpressing and control cells (Figure 2.11 A and B), and both show similar actin accumulation beneath migrating nuclei (Figure 2.11 C and D). This actin buildup, driven by formin-mediated pushing forces, is known to facilitate nuclear movement in the zebrafish retinal neuroepithelium

(Yanakieva et al., 2019). These findings indicate that cytoskeletal organization is not significantly affected by Lamin A overexpression, and that the forces driving nuclear migration are preserved. Thus, differences in migration efficiency are unlikely to result from cytoskeletal defects.

Another possible explanation for the observed G2 elongation is impaired nuclear envelope breakdown (NEB). Given that Lamin A is a key structural component of the nuclear envelope (Dauer and Worman, 2009; Davidson et al., 2014; Friedl et al., 2011), its overexpression could theoretically lead to excessive accumulation at the nuclear periphery, potentially hindering NEB and delaying mitotic entry. However, my results show that NEB occurs at similar rates in Lamin A-overexpressing and control nuclei (Figure 2.17 E), ruling out NEB defects as the cause of the prolonged G2 phase. As discussed previously, both NEB and mitotic rounding are influenced by nuclear properties primarily in a non-cell-autonomous manner. This raises the intriguing question of how nuclear and tissue mechanics together regulate mitotic entry during development. Exploring this relationship could provide valuable insights into how physical constraints integrate with cell cycle control in proliferative tissues.

3.2.2 Conclusion: Nuclear mechanics are the primary effect of Lamin A overexpression in zebrafish neuroepithelia

While we cannot fully exclude minor effects of Lamin A overexpression on gene regulation or cytoskeletal force transmission, my results strongly support the conclusion that the observed delays in apical nuclear migration and mitotic rounding are primarily driven by changes in nuclear mechanics. There is no evidence for significant disruptions to cell cycle progression, transcriptional regulation, cytoskeletal organization, or nuclear envelope integrity. Instead, the tissue-specific G2 elongation observed in the densely packed retina further underscores the importance of nuclear deformability for migration in confined environments.

To my knowledge, this is the first in vivo study to directly examine the impact of Lamin A/C on nuclear mechanics within a developing tissue. These findings offer important insights into how nuclear material properties contribute to cellular behavior during organogenesis, particularly in spatially constrained architectures like pseudostratified epithelia. They also suggest that nuclear properties are not only cell-intrinsic but must be coordinated at the tissue

level to ensure robust development. Because nuclear deformability is central to key processes like mitotic entry and nuclear positioning during organogenesis, it would be fascinating to investigate how the importance of nuclear material properties varies across tissues and what strategies cells have evolved to modulate nuclear mechanics in confined environments.

Additionally, the needs of tissues can vary across development and maintenance, and it remains unexplored whether nuclear material properties change or adapt to these different contexts. Overall, how material properties are integrated at both the nuclear and tissue levels to support the diverse mechanical demands of morphogenesis is still an open question.

3.3 Low level of Lamin A expression may facilitate morphogenesis

Nuclear material properties must be precisely regulated during morphogenesis, a process characterized by extensive movements at the tissue, cellular, and nuclear levels. These dynamic events unfold within confined environments, where cells must optimize space and undergo considerable shape changes. My results show that nuclear deformability plays a key role in enabling efficient nuclear positioning and timely mitotic entry in densely packed tissues. This supports the idea that low levels of Lamin A/C, by preserving nuclear deformability, allow cells and nuclei to navigate spatial constraints (Bell et al., 2022; Harada et al., 2014; McGregor et al., 2016) and support proper tissue development. Interestingly, the expression of Lamin A is typically low during early development, as observed in zebrafish retinal and hindbrain neuroepithelia (Yanakieva et al., 2019), the developing mouse brain (Röber et al., 1989) and both mouse and human embryonic stem cells (Constantinescu et al., 2006). To further explore the context-specific roles of nuclear mechanics, it would be valuable to elevate Lamin A expression in other epithelial tissues and assess how nuclear deformability influences organogenesis under distinct morphogenetic constraints. One compelling example is lumen formation in the zebrafish otic vesicle, where epithelial thinning and mitotic rounding drive tissue morphogenesis. While the mechanical forces influencing lumen growth and shape have been characterized (Hoijman et al., 2015) the potential role of nuclear material properties in this process remains unexplored. Another intriguing context is the epithelial-to-mesenchymal transition (EMT), which can be triggered by increased tissue stiffness, as observed in Xenopus laevis neural crest cells (Barriga et al., 2018). Investigating how changes in tissue stiffness

intersect with nuclear mechanics in such settings could yield valuable insights into how nuclear properties contribute to morphogenesis.

Although low levels of Lamin A/C expression appear to confer advantages during morphogenesis, its expression progressively increases in developing tissues that experience elevated mechanical stress, particularly in the bone, musculoskeletal, and cardiovascular systems (Iyer et al., 2021; Malashicheva and Perepelina, 2021; Swift et al., 2013). The critical role of Lamin A/C in mature tissues is underscored by the wide range of disease phenotypes, known as laminopathies, that result from mutations in the *lmna* gene, highlighting the diverse functions this protein family serves in tissue homeostasis and integrity (reviewed in (Zuela et al., 2012). One possible explanation is that, once tissue architecture is established and large-scale cellular movements decrease, the functional demands on the nucleus shift. In this more stable context, high nuclear deformability is no longer necessary. Instead, structural integrity and genomic protection become priorities. Lamin A, being a key structural component of the nuclear lamina, likely plays an essential role at this stage by enhancing nuclear stiffness, maintaining nuclear shape, and safeguarding DNA from mechanical stress. This idea is supported by studies showing that low Lamin A levels during confined cell migration can lead to nuclear envelope ruptures, exposing genetic material to the cytoplasm and resulting in DNA damage (Denais et al., 2016). In both migrating cancer cells and fibroblasts, the frequency of nuclear envelope rupture rises with increased physical confinement and reduced lamin expression (Denais et al., 2016). These findings highlight the protective role of Lamin A in maintaining nuclear integrity under mechanical stress, suggesting that its expression must be finely tuned to balance nuclear deformability with genome stability.

Additionally, elevated Lamin A levels may serve to preserve tissue integrity by limiting cellular mobility. In 3D environments, nuclear stiffness can be a major physical constraint on cell movement, particularly through confined spaces. By increasing nuclear rigidity, high Lamin A levels can effectively act as a barrier to unnecessary or aberrant cell migration. This function is especially relevant in maintaining the organization and cohesion of mature tissues, where unwarranted cellular movement could disrupt tissue architecture and function. One example being neuronal migration and lamination in the vertebrate retina and brain. Here, developing neurons must arrange in distinct layers to ensure correct organ function (Amini et al., 2018). Consistent with this, epithelial-to-mesenchymal transition (EMT), a process that provides epithelial cells with migratory and invasive properties during development and cancer

metastasis, is frequently accompanied by a downregulation of Lamin A/C (Bell et al., 2022). This reduction in nuclear stiffness facilitates the enhanced deformability required for cells to navigate dense tissue environments.

Thus, the dynamic regulation of Lamin A/C expression may represent a key mechanism by which cells balance the competing demands of structural stability and deformability during different stages of development or in response to physiological cues. During early development, tissues undergo extensive cell movements and shape changes. In this context, low levels of Lamin A/C may help maintain nuclear deformability, enabling cells to migrate and divide more efficiently in densely packed and mechanically active environments. Conversely, as tissues mature and cellular organization stabilizes, increased Lamin A/C expression may enhance nuclear stiffness, contributing to the maintenance of nuclear integrity, protection of genomic material, and overall tissue resilience. This regulatory deformability in Lamin A/C levels may allow cells to adapt their nuclear mechanics to the mechanical and functional demands of different developmental stages or tissue contexts.

3.4 Nuclear deformability ensures robustness in densely packed tissues

Despite reduced efficiency in apical migration, nuclei overexpressing Lamin A in the zebrafish retina ultimately reach the apical surface and divide apically. This is crucial because apical nuclear migration is essential for maintaining tissue integrity and supporting neurogenesis: subapical divisions lead to clusters of proliferating cells that lose apical attachment and fail to differentiate (Strzyz et al., 2015). Thus, ensuring robust apical nuclear migration is crucial for preserving proper tissue architecture.

Pseudostratified epithelia (PSE) can adapt their cytoskeletal mechanisms that drives nuclear positioning depending on cell length and nuclear density. In intermediate-length PSE, actin-dependent forces suffice for nuclear movement, whereas in longer and denser PSE, microtubules and dynein likely provide a more effective mechanism (Strzyz et al., 2016). Similarly, in zebrafish neuroepithelia, actin-driven nuclear positioning depends on tissue morphology—actomyosin contractility via ROCK activity in straight PSE, and formin-dependent actin polymerization in curved PSE (Yanakieva et al., 2019). These observations indicate that cell and tissue morphology can influence the cytoskeletal mechanisms driving nuclear positioning. The fact that different pseudostratified epithelia regulate their cytoskeleton

differently to achieve apical division highlights the robustness of apical nuclear migration. It is therefore likely that different PSEs have evolved distinct strategies to ensure efficient apical migration depending on their specific architectural constraints.

In this context, my findings highlight the robustness of apical nuclear migration, demonstrating that nuclei still divide apically even when migration efficiency is reduced by increased nuclear stiffness. Notably, the impact of increased nuclear stiffness on migration appears to be context-dependent: Lamin A overexpression had only a minor effect on apical nuclear migration in the loosely packed hindbrain, where nuclear packing and cell density are lower. These observations suggest that nuclear deformability plays a crucial role in enabling cells to overcome spatial constraints. It is therefore possible that enhanced nuclear deformability is an adaptation to the high cell density characteristic of pseudostratified epithelia, contributing to the robustness of apical divisions and ensuring efficient nuclear migration.

Despite the reduced efficiency of apical nuclear migration caused by increased nuclear stiffness, neuronal differentiation and lamination remained unaffected. This provides new evidence highlighting the robustness of apical mitosis as a key mechanism ensuring successful organogenesis. One might expect that impaired nuclear migration could lead to sub-apical divisions, which are known to compromise tissue integrity in other contexts. However, my data show that even nuclei requiring twice as much time to migrate still divide at the apical surface. Importantly, G2 phase is elongated under these conditions, and cells do not enter mitosis until their nuclei reach the apical side. It remains an open question whether G2 elongation acts as a regulatory mechanism that actively prevents sub-apical divisions by delaying mitotic entry, or whether it simply reflects a passive consequence of slowed nuclear migration.

4. Future directions

The findings presented in my thesis contribute to a deeper understanding of how nuclear material properties can influence fundamental aspects of organ development. By overexpressing Lamin A in zebrafish neuroepithelia, I demonstrate that increased nuclear stiffness is sufficient to impair apical nuclear migration and delay mitotic entry, depending on tissue density and stiffness. These results not only provide new insights into the mechanical regulation of cell behaviour and nuclear positioning during development, but also raise important new questions, opening avenues for future research.

4.1 The effect of nuclear properties on nuclear positioning beyond zebrafish neuroepithelium

Our findings underscore the critical role of nuclear material properties in regulating nuclear positioning within densely packed tissues. A key next step will be to investigate whether these principles extend to other pseudostratified epithelia with different architectural features and to tissues with distinct cellular organizations. First, it would be interesting to compare nuclear deformability and migration efficiency across short, intermediate, and long pseudostratified epithelia, such as Drosophila imaginal discs and the vertebrate neural tube, to assess how variations in cell height and nuclear packing influence the effect of nuclear material properties on nuclear positioning. Further, it could be tested whether nuclear stiffness similarly affects nuclear positioning and mitotic division in non-pseudostratified contexts, including simple epithelia and mesenchymal tissues, where cell packing and cytoskeletal arrangements differ markedly. Finally, by combining atomic force microscopy with our live-imaging deformation assays, it will be important to explore possible correlations between nuclear stiffness with overall tissue stiffness across these models, probing how nuclear volume fraction and cytoplasmic architecture shape tissue-level mechanics. Extending our analysis beyond the zebrafish neuroepithelia will allow to determine the generality of nuclear deformability as a regulator of morphogenetic movements and organogenesis.

4.2 How is DNA damaged prevented in the densely packed zebrafish neuroepithelia

A critical function of Lamin A is to protect the genetic material and prevent DNA damage (Denais et al., 2016; Harada et al., 2014; Hutchison and Worman, 2004; Wang et al., 2022). In vitro studies have shown that low Lamin A levels are associated with nuclear envelope ruptures during migration through confined 3D environments, exposing DNA to the cytoplasm and leading to damage. Specifically, in mammalian tumour cells undergoing confined migration, nuclear deformations cause localized nuclear envelope rupture, which correlates with increased DNA damage. Both increased cell confinement and depletion of nuclear lamins exacerbate the frequency of these rupture events (Denais et al., 2016).

Interestingly, in the zebrafish retina, nuclei express only low levels of Lamin A/C while existing within a densely packed, highly confined environment. During the proliferative phase of retinal development, nuclei must migrate apically through this crowded tissue architecture. Despite these conditions, I find no evidence of nuclear envelope rupture or DNA damage in this system.

This raises an important question: how is DNA integrity preserved in developing tissues that undergo extensive nuclear deformation in confined environments? Understanding the mechanisms that protect the genome during these critical developmental movements could reveal important tissue-specific strategies that differ from those observed in vitro.

One possible explanation is that the deformability of the tissue-wide nuclei provides a mechanically permissive environment that prevents nuclear envelope rupture. In a soft, compliant tissue where neighbouring nuclei are also highly deformable, mechanical resistance against a migrating and deforming nucleus is minimized. As a result, nuclei may experience less severe localized stresses, reducing the likelihood of envelope rupture and protecting DNA integrity during movement. Breaking an object typically requires a stiffer surface against a softer one, and if all nuclei share similar mechanical properties, the risk of rupture may be minimized. This hypothesis could be tested using the NLS-GFP transgenic zebrafish line in the transplantation setup, where deformable nuclei migrate in a stiffer environment. My observations show that increased stiffness tissue-wide impairs nuclear dynamics (Figure 2.15 A-F), leading to an elongated G2 phase (Figure 2.16 F). However, I have not analysed whether this stiffer environment induces nuclear envelope rupture in control cells. Another approach to test whether tissue-wide nuclear deformability prevents nuclear envelope rupture would

be to introduce stiff beads into the pseudostratified epithelium (PSE). By locally increasing mechanical resistance within the otherwise soft and deformable tissue, these beads would mimic the presence of rigid obstacles. If nuclear envelope integrity depends on the mechanical compliance of the surrounding environment, then nuclei migrating past or contacting these stiff beads would be expected to experience greater deformation and a higher incidence of localized nuclear envelope rupture.

To further refine this approach, beads of varying stiffness could be used to systematically tune the mechanical challenge presented to migrating nuclei. This would allow the determination of whether there is a critical stiffness threshold above which nuclear envelope rupture becomes more frequent, providing quantitative insight into how mechanical heterogeneity within a tissue influences nuclear stability.

Another hypothesis to explain how does DNA integrity is maintained in developing confined tissues is that cytoskeletal components play a protective role in preventing nuclear damage. Microtubule arrangements, which span the entire apico-basal axis, and intermediate filaments such as vimentin may act as a structural shield around the nucleus. To test this, it would be interesting to disrupt these structures using a morpholino knockdown approach or a low-dose colcemid treatment to depolymerize microtubules and observe whether this increases nuclear envelope ruptures and/or DNA damage.

These experiments will help clarify how nuclear material properties contribute to DNA protection and how tissues cope with potential nuclear damage in highly confined environments. Understanding these mechanisms could provide key insights into how developing tissues balance nuclear deformability with genomic stability.

5. Conclusions

This study advances our understanding of how nuclear deformability shapes key nuclear and cellular processes that are critical for proper organ development. By employing high-resolution live imaging and quantitative approaches to track individual nuclear movements and shape changes during interkinetic nuclear migration, this work demonstrates that increased nuclear stiffness impairs apical nuclear migration in both cell-autonomous and non-cell-autonomous manners. This work further shows that the effect of nuclear deformability on nuclear movements is dependent on the confined state of the tissue.

These findings were made possible by the use and characterization of a genetic tool and transgenic line that induces Lamin A overexpression, leading to increased nuclear and tissue-wide stiffness. A key methodological advancement of this study was the application of root mean squared deviations as a novel metric to quantify nuclear shape changes directly from imaging data. This approach overcomes limitations of previous techniques, such as atomic force microscopy, which are easier to apply to isolated cells in vitro but are much more challenging to use for assessing nuclei inside living tissues, where access and mechanical complexity are greater. Furthermore, by integrating this analysis with the theory of compressible droplets and atomic force microscopy measurements of PSE apparent elastic modulus, this work establishes a link between nuclear deformability and efficient apical migration, highlighting the role of nuclear material properties in morphogenesis.

Future research on how Lamin A/C expression is regulated in both progenitor and differentiated cells will be crucial for understanding how nuclear material properties influence tissue development and maintenance. This could help uncover how nuclear mechanics drive proper organ development and shape the mechanical foundations of tissue formation. By controlling nuclear deformability, cells can fine-tune their ability to move, divide, and organize in confined, crowded environments. Understanding how these nuclear properties are regulated will provide deeper insights into how the material properties of living cells contribute to the emergence of complex biological forms. Ultimately, this research could open a new chapter in developmental biology, highlighting the critical role of nuclear mechanics in morphogenesis and tissue integrity.

6. Material and Methods

6.1 Experimental model and study participants details

Wild-type zebrafish (Danio rerio; AB and Tupfel long-fin (TL) strains) and various transgenic lines were housed in mixed-sex groups (10 adults per liter) within a recirculating life support system (Tecniplast). Environmental conditions were maintained at 28°C, pH 7.0, conductivity of 1000 µS/cm, and a 14-hour light/10-hour dark photoperiod. Juvenile fish were fed a diet combining saltwater rotifers (Brachionus plicatilis) and processed feed (Gemma 150, Skretting). Adult zebrafish were nourished with a mixture of live Artemia salina and commercially processed dry food (Gemma 300, Skretting). Detailed descriptions of husbandry procedures, water quality parameters, and health monitoring programs have been previously documented. Embryos were incubated at 28.5°C in E3 medium. Developmental staging of larvae was determined in hours post-fertilization (hpf) following the criteria established by Kimmel et al. (1995). Starting from 8 hpf, the medium was replenished daily and supplemented with 0.2 mM 1-phenyl-2-thiourea (10107703, Acros Organics) to prevent pigmentation. Zebrafish larvae were analyzed between 24 and 36 hpf, a developmental window characterized by limited neurogenesis in the retina, with most cells being proliferative progenitors. Prior to live imaging and dissections, larvae were anesthetized by incorporating 0.04% tricaine methanesulfonate (MS-222, 1004671, Pharmaq) into the E3 medium. All experimental procedures adhered to institutional standard operating protocols, under licensing by the Direcção Geral de Alimentação e Veterinária (DGAV, Portugal) and in compliance with European Directive 2010/63/EU and Portuguese Decree Law No. 113/2013.

For nuclear visualization, the Tg(hsp70:H2B-RFP) and Tg(b-actin:PCNA-GFP) transgenic lines were employed. The Tg(b-actin:PCNA-GFP) line was further utilized for assessing nuclear cell cycle dynamics, as described previously, and illustrated in Figure S2B. Lamin A overexpression was induced in a tissue-wide manner using the Tg(hsp70:LMNA-mKate2) transgenic zebrafish line. The Tg(b-actin:Ras-GFP) line facilitated plasma membrane visualization.

6.2 DNA Cloning and Constructs used

To observe actin distribution, the Actin-Chromobody (acg, Chromotek) was cloned via Gateway recombination (Thermo Fisher Scientific) using the Tol2 system, generating the bactin:Actin-VHH-tagGFP2 construct.

6.3 DNA and RNA microinjections

Plasmid DNA constructs were microinjected into one-cell stage embryos, ensuring mosaic expression in a subset of cells. The injection mix was prepared in Milli-Q water at a final concentration of 50 ng/µl DNA, with an injection volume of 0.5–1 nl per embryo.

Messenger RNA (mRNA) was synthesized using the Thermo Fisher Scientific mMESSAGE mMACHINE SP6 Transcription Kit (AM1340), following the manufacturer's protocol. GFP-Ras mRNA (1 nl at 50 ng/µl) was injected into one-cell stage embryos to label plasma membranes, as depicted in Figure 1H. A list of constructs used in the study is provided in the accompanying table (table is published in Maia-Gil et al. 2024).

DNA construct	Labelled structure / function	Reference
βactin:Actin-VHH-tagGFP2	Actin "cloud-like" structure	This study
pCS2+GFP-ras	Used to produce the RAS-GFP mRNA and visualize the plasma membrane	Sidhaye et al., 2017(Sidhaye and Norden, 2017)
βactin:mkate-UtrophinCH	Stable F-actin structures, used to identify cell's apical side	Amini et al., 2022(Amini et al., 2022b)
hsp70:GFP-UtrophinCH	F-actin, used to identify cell's apical side	Strzyz et al., 2015[2]
hsp70:PCNA-GFP	Live cell-cycle phase marker	Strzyz et al., 2015[2]
hsp70:LmnA-mKate2	Overexpression of Lamin A	Yanakieva et al., 2019[35]
hsp70:EGFP-LAP2b	Lamina-associated polypeptide 2	Yanakieva et al., 2019[16]
βactin:EGFP-DCX	Microtubules	Icha et al., 2016(Icha et al., 2016a)
hsp70:H2B-RFP	Histone marker	Matejcic et al., 2018(Matejčić et al., 2018)

6.4 Blastomere transplantation

Blastomere transplantations were performed between donor (Tg(b-actin:PCNA-GFP)) and recipient (Tg(hsp70:H2B-RFP) or Tg(hsp70:LMNA-mKate2)) embryos. At the 256-cell stage,

embryos were dechorionated using 2 mg/ml Pronase (P8811, Sigma-Aldrich) for five minutes, followed by three washes in Danieus buffer (58 mM NaCl, 0.7 mM KCl, 0.4 mM MgSO4•7H2O, 0.6 mM Ca(NO3)2, and 5 mM HEPES). Embryos were transferred via glass pipette to agarose-coated Petri dishes containing 6×25 wells. Transplantations were conducted in E3 medium using an Olympus SZX10 stereomicroscope equipped with a micromanipulator and a 0.1-mm diameter glass needle. Approximately 15-25 blastomeres were transplanted per embryo at the mid-blastula stage. Post-transplantation, embryos were incubated at 32°C for 1–2 hours, then transferred to fresh E3 medium with 0.2 mM 1-phenyl-2-thiourea (10107703, Acros Organics) and maintained at 28.5°C overnight.

6.5 Heat-shock treatment and screening

To activate hsp70-driven transgenes, zebrafish larvae were exposed to a 39°C water bath for 30 minutes at the 16-somite stage (for hindbrain imaging) and between 22 and 23 hpf (for retinal imaging). After heat shock, larvae were returned to 28.5°C in fresh E3 medium containing 0.2 mM 1-phenyl-2-thiourea. Fluorescent-positive larvae were screened under an Olympus SZX16 stereomicroscope equipped with a fluorescence lamp (Olympus U-HGLGPS) 2–4 hours post-induction and selected for further analysis. To activate hsp70-driven transgenes, zebrafish larvae were exposed to a 39°C water bath for 30 minutes at the 16-somite stage (for hindbrain imaging) and between 22 and 23 hpf (for retinal imaging). After heat shock, larvae were returned to 28.5°C in fresh E3 medium containing 0.2 mM 1-phenyl-2-thiourea. Fluorescent-positive larvae were screened under an Olympus SZX16 stereomicroscope equipped with a fluorescence lamp (Olympus U-HGLGPS) 2–4 hours post-induction and selected for further analysis.

6.6 Dissection of zebrafish heads

Prior to dissection, larvae were manually or chemically dechorionated using 2 mg/ml Pronase (P8811, Sigma-Aldrich) and anesthetized with 0.04% tricaine methanesulfonate. Anesthetized larvae were placed in chilled 1× PBS on a glass-bottom dish. Heads were dissected manually using fine forceps (size 55) and transferred into 1.5 ml microtubes with minimal liquid volume. Samples were snap-frozen on dry ice immediately post-dissection. Larvae from different experimental conditions (no heat shock; 2, 6, and 14 hours post-heat shock) underwent identical

processing, with three biological replicates per condition. Samples were stored at -80°C until further analysis.

6.7 Immunoblotting

Prior to Heads were lysed by adding RIPA lysis buffer supplemented with protease inhibitors (A32953, Pierce), 50 mM dithiothreitol (MB03101, NZYTech), and 10 mM sodium orthovanadate (S6508, Merck). Lysis was performed using an electric pestle in 10-second bursts. The samples were then incubated on ice for 20 minutes, heated at 95°C for 5 minutes, and centrifuged at 18,000 RCF for 10 minutes at 4°C. Supernatants were collected and mixed with protein loading buffer (928-40004, LI-COR Biosciences) before being loaded onto pre-cast NuPAGE 4–12% Bis-Tris protein gels (NP0322BOX, Thermo Fisher Scientific).

Electrophoresis was performed using a running buffer containing 50 mM Tris base, 50 mM MOPS, 0.1% SDS, and 0.1 mM EDTA (M00138, GenScript). Gels were run at 100 V for 200 minutes in a Mini Gel Tank system (Thermo Fisher Scientific). The molecular weight marker used was the Chameleon Duo Pre-stained Protein Ladder (928-60000, LI-COR Biosciences).

Proteins were transferred from gels to nitrocellulose membranes (926-31092, LI-COR Biosciences) using the Mini Gel Tank system, following the manufacturer's recommendations. The transfer was performed at 20 V for 1 hour in a buffer containing 25 mM Tris base, 25 mM Bicine (M00139, GenScript), and 10% absolute ethanol (20821.330, VWR Chemicals).

Immunoblotting was carried out by blocking membranes for 15 minutes in PBS (137 mM NaCl, 2.7 mM KCl, 8.1 mM $Na_2HPO_4 \cdot 2H_2O$, 1.8 mM KH_2PO_4) containing 10% non-fat milk (Molico, Nestlé) and 0.05% Tween-20. Membranes were incubated overnight at 4°C with primary antibodies under slight agitation, followed by three washes with PBS containing 0.05% Tween-20. Secondary antibodies were then applied, followed by three additional washes with PBS containing 0.05% Tween-20 and two final washes with PBS. Membranes were developed using the WesternBright Sirius HRP substrate (K-12043-D10, Advansta), according to the manufacturer's instructions. The primary antibodies used were: Anti-Lamin A/C (NBP1-85550, NovusBio) at 1:1000; Anti-Lamin B1 (ab16048, Abcam) at 1:2000; Anti-Lamin B2 (sc-56146, Santa Cruz Biotechnology) at 1:2000 and Anti-actin (A2066, Sigma-Aldrich) at 1:2000. The secondary antibodies used were: Anti-rabbit-HRP conjugated (711-035-152, Jackson Immuno Research) at 1:10,000 and Anti-mouse-HRP conjugated (715-035-151, Jackson Immuno

Research) at 1:10,000. Anti-Lamin A/C, Lamin B1, and Lamin B2 antibodies were diluted in buffer containing 50 mM Tris-HCl (pH 7.5), 150 mM NaCl, 0.1% Triton X-100, and 2% BSA. Anti-actin and secondary antibodies were diluted in PBS containing 5% non-fat milk and 0.05% Tween-20.

6.8 Whole-mount immunostaining

For whole-mount immunostaining, zebrafish larvae were manually dechorionated and fixed in 4% PFA (043368-9M, Thermo Fisher Scientific) in PBS at 22 hpf for hindbrain imaging and at 28–30 hpf for retina imaging. Fixation was performed overnight at 4°C.

Following fixation, larvae were rinsed with 1× PBS and washed five times with PBS containing 0.8% Triton X-100 (28817295, VWR) for 10 minutes with slight agitation. Permeabilization was carried out using trypsin-EDTA (sc-391060, Santa Cruz Biotechnology) on ice for 7–10 minutes. The larvae were then rinsed twice with PBS-Triton 0.8% and incubated in the same buffer on ice for 30 minutes. Blocking was performed at room temperature for 3 hours in PBS-Triton 0.8% containing 10% goat serum (16210064, Gibco). Larvae were then incubated with primary antibodies in PBS-Triton 0.8% supplemented with 1% goat serum for 3 days at 4°C, with slight agitation. The primary antibodies used were: Anti-phospho-Histone H3 (Ser10) (Cat No. 631257, Sigma-Aldrich) at 1:500 and Histone H2A.XS139ph (phospho-Ser139) (Cat No. GTX127342, RRID: AB_2833105, GeneTex) at 1:200. After incubation, larvae were washed five times for 30 minutes in PBS-Triton 0.8%. Secondary antibody incubation was performed in PBS-Triton 0.8% containing 1% goat serum for 2 days at 4°C with slight agitation. The secondary antibodies used were: Alexa Fluor 488 anti-rabbit (RRID: AB_2535792, Thermo Fisher Scientific) at 1:500 and DAPI (MBD0015, Sigma-Aldrich) at 1:1000.

6.9 Dissection of retinal pseudostratified epithelium

For atomic force microscopy (AFM) analysis, zebrafish larvae at 26–30 hpf were manually dechorionated 2–4 hours after heat shock and anesthetized by supplementing E3 medium with 0.04% tricaine methanesulfonate (MS-222, 1004671, Pharmaq). Anesthetized larvae were then transferred to a glass-bottom dish containing chilled 1× PBS, where their heads were manually dissected. The two eyes were then separated from each head.

To ensure that only the stiffness of cells from the retinal pseudostratified epithelium (PSE) was measured, the retinal pigmented epithelium (RPE) and the lens were removed from all eyes.

To visualize the RPE, larvae were not treated with 1-phenyl-2-thiourea (PTU), allowing melanocyte development. Dissected retinal cells were transferred to a 1.5 ml microtube and kept on ice. This process was repeated for 10–14 retinas per condition.

Following dissection, retinal cells from both conditions were plated on a Poly-D-Lysine (A3890401, Gibco)-coated glass-bottom dish and incubated at 28.5°C for 30 minutes to allow cell attachment. Once attached, cells were supplemented with Leibovitz's L-15 Medium (11415049, Gibco) containing 20 mM HEPES (10397023, Fisher Bioreagents) and 2% FBS (10270106, Gibco).

6.9.1 Atomic Force Microscopy (AFM) measurements

All AFM measurements were performed using a FLEX-ANA (Nanosurf) automated AFM device. The AFM head was mounted on a Leica DMI 6000 inverted microscope fitted with an x–y-motorized stage, allowing imaging of cells using a 10×/0.30 Leica dry objective while acquiring AFM data. Cantilevers coated with 2.25 mm diameter colloidal spheres (CP-qp-SCONT-Au-A, NanoAndMore GmbH) were used to ensure that indentations captured mechanical properties at the cellular level rather than the tissue level.

Cantilevers were mounted on the AFM device, and their spring constants were determined using the thermal noise method. Only cantilevers with spring constants between 0.01 and 0.03 N/m were selected. Extracted retinas were mounted as described previously, and 25 indentations were performed per cell within a 50×50 mm region of interest (ROI). The following modulation parameters were used: Maximum indentation force: 5–7 nN; Approach speed: 5 mm/s; Retraction speed: 50 mm/s and Sample rate: 2400 Hz. AFM curves were selected for analysis as described in the AFM data analysis section.

In brief, AFM measurements were performed using a set force of 5 nN, ensuring uniform application across all conditions. An active z-loop was used to maintain constant force application. Analysis was conducted with a standardized indentation depth of 2 mm across all conditions, allowing results to be interpreted in terms of the apparent elastic moduli of the probed material.

6.9.2 AFM data analysis and image treatment

AFM data were analyzed using AtomicJ software (v2.3.1). Raw force–distance curve data were fitted to the Hertz model for a spherical indenter:

$$F = \frac{4}{3} K \sqrt{r} \delta^{3/2} = \frac{4}{3} \frac{E}{1 - v^2} \sqrt{r} \delta^{3/2}$$

where F is the applied force, E represents Young's modulus, v is Poisson's ratio, r is the indenter radius, and d denotes the indentation depth. The term K = E/(1 - v^2) represents the apparent elastic modulus, referred to as "stiffness" in the text and labeled as "apparent elasticity (Pa)" on the y-axis of each graph.

Curve quality was assessed based on shape. For selected curves, AtomicJ was used to detect the contact point, and elastic moduli were extracted from this point up to a 2 µm indentation depth, as previously described. The median value from each grid covering a single cluster of retinal cells was calculated and subsequently processed for statistical analysis.

6.10 Microscope image acquisition

Zebrafish retinas were imaged during the proliferative phase, between 26 and 36 hpf.

6.10.1 Confocal scans

Fixed samples were imaged 6–8 hours after heat shock using three different confocal microscope systems:

Leica Stellaris 5 Upright Confocal Microscope

The majority of images were captured using a HC PL APO 40×/1.1 Water CORR CS2 objective (#506425, Leica) and operated with LAS X software (v4.5.0.25531).

Zeiss LSM 900 Confocal Microscope

Later developmental time points and cytoskeletal structures were imaged using a LD LCI Plan-Apochromat 40×/1.2 Imm Corr DIC M27 objective with water immersion. Acquired z-stacks spanned the entire retina or measured 20–60 µm in thickness, with a step size of 0.5–1 µm. The microscope was controlled via Zen v3.5.093.00010 software (Zeiss).

Zeiss LSM 980 Airyscan Confocal Microscope

High-resolution nuclear imaging was performed using a C Plan-Apochromat 63×/1.4 Oil DIC M27 objective with glycerol immersion. Datasets were processed using joint deconvolution, with z-stack thicknesses of 17–20 µm and a step size of 0.17 µm. The microscope was operated using Zen v3.3.89.0000 software (Zeiss).

All samples were mounted in 1% glycerol on glass-bottom dishes (MatTek) for imaging.

6.10.2 Time-lapse imaging using Light Sheet Fluorescent Microscopy (LSFM)

Live imaging of individual nuclei in the hindbrain (18–24 hpf) and retina (26–36 hpf) of zebrafish larvae was conducted using a Zeiss Z.1 Light Sheet Microscope, operated with ZEN 2014 SP1 software (v9.2.8.60, Black Edition). Imaging commenced 4–6 hours post-heat shock.

Larvae at 18 or 26 hpf were embedded in 0.6% low-melting agarose (prepared in filtered E3 medium) within a cylindrical column. The sample chamber was filled with E3 medium supplemented with 0.2 mM 1-phenyl-2-thiourea (10107703, Acros Organics) and 0.04% tricaine methanesulfonate (MS-222, 1004671, Pharmaq) as described previously. Entire hindbrains and retinas were captured in single-view mode at 1-minute intervals over a 6–10 hour period. Images were acquired at 0.5–1 µm step sizes using dual-sided illumination with 10×/0.2 objectives (Carl Zeiss Microscopy). Time-lapse images were recorded using a Plan-Apochromat 40×/1.0-W detection objective and two PCO.Edge 4.2 sCMOS cameras. The multiview imaging option enabled the simultaneous capture of both retinas in each zebrafish larva.

6.11 Image processing and analysis

Before analysis, basic image preprocessing was performed. Using ZEN 2014 SP1 (v9.2.8.54 & v9.3.1.393, Black Edition) or Fiji, images were averaged, cropped, and drift-corrected. Image analysis was conducted using IMARIS (v10.0.0), AMIRA v2020.2 (Thermo Fisher), and Fiji, while statistical analyses and data visualization were performed using Microsoft Excel, GraphPad Prism (v9.4.0, Windows), and Python.

6.12 Nuclear segmentations, volume and shape analysis

Zebrafish retinas at 28–30 hpf (6–8 hours post-heat shock) expressing H2B-GFP, following hsp70:H2B-GFP plasmid injection at the one-cell stage, were segmented using the Surface Tool in IMARIS (v10.0.0). 3D segmentation was performed by fitting an ellipsoid to the fluorescently labeled nuclei. The long and short semi-axes and their respective aspect ratios were extracted from these 3D reconstructions. Nuclear volume was calculated by determining the total voxel count occupied by each segmented nucleus.

6.13 Nuclear deformations during S and G2 phases

AFM data Zebrafish expressing Tg(hsp70:H2B-RFP) and Tg(hsp70:LMNA-mKate2) were mosaically labeled with the nuclear envelope marker hsp70:EGFP-LAP2b DNA via injection at the one-cell stage. Hindbrains and retinas were live-imaged at 18–24 hpf and 26–36 hpf, respectively, using light sheet microscopy as described above. Imaging began 4–6 hours post-heat shock.

Based on previous studies, hindbrain nuclei were classified as S-phase 30–50 minutes before reaching the apical side and G2-phase 15 minutes before apical arrival. Retinal nuclei were designated as S-phase 40–60 minutes and G2-phase 20 minutes before reaching the apical surface. 3D segmentation of nuclei was performed using the LimeSeg plugin in Fiji (LimeSeg plugin).

To quantify nuclear shape dynamics, the Root Mean Squared Deviation (RMSD) of each segmented nucleus was computed and compared against a perfect ellipsoid. RMSD variations over time reflected stochastic nuclear shape fluctuations in S-phase and the morphological changes associated with apical nuclear migration in G2-phase. Standard Deviation (SD) values were used as a proxy for nuclear deformability, representing the extent of shape fluctuations.

6.14 Analysis of cell cycle nuclear dynamics

To track cell cycle progression, nuclei were labeled with PCNA, a live-cell cycle marker identifying replication foci. Imaging began 4–6 hours post-heat shock. PCNA-positive nuclei displayed replication foci during S-phase. Once these foci disappeared, G2-phase commenced and lasted until nuclear envelope breakdown (NEB). After apical mitosis, nuclei transitioned into G1-phase until PCNA replication foci reappeared.

To assess apical nuclear migration, nuclei were analyzed from the onset of G2-phase (marked by PCNA foci disappearance) until reaching the apical surface. The bactin:mkate-UtrophinCH or bactin:mkate-UtrophinCH DNA markers were used to label the apical region.

6.15 Sample Drift Correction

The apical side of the cell was designated as a reference point for nuclear position tracking. Utrophin, which labels F-actin, was used to visualize the apical boundary. In transplantation experiments, the apical surface was identified by the universal expression of H2B across nuclei. Drift correction for each cell crop was performed using the Manual Drift Correction plugin in Fiji (Manual Drift Correction).

6.16 MIP, rotation and nuclei tracking

Since nuclear movement predominantly occurs along the y-axis, with minimal displacement in the x- and z-axes, a maximum intensity projection (MIP) of the z-stack was applied to each cell crop. The images were then rotated to align the cell's principal axis with the y-axis using ZEN 2014 SP1 (v9.2.8.54 & v9.3.1.393, Black Edition) and/or Fiji. Consequently, nuclear motion was assessed in one dimension (1D), employing the MTrackJ plugin in Fiji (https://imagej.net/plugins/manual-drift-correction). The nuclear center was manually selected at different time points, serving as a reference for position tracking.

6.17 Kinetics of apical nuclear migration

The duration and position of nuclear movements were extracted from MTrackJ and analyzed using Microsoft Excel and Wolfram Mathematica.81 Mean squared displacement (MSD) and directionality ratio were computed for the first 18 minutes of either apical nuclear migration or S-phase. These calculations were performed in Microsoft Excel utilizing the open-source software DiPer (Gorelik and Gautreau, 2014).

6.18 Quantification and Statistical analysis

To quantify apical mitotic events, DAPI-stained retinas at 28–30 hpf were used to generate a 3D retinal surface with the Surface Tool in IMARIS. Next, spot detection was applied to identify pH3-positive nuclei, as described earlier, to count mitotic cells. To determine the percentage of pH3-positive nuclei dividing at the apical side, detected spots were filtered based on their shortest distance from the retinal surface and categorized into: Green spots - nuclei within 5 µm of the apical surface; and Orange spots - nuclei beyond this threshold. This classification was performed in IMARIS (v10.0.0).

6.19 Statistical analysis

All statistical tests were conducted using GraphPad Prism (v9.4.0, Windows, GraphPad Software). A two-tailed approach was applied with a 95% confidence interval. Normality tests: Data distribution was assessed using the D'Agostino-Pearson and/or Shapiro-Wilk tests.

Comparative analyses: Gaussian-distributed data - Compared using an unpaired t-test; Non-parametric data - Analyzed with a Mann-Whitney test. All p-values are provided in the corresponding figure legends.

6.20 Table of experimental repeats and statistical parameters used

Parameter in this thesis	Equivalent figure in Maia-Gil et al., 2024	Condition 1, n nuclei, N embryos, mean ± SD	Condition 2, n nuclei, N embryos, mean ± SD	Statistical test, p-value
Figure 2.2 B – Nuclear Volume (μm^3)	Figure 1 C – Nuclear Volume (μm^3)	Control, 83, 11, 169.8 ± 47.83	Lamin A OE transgenic line, 61, 6, 130.4 ± 27.47	Mann Whitney test, p < 0.0001
Figure 2.2 C – Nuclear Aspect Ratio	Figure 1 D – Nuclear Aspect Ratio	Control, 83, 11, 0.4188 ± 0.1113	Lamin A OE transgenic line, 61, 6, 0.402 ± 0.06388	Mann Whitney test, p = 0.5891

Figure 2.2 F – Standard deviations of RMSD (µm)	Figure 1 F – Standard deviations of RMSD (µm)	Control, 7, 2, 0.2449± 0.1256	Lamin A OE transgenic line, 7, 2, 0.1102 ± 0.08810	Mann Whitney test, p = 0.0262
Figure 2.3 B – Preferred volume (μm^3)	Figure S1 E – Preferred volume (μm^3)	Control, 7, 2, 1056 ± 360.5	Lamin A OE transgenic line, 7, 2, 885.7 ± 182.8	Mann Whitney test, p = 0.6200
Figure 2.3 C – Surface Tension		Control, 7, 2, 0.2622 ± 0.072	Lamin A OE transgenic line, 7, 2, 0.5190 ± 0.210	Mann Whitney test, p = 0.004
Figure 2.3 D – Volume elastic coefficient ((μm^{-4}) 10^{-3})	Figure 1 G – Volume elastic coefficient ((μm^{-4}) 10^{-3})	Control, 7, 2, 3.158± 1.614	Lamin A OE transgenic line, 7, 2, 6.397 ± 3.584	Mann Whitney test, p = 0.0111
Figure 2.4 E – Apparent Elasticity (Pa)	Figure 1 I – Apparent Elasticity (Pa)	Control, 17, 2, 251.2 ± 125.3*	Lamin A OE transgenic line, 21, 2, 462.2 ± 161.3*	Unpaired t-test, p > 0.0001
Figure 2.5 C – Cell Cycle length (min)	Figure 2 A – Cell Cycle length (min)	Control, 15, 3, 361.5 ± 36.99	Lamin A OE transgenic line, 13, 3, 377.9 ± 57.23	Mann Whitney test, p = 0.0245
Figure 2.5 C – Cell Cycle length (min)	Figure 2 A – Cell Cycle length (min)	Control, 15, 3, 361.5 ± 36.99	Lamin A OE mosaic, 13, 4, 336.8 ± 108.7	Unpaired t-test, p = 0.3701
Figure 2.5 D – G1-phase length (min)	Figure 2 B – G1-phase length (min)	Control, 19, 3, 90.42 ± 25.57	Lamin A OE transgenic line, 29, 3, 107.6 ± 43.93	Unpaired t-test, p = 0.8337
Figure 2.5 D – G1-phase length (min)	Figure 2 B – G1-phase length (min)	Control, 19, 3, 90.42 ± 25.57	Lamin A OE mosaic, 17, 4, 87.88 ± 44.81	Unpaired t-test, p = 0.1302

Figure 2.5 E – S-phase length (min)	Figure 2 C – S-phase length (min)	Control, 12 ,2, 245.8 ± 54.81	Lamin A OE transgenic line, 15, 3, 253.1 ± 44.74	Mann Whitney test, p = 0.0188
Figure 2.5 E – S-phase length (min)	Figure 2 C – S-phase length (min)	Control, 12 ,2, 245.8 ± 54.81	Lamin A OE mosaic, 13 ,3, 225.4 ± 94.41	Mann Whitney test, p = 0.3792
Figure 2.5 F – G2-phase length (min)	Figure 2 D – G2-phase length (min)	Control, 90, 4, 28,64 ± 9.126	Lamin A OE transgenic line, 69, 6, 43.43 ± 19.28	Mann Whitney test, p < 0.0001
Figure 2.5 F – G2-phase length (min)	Figure 2 D – G2-phase length (min)	Control, 90, 4, 28,64 ± 9.126	Lamin A OE mosaic, 75, 6, 40.43 ± 22.98	Mann Whitney test, p < 0.0001
Figure 2.7 B – % of pH3 positive cells at less than 5 µm from the apical side	Figure 2 F – % of pH3 positive cells at less than 5 µm from the apical side	Control, 6, 2, 91.62 ± 3.814 **	Lamin A OE transgenic line, 8, 3, 89.81 ± 7.905 **	Mann Whitney test, p > 0.9999
Figure 2.10 A – Duration of apical nuclear migration (min)	Figure 3 G – Duration of apical nuclear migration (min)	Control, 57, 4, 20.32 ± 8.386	Lamin A OE transgenic line, 29, 4, 30.62 ± 17.46	Mann Whitney test, p = 0.0080
Figure 2.10 A – Duration of apical nuclear migration (min)	Figure 3 G – Duration of apical nuclear migration (min)	Control, 57, 4, 20.32 ± 8.386	Lamin A OE mosaic, 39, 6, 36.95 ± 23.38	Mann Whitney test, p < 0.0001
Figure 2.10 B – Total path (T) (µm)	Figure S4 C – Total path covered (T) (µm)	Control, 54, 4, 13.05 ± 5.957	Lamin A OE transgenic line, 29, 4, 16.95 ± 9.008	Mann Whitney test, p = 0.0720

Figure 2.10 B – Total path (T) (µm)	Figure S4 C – Total path covered (T) (µm)	Control, 54, 4, 13.05 ± 5.957	Lamin A OE mosaic, 39, 6, 18.88 ± 11.28	Mann Whitney test, p = 0.0096
Figure 2.10 C – Shortest distance between starting and division positions (d) (µm)	Figure S4 B – Shortest distance between starting and apical positions (d) (µm)	Control, 54, 4, 9.394 ± 5.355	Lamin A OE transgenic line, 29, 4, 5.928 ± 3.352	Mann Whitney test, p = 0.0020
Figure 2.10 C – Shortest distance between starting and division positions (d) (µm)	Figure S4 B – Shortest distance between starting and apical positions (d) (µm)	Control, 54, 4, 9.394 ± 5.355	Lamin A OE mosaic, 39, 6, 8.131 ± 5.843	Mann Whitney test, p = 0.1566
Figure 2.10 D – Surplus of distance travelled (T – d) (µm)	Figure 3 H – Surplus of distance travelled (T – d) (µm)	Control, 52, 4, 3,793 ± 3.284	Lamin A OE transgenic line, 29, 4, 11.02 ± 8.183	Mann Whitney test, p < 0.0001
Figure 2.10 D – Surplus of distance travelled (T – d) (µm)	Figure 3 H – Surplus of distance travelled (T – d) (µm)	Control, 52, 4, 3,793 ± 3.284	Lamin A OE mosaic, 39, 6, 10.75 ± 10.43	Mann Whitney test, p < 0.0001
Figure 2.10 F - Instantaneous velocity during apical nuclear migration (µm/min)	Figure S4 D - Instantaneous velocity during apical nuclear migration (µm/min)	Control, 1065, 4, 0.4763 ± 0.7184	Lamin A OE transgenic line, 888, 4, 0.1936 ± 0.6579	Mann Whitney test, p < 0.0001

Figure 2.10 F- Instantaneous velocity during apical nuclear migration (µm/min)	Figure S4 D - Instantaneous velocity during apical nuclear migration (µm/min)	Control, 1065, 4, 0.4763 ± 0.7184***	Lamin A OE mosaic, 1414, 6, 0.224 ± 0.6793***	Mann Whitney test, p < 0.0001
Figure 2.12 C – Standard deviations from RMSD (µm)	Figure 3 J – Standard deviations from RMSD (µm)	Control (S), 6, 2, 0.2045 ± 0.07231	Control (G2), 10, 2, 0.3453 ± 0.09288	Mann Whitney test, p = 0.0030
Figure 2.12 C – Standard deviations from RMSD (µm)	Figure 3 J – Standard deviations from RMSD (µm)	Lamin A OE transgenic line (S), 6, 2, 0.07841 ± 0.02913	Lamin A OE transgenic line (G2), 10, 2, 0.1482 ± 0.08776	Mann Whitney test, p = 0.1471
Figure 2.13 F – Duration of apical nuclear migration (min)	Figure 4 E – Duration of apical nuclear migration (min)	Control, 35, 3, 20.29 ± 6.819	Lamin A OE transgenic mosaic, 27, 3, 22.04 ± 5.788	Mann Whitney test, p = 0.1859
Figure 2.13 G – Surplus of distance travelled (T – d) (µm)	Figure 4 F – Surplus of distance travelled (T – d) (µm)	Control, 35, 3, 4.434 ± 4.344	Lamin A OE mosaic, 27, 3, 4.090 ± 3.509	Mann Whitney test, p = 0.8740
Figure 2.13 K – Standard deviations from RMSD (µm)	Figure 4 H – Standard deviations from RMSD (µm)	Control (S), 5, 2, 0.2052 ± 0.09643	Control (G2), 5, 2, 0.3314 ± 0.1048	Mann Whitney test, p = 0.0556
Figure 2.13 K – Standard deviations from RMSD (µm)	Figure 4 H – Standard deviations from RMSD (µm)	Lamin A OE mosaic (S), 5, 1, 0.1002 ± 0.05054	Lamin A OE mosaic (G2), 5, 1, 0.2277 ± 0.1634	Mann Whitney test, p = 0.1508
Figure 2.14 B – Duration of apical	Figure 5 F – Duration of	Control → Control, 33, 2, 21.64 ± 8.536	Control → Lamin A OE transgenic line, 17, 3, 42.29 ± 26.53	Unpaired t-test, p = 0.0002

nuclear migration (min)	apical nuclear migration (min)			
Figure 2.15 A – Shortest distance between starting and apical positions (d) (µm)	Figure S6 E – Shortest distance between starting and apical positions (d) (µm)	Control → Control, 31, 2, 6.410 ± 4.119	Control → Lamin A OE transgenic line, 16, 3, 7.239 ± 4.123	Mann Whitney test, p = 0.3409
Figure 2.15 B – Total path covered (T) (µm)	Figure S6 F – Total path covered (T) (µm)	Control → Control, 31, 2, 11.49 ± 5.292	Control → Lamin A OE transgenic line, 16, 3, 22.39 ± 16.04	Mann Whitney test, p = 0.0059
Figure 2.15 C – Surplus of distance travelled (T – d) (µm)	Figure 5 G – Surplus of distance travelled (T – d) (µm)	Control → Control, 31, 2, 5.081 ± 3.941	Control → Lamin A OE transgenic line, 16, 3, 15.15 ± 17.09	Mann Whitney test, p = 0.0247
Figure 2.15 E – Instantaneous velocity (µm/min)	Figure S6 G - Instantaneous velocity during apical nuclear migration (µm/min)	Control → Control, 647, 2, 0.3071 ± 0.6236***	Control → Lamin A OE transgenic line, 643, 3, 0.1801 ± 0.6792***	Mann Whitney test, p = 0.0015
Figure 2.15 F – G2 length (min)	Figure S6 H – G2 phase length (min)	Control → Control, 37, 2,29.70 ± 8.168	Control → Lamin A OE transgenic line, 18, 3, 70.94 ± 37.62	Mann Whitney test, p < 0.0001
Figure 2.16 E – Time between apical arrival and NEB (min)	Figure 6 E – Time between apical arrival and NEB (min)	Control, 57, 4, 7.947 ± 5.935	Lamin A OE transgenic line, 29, 4, 14.55 ± 14.02	Mann Whitney test, p = 0.0282
Figure 2.16 E – Time between	Figure 6 E – Time between	Control, 57, 4, 7.947 ± 5.935	Lamin A OE mosaic, 39, 6, 9.513 ± 14.30	Mann Whitney

apical arrival and NEB (min)	apical arrival and NEB (min)			test, p = 0.2386
Figure 2.16 F – Time between apical arrival and NEB (min)	Figure 6 F – Time between apical arrival and NEB (min)	Control → Control, 34, 2, 9.412 ± 7.370	Control → Lamin A OE transgenic line, 17, 3, 23.24 ± 15.71	Mann Whitney test, p = 0.0027
Figure 2.16 G – Time between apical arrival and Rounding (min)	Figure 6 G – Time between apical arrival and Rounding (min)	Control inj with RAS-GFP, 10, 1, 5.500 ± 1.900	Control → Lamin A OE transgenic line, 15, 3, 38.27 ± 23.83	Mann Whitney test, p < 0.0001
Figure 2.16 G – Time between apical arrival and Rounding (min)	Figure 6 G – Time between apical arrival and Rounding (min)	Control → Control, 4, 1, 5.750 ± 6.292	Control → Lamin A OE transgenic line, 15, 3, 38.27 ± 23.83	Mann Whitney test, p = 0.0021

7. List of Figures

Figure 1.1 Schematic of the Linker of Nucleoskeleton and Cytoskeleton (LINC) complex 15

Figure 1.2 Schematic of the nuclear lamina interactions (Adapted from (Capell and Collins, 2006): 17

Figure 1.3 Schematic showing microtubule-based mechanisms of nuclear positioning: 19

Figure 1.4 Schematic showing Actin-based mechanisms of nuclear positioning: 20

Figure 1.5 Nuclear positioning in Pseudostratified epithelia (PSE): (A) PSE classification according to cell length and density 35

Figure 2. 1 Lamin A overexpression leads to increased Lamin A levels, which integrate into the nuclear lamina .. 41

Figure 2. 2 Upon Lamin A overexpression, nuclei become smaller, maintain their aspect ratio, and exhibit reduced surface deformability: 44

Figure 2. 3 Model of compressible droplets predicts an increase in nuclear stiffness upon Lamin A overexpression: 46

Figure 2. 4 Apparent elasticity (Pa) increases upon Lamin A overexpression, as measured by Atomic Force Microscopy (AFM): 47

Figure 2. 5 Overexpression of Lamin A does not induce DNA damage or overall cell cycle alterations. However, nuclei with Lamin A overexpression exhibit a slower G2 phase: 50

Figure 2. 6 Lamin A overexpression does not influence neurogenesis or lamination: 52

Figure 2. 7 Nuclei overexpressing Lamin A divide apically: 53

Figure 2. 8 Trajectories of Lamin A overexpressing nuclei during S- and G1-phases are similar to controls: 56

Figure 2. 9 Time-lapse images showing that nuclear trajectories to the apical surface are influenced by Lamin A overexpression: 57

Figure 2. 10 Quantifications of apical nuclear migration showing the Lamin A overexpressing nuclei are less directly and slower: 59

Figure 2. 11 Lamin A overexpression does not interfere with cytoskeletal organization: 61

Figure 2. 12 Quantification of nuclear deformability showing reduced nuclear deformations when apical migration is impaired: 63

Figure 2. 13 G2 phase length and nuclear apical migration in the less packed hindbrain: 64

Figure 2. 14 Lamin A overexpression shows less pronounced effects on apical nuclear migration in the hindbrain neuroepithelium: 66

Figure 2. 15 Lamin A overexpression in the environment affects apical nuclear migration of control nuclei: 67

Figure 2. 16 Quantitative Analysis of Apical Migration in a Lamin A overexpressing environment: 69

Figure 2. 17 Lamin A Overexpression in the Environment Affects NEB Timing and Mitotic Rounding: 71

Figure 3. 1 Nuclear deformability facilitates apical nuclear migration in the zebrafish retina: 74

8. List of Abbreviations

3D	Three-Dimensional
AFM	Atomic Force Microscopy
ANM	Apical Nuclear Migration
Arp	Actin-Related Protein
Ath5	Atonal bHLH transcription factor 7
Cdc42	Cell Division Cycle 42
CNM	Centronuclear Myopathies
CNS	Central Nervous System
DAPI	4′,6-Diamidino-2-Phenylindole
DCX	Doublecortin
DNA	Deoxyribonucleic acid
DRF	Diaphanous-Related Formin
EDMD	Emery-Dreifuss Muscular Dystrophy
ER	Endoplasmic Reticulum
ESC	Embryonic Stem Cell
GFP	Green Fluorescence Protein
H2B	Histone 2B
hpf	Hours post fertilisation
hsp	Heat Shock Promoter
IgG fold	Immunoglobulin-fold
IKNM	Interkinetic Nuclear Migration
INM	Inner Nuclear Membrane
KASH	klarsicht, Anc1, and Syne homology
LAD	Lamina-Associated Domain
LINC	Linker of the Nucleoskeleton and Cytoskeleton
lmna	Lamin A
lmnb	Lamin B
LSFM	Light-Sheet Fluorescence Microscope

min	minutes
MEF	Mouse Embryonic Fibroblast
MIP	Maximum Intensity Projection
MLCK	Myosin Light Chain Kinase
MRLC	Myosin Regulatory Light Chain
mRNA	Messenger Ribonucleic Acid
MSD	Mean Squared Deviation
MT	Microtubules
MTOC	Microtubule-organising centre
NEB	Nuclear Envelope Breakdown
Nesprin	Nuclear Envelope Spectrin Repeat Proteins
NLS	Nuclear Localisation Signal
NPC	Nuclear Pore Complex
NPC	Nuclear Pore Complex
OE	Overexpression
ONM	Outer Nuclear Membrane
PBS	Phosphate Buffered Saline solution
PCNA	Proliferating Cell Nuclear Antigen
PFA	Paraformaldehyd
PH3	phospho-histone 3
PNS	Perinuclear Space
PDGF	Platelet derived growth factor
PR	Photoreceptors
PSE	Pseudostratified Epithelia
PTU	1-phenyl-2-thiourea
RFP	Red Fluorescence Protein
RGC	Retinal Ganglion Cells
RMSD	Root Mean Squared Deviations
RNA	Ribonucleic acid
ROCK	Rho-associated kinase
SD	Standard Deviation

SEM	Standart Error of the Mean
SUN	Sad1 and Unc-83
TAN line	Transmembrane Actin-associated Nuclear line
TF	Transcriptor Factor
WASP	Wiskott–Aldrich Syndrome protein
WB	Western Blot
WT	Wild Type

9. References

Amini R, Bhatnagar A, Schlüßler R, Möllmert S, Guck J, Norden C. 2022a. Amoeboid-like migration ensures correct horizontal cell layer formation in the developing vertebrate retina. *eLife* **11**:e76408. doi:10.7554/eLife.76408

Amini R, Bhatnagar A, Schlüßler R, Möllmert S, Guck J, Norden C. 2022b. Amoeboid-like migration ensures correct horizontal cell layer formation in the developing vertebrate retina. *eLife* **11**:e76408. doi:10.7554/eLife.76408

Amini R, Rocha-Martins M, Norden C. 2018. Neuronal Migration and Lamination in the Vertebrate Retina. *Front Neurosci* **11**:742. doi:10.3389/fnins.2017.00742

Barriga EH, Franze K, Charras G, Mayor R. 2018. Tissue stiffening coordinates morphogenesis by triggering collective cell migration in vivo. *Nature* **554**:523–527. doi:10.1038/nature25742

Bell ES, Shah P, Zuela-Sopilniak N, Kim D, Varlet A-A, Morival JLP, McGregor AL, Isermann P, Davidson PM, Elacqua JJ, Lakins JN, Vahdat L, Weaver VM, Smolka MB, Span PN, Lammerding J. 2022. Low lamin A levels enhance confined cell migration and metastatic capacity in breast cancer. *Oncogene* **41**:4211–4230. doi:10.1038/s41388-022-02420-9

Calero-Cuenca FJ, Janota CS, Gomes ER. 2018. Dealing with the nucleus during cell migration. *Current Opinion in Cell Biology* **50**:35–41. doi:10.1016/j.ceb.2018.01.014

Capell BC, Collins FS. 2006. Human laminopathies: nuclei gone genetically awry. *Nat Rev Genet* **7**:940–952. doi:10.1038/nrg1906

Chang W, Antoku S, Östlund C, Worman HJ, Gundersen GG. 2015. Linker of nucleoskeleton and cytoskeleton (LINC) complex-mediated actin-dependent nuclear positioning orients centrosomes in migrating myoblasts. *Nucleus* **6**:77–88. doi:10.1080/19491034.2015.1004947

Constantinescu D, Gray HL, Sammak PJ, Schatten GP, Csoka AB. 2006. Lamin A/C Expression Is a Marker of Mouse and Human Embryonic Stem Cell Differentiation. *Stem Cells* **24**:177–185. doi:10.1634/stemcells.2004-0159

Dauer WT, Worman HJ. 2009. The Nuclear Envelope as a Signaling Node in Development and Disease. *Developmental Cell* **17**:626–638. doi:10.1016/j.devcel.2009.10.016

Davidson PM, Denais C, Bakshi MC, Lammerding J. 2014. Nuclear Deformability Constitutes a Rate-Limiting Step During Cell Migration in 3-D Environments. *Cel Mol Bioeng* **7**:293–306. doi:10.1007/s12195-014-0342-y

Dechat T, Pfleghaar K, Sengupta K, Shimi T, Shumaker DK, Solimando L, Goldman RD. 2008. Nuclear lamins: major factors in the structural organization and function of the nucleus and chromatin. *Genes Dev* **22**:832–853. doi:10.1101/gad.1652708

Denais CM, Gilbert RM, Isermann P, McGregor AL, Te Lindert M, Weigelin B, Davidson PM, Friedl P, Wolf K, Lammerding J. 2016. Nuclear envelope rupture and repair during cancer cell migration. *Science* **352**:353–358. doi:10.1126/science.aad7297

Deshpande O, Telley IA. 2021. Nuclear positioning during development: Pushing, pulling and flowing. *Seminars in Cell & Developmental Biology* **120**:10–21. doi:10.1016/j.semcdb.2021.09.020

Ferme LC, Ryan AQ, Haase R, Modes CD, Norden C. 2024. Timely neurogenesis enables increased nuclear packing order during neuronal lamination. doi:10.1101/2024.11.12.623216

Folker ES, Baylies MK. 2013. Nuclear positioning in muscle development and disease. *Front Physiol* **4**. doi:10.3389/fphys.2013.00363

Friedl P, Wolf K, Lammerding J. 2011. Nuclear mechanics during cell migration. *Current Opinion in Cell Biology* **23**:55–64. doi:10.1016/j.ceb.2010.10.015

Gleeson JG, Allen KM, Fox JW, Lamperti ED, Berkovic S, Scheffer I, Cooper EC, Dobyns WB, Minnerath SR, Ross ME, Walsh CA. 1998. doublecortin, a Brain-Specific Gene Mutated in Human X-Linked Lissencephaly and Double Cortex Syndrome, Encodes a Putative Signaling Protein. *Cell* **92**:63–72. doi:10.1016/S0092-8674(00)80899-5

Gomes ER, Jani S, Gundersen GG. 2005. Nuclear Movement Regulated by Cdc42, MRCK, Myosin, and Actin Flow Establishes MTOC Polarization in Migrating Cells. *Cell* **121**:451–463. doi:10.1016/j.cell.2005.02.022

Gönczy P, Pichler S, Kirkham M, Hyman AA. 1999. Cytoplasmic Dynein Is Required for Distinct Aspects of Mtoc Positioning, Including Centrosome Separation, in the One Cell Stage *Caenorhabditis elegans* Embryo. *The Journal of Cell Biology* **147**:135–150. doi:10.1083/jcb.147.1.135

Gruenbaum Y, Foisner R. 2015. Lamins: Nuclear Intermediate Filament Proteins with Fundamental Functions in Nuclear Mechanics and Genome Regulation. *Annu Rev Biochem* **84**:131–164. doi:10.1146/annurev-biochem-060614-034115

Gundersen GG, Worman HJ. 2013. Nuclear Positioning. *Cell* **152**:1376–1389. doi:10.1016/j.cell.2013.02.031

Harada T, Swift J, Irianto J, Shin J-W, Spinler KR, Athirasala A, Diegmiller R, Dingal PCDP, Ivanovska IL, Discher DE. 2014. Nuclear lamin stiffness is a barrier to 3D migration, but softness can limit survival. *Journal of Cell Biology* **204**:669–682. doi:10.1083/jcb.201308029

Herrera I, Fernandes JAL, Shir-Mohammadi K, Levesque J, Mattar P. 2023. Lamin A upregulation reorganizes the genome during rod photoreceptor degeneration. *Cell Death Dis* **14**:701. doi:10.1038/s41419-023-06224-x

Hoijman E, Rubbini D, Colombelli J, Alsina B. 2015. Mitotic cell rounding and epithelial thinning regulate lumen growth and shape. *Nat Commun* **6**:7355. doi:10.1038/ncomms8355

Hu DJ-K, Baffet AD, Nayak T, Akhmanova A, Doye V, Vallee RB. 2013. Dynein Recruitment to Nuclear Pores Activates Apical Nuclear Migration and Mitotic Entry in Brain Progenitor Cells. *Cell* **154**:1300–1313. doi:10.1016/j.cell.2013.08.024

Hutchison CJ. 2002. Lamins: building blocks or regulators of gene expression? *Nat Rev Mol Cell Biol* **3**:848–858. doi:10.1038/nrm950

Hutchison CJ, Worman HJ. 2004. A-type lamins: Guardians of the soma? *Nat Cell Biol* **6**:1062–1067. doi:10.1038/ncb1104-1062

Icha J, Kunath C, Rocha-Martins M, Norden C. 2016a. Independent modes of ganglion cell translocation ensure correct lamination of the zebrafish retina. *Journal of Cell Biology* **215**:259–275. doi:10.1083/jcb.201604095

Icha J, Schmied C, Sidhaye J, Tomancak P, Preibisch S, Norden C. 2016b. Using Light Sheet Fluorescence Microscopy to Image Zebrafish Eye Development. *JoVE* 53966. doi:10.3791/53966

Icha J, Weber M, Waters JC, Norden C. 2017. Phototoxicity in live fluorescence microscopy, and how to avoid it. *BioEssays* **39**:1700003. doi:10.1002/bies.201700003

Isermann P, Lammerding J. 2013. Nuclear Mechanics and Mechanotransduction in Health and Disease. *Current Biology* **23**:R1113–R1121. doi:10.1016/j.cub.2013.11.009

Iyer KV, Taubenberger A, Zeidan SA, Dye NA, Eaton S, Jülicher F. 2021. Apico-basal cell compression regulates Lamin A/C levels in epithelial tissues. *Nat Commun* **12**:1756. doi:10.1038/s41467-021-22010-9

Jungbluth H, Wallgren-Pettersson C, Laporte J. 2008. Centronuclear (myotubular) myopathy. *Orphanet J Rare Dis* **3**:26. doi:10.1186/1750-1172-3-26

Kalukula Y, Stephens AD, Lammerding J, Gabriele S. 2022. Mechanics and functional consequences of nuclear deformations. *Nat Rev Mol Cell Biol* **23**:583–602. doi:10.1038/s41580-022-00480-z

Kim S, Amini R, Yen S-T, Pospíšil P, Boutillon A, Deniz IA, Campàs O. 2024. A nuclear jamming transition in vertebrate organogenesis. *Nat Mater*. doi:10.1038/s41563-024-01972-3

Kosodo Y, Suetsugu T, Suda M, Mimori-Kiyosue Y, Toida K, Baba SA, Kimura A, Matsuzaki F. 2011. Regulation of interkinetic nuclear migration by cell cycle-coupled active and passive mechanisms in the developing brain: Mechanisms of interkinetic nuclear migration. *The EMBO Journal* **30**:1690–1704. doi:10.1038/emboj.2011.81

Lammerding J, Fong LG, Ji JY, Reue K, Stewart CL, Young SG, Lee RT. 2006. Lamins A and C but Not Lamin B1 Regulate Nuclear Mechanics. *Journal of Biological Chemistry* **281**:25768–25780. doi:10.1074/jbc.M513511200

Lancaster OM, Le Berre M, Dimitracopoulos A, Bonazzi D, Zlotek-Zlotkiewicz E, Picone R, Duke T, Piel M, Baum B. 2013. Mitotic Rounding Alters Cell Geometry to Ensure Efficient Bipolar Spindle Formation. *Developmental Cell* **25**:270–283. doi:10.1016/j.devcel.2013.03.014

Lee HO, Norden C. 2013. Mechanisms controlling arrangements and movements of nuclei in pseudostratified epithelia. *Trends in Cell Biology* **23**:141–150. doi:10.1016/j.tcb.2012.11.001

Lehner CF, Stick R, Eppenberger HM, Nigg EA. 1987. Differential expression of nuclear lamin proteins during chicken development. *The Journal of cell biology* **105**:577–587. doi:10.1083/jcb.105.1.577

Leung L, Klopper AV, Grill SW, Harris WA, Norden C. 2011. Apical migration of nuclei during G2 is a prerequisite for all nuclear motion in zebrafish neuroepithelia. *Development* **138**:5003–5013. doi:10.1242/dev.071522

Lomakin AJ, Cattin CJ, Cuvelier D, Alraies Z, Molina M, Nader GPF, Srivastava N, Sáez PJ, Garcia-Arcos JM, Zhitnyak IY, Bhargava A, Driscoll MK, Welf ES, Fiolka R, Petrie RJ, De Silva NS, González-Granado JM, Manel N, Lennon-Duménil AM, Müller DJ, Piel M. 2020. The nucleus acts as a ruler tailoring cell responses to spatial constraints. *Science* **370**:eaba2894. doi:10.1126/science.aba2894

Luxton GWG, Gomes ER, Folker ES, Vintinner E, Gundersen GG. 2010. Linear Arrays of Nuclear Envelope Proteins Harness Retrograde Actin Flow for Nuclear Movement. *Science* **329**:956–959. doi:10.1126/science.1189072

Luxton GWG, Gomes ER, Folker ES, Worman H, Gundersen GG. 2011. TAN lines: A novel nuclear envelope structure involved in nuclear positioning. *Nucleus* **2**:173–181. doi:10.4161/nucl.2.3.16243

Malashicheva A, Perepelina K. 2021. Diversity of Nuclear Lamin A/C Action as a Key to Tissue-Specific Regulation of Cellular Identity in Health and Disease. *Front Cell Dev Biol* **9**:761469. doi:10.3389/fcell.2021.761469

Matejčić M, Salbreux G, Norden C. 2018. A non-cell-autonomous actin redistribution enables isotropic retinal growth. *PLoS Biol* **16**:e2006018. doi:10.1371/journal.pbio.2006018

McGregor AL, Hsia C-R, Lammerding J. 2016. Squish and squeeze — the nucleus as a physical barrier during migration in confined environments. *Current Opinion in Cell Biology* **40**:32–40. doi:10.1016/j.ceb.2016.01.011

Meyer EJ, Ikmi A, Gibson MC. 2011. Interkinetic Nuclear Migration Is a Broadly Conserved Feature of Cell Division in Pseudostratified Epithelia. *Current Biology* **21**:485–491. doi:10.1016/j.cub.2011.02.002

Moore JK, Stuchell-Brereton MD, Cooper JA. 2009. Function of dynein in budding yeast: Mitotic spindle positioning in a polarized cell. *Cell Motil Cytoskeleton* **66**:546–555. doi:10.1002/cm.20364

Nakajima Y, Meyer EJ, Kroesen A, McKinney SA, Gibson MC. 2013. Epithelial junctions maintain tissue architecture by directing planar spindle orientation. *Nature* **500**:359–362. doi:10.1038/nature12335

Nerli E, Kretzschmar J, Bianucci T, Rocha-Martins M, Zechner C, Norden C. 2023. Deterministic and probabilistic fate decisions co-exist in a single retinal lineage. *The EMBO Journal* **42**:e112657. doi:10.15252/embj.2022112657

Nerli E, Rocha-Martins M, Norden C. 2020. Asymmetric neurogenic commitment of retinal progenitors is regulated via the Notch endocytic pathway (preprint). Developmental Biology. doi:10.1101/2020.06.30.179499

Norden C. 2017. Pseudostratified epithelia – cell biology, diversity and roles in organ formation at a glance. *Journal of Cell Science* jcs.192997. doi:10.1242/jcs.192997

Norden C, Young S, Link BA, Harris WA. 2009. Actomyosin Is the Main Driver of Interkinetic Nuclear Migration in the Retina. *Cell* **138**:1195–1208. doi:10.1016/j.cell.2009.06.032

Padilla JR, Ferreira LM, Folker ES. 2022. Nuclear movement in multinucleated cells. *Development* **149**:dev200749. doi:10.1242/dev.200749

Röber R-A, Weber K, Osborn M. 1989. Differential timing of nuclear lamin A/C expression in the various organs of the mouse embryo and the young animal: a developmental study. *Development* **105**:365–378. doi:10.1242/dev.105.2.365

Roman W, Martins JP, Carvalho FA, Voituriez R, Abella JVG, Santos NC, Cadot B, Way M, Gomes ER. 2017. Myofibril contraction and crosslinking drive nuclear movement to the periphery of skeletal muscle. *Nat Cell Biol* **19**:1189–1201. doi:10.1038/ncb3605

Rowat AC, Jaalouk DE, Zwerger M, Ung WL, Eydelnant IA, Olins DE, Olins AL, Herrmann H, Weitz DA, Lammerding J. 2013. Nuclear Envelope Composition Determines the Ability of Neutrophil-type Cells to Passage through Micron-scale Constrictions. *Journal of Biological Chemistry* **288**:8610–8618. doi:10.1074/jbc.M112.441535

Salina D, Bodoor K, Eckley DM, Schroer TA, Rattner JB, Burke B. 2002. Cytoplasmic Dynein as a Facilitator of Nuclear Envelope Breakdown. *Cell* **108**:97–107. doi:10.1016/S0092-8674(01)00628-6

Sauer FC. 1935. Mitosis in the neural tube. *Journal of Comparative Neurology* **62**:377–405. doi:10.1002/cne.900620207

Sellers JR, Wang F, Chantler PD. 2003. Trifluoperazine inhibits the MgATPase activity and in vitro motility of conventional and unconventional myosins. *J Muscle Res Cell Motil* **24**:579–585. doi:10.1023/B:JURE.0000009969.04562.58

Shu T, Ayala R, Nguyen M-D, Xie Z, Gleeson JG, Tsai L-H. 2004. Ndel1 Operates in a Common Pathway with LIS1 and Cytoplasmic Dynein to Regulate Cortical Neuronal Positioning. *Neuron* **44**:263–277. doi:10.1016/j.neuron.2004.09.030

Sidhaye J, Norden C. 2017. Concerted action of neuroepithelial basal shrinkage and active epithelial migration ensures efficient optic cup morphogenesis. *eLife* **6**:e22689. doi:10.7554/eLife.22689

Skop AR, White JG. 1998. The dynactin complex is required for cleavage plane specification in early Caenorhabditis elegans embryos. *Current Biology* **8**:1110–1117. doi:10.1016/S0960-9822(98)70465-8

Snider NT, Omary MB. 2014. Post-translational modifications of intermediate filament proteins: mechanisms and functions. *Nat Rev Mol Cell Biol* **15**:163–177. doi:10.1038/nrm3753

Solecki DJ, Model L, Gaetz J, Kapoor TM, Hatten ME. 2004. Par6α signaling controls glial-guided neuronal migration. *Nat Neurosci* **7**:1195–1203. doi:10.1038/nn1332

Strzyz PJ, Lee HO, Sidhaye J, Weber IP, Leung LC, Norden C. 2015. Interkinetic Nuclear Migration Is Centrosome Independent and Ensures Apical Cell Division to Maintain Tissue Integrity. *Developmental Cell* **32**:203–219. doi:10.1016/j.devcel.2014.12.001

Strzyz PJ, Matejcic M, Norden C. 2016. Heterogeneity, Cell Biology and Tissue Mechanics of Pseudostratified Epithelia: Coordination of Cell Divisions and Growth in Tightly Packed TissuesInternational Review of Cell and Molecular Biology. Elsevier. pp. 89–118. doi:10.1016/bs.ircmb.2016.02.004

Swift J, Ivanovska IL, Buxboim A, Harada T, Dingal PCDP, Pinter J, Pajerowski JD, Spinler KR, Shin J-W, Tewari M, Rehfeldt F, Speicher DW, Discher DE. 2013. Nuclear Lamin-A Scales with Tissue Stiffness and Enhances Matrix-Directed Differentiation. *Science* **341**:1240104. doi:10.1126/science.1240104

Tanaka T, Serneo FF, Higgins C, Gambello MJ, Wynshaw-Boris A, Gleeson JG. 2004. Lis1 and doublecortin function with dynein to mediate coupling of the nucleus to the centrosome in neuronal migration. *The Journal of Cell Biology* **165**:709–721. doi:10.1083/jcb.200309025

Tsai J-W, Bremner KH, Vallee RB. 2007. Dual subcellular roles for LIS1 and dynein in radial neuronal migration in live brain tissue. *Nat Neurosci* **10**:970–979. doi:10.1038/nn1934

Tsai J-W, Lian W-N, Kemal S, Kriegstein AR, Vallee RB. 2010. Kinesin 3 and cytoplasmic dynein mediate interkinetic nuclear migration in neural stem cells. *Nat Neurosci* **13**:1463–1471. doi:10.1038/nn.2665

Urciuoli E, D'Oria V, Petrini S, Peruzzi B. 2021. Lamin A/C Mechanosensor Drives Tumor Cell Aggressiveness and Adhesion on Substrates With Tissue-Specific Elasticity. *Front Cell Dev Biol* **9**:712377. doi:10.3389/fcell.2021.712377

Varshney N, Sanyal K. 2019. Nuclear migration in budding yeasts: position before division. *Curr Genet* **65**:1341–1346. doi:10.1007/s00294-019-01000-x

Wang Y, Elsherbiny A, Kessler L, Cordero J, Shi H, Serke H, Lityagina O, Trogisch FA, Mohammadi MM, El-Battrawy I, Backs J, Wieland T, Heineke J, Dobreva G. 2022. Lamin A/C-dependent chromatin architecture safeguards naïve pluripotency to prevent aberrant cardiovascular cell fate and function. *Nat Commun* **13**:6663. doi:10.1038/s41467-022-34366-7

Yamada KM, Sixt M. 2019. Mechanisms of 3D cell migration. *Nat Rev Mol Cell Biol* **20**:738–752. doi:10.1038/s41580-019-0172-9

Yanakieva I, Erzberger A, Matejčić M, Modes CD, Norden C. 2019. Cell and tissue morphology determine actin-dependent nuclear migration mechanisms in neuroepithelia. *Journal of Cell Biology* **218**:3272–3289. doi:10.1083/jcb.201901077

Yanakieva I, Matejčić M, Norden C. 2018. Choosing the right microscope to image mitosis in zebrafish embryos: A practical guideMethods in Cell Biology. Elsevier. pp. 107–127. doi:10.1016/bs.mcb.2018.03.017

Zhao T, Graham OS, Raposo A, St Johnston D. 2012. Growing Microtubules Push the Oocyte Nucleus to Polarize the *Drosophila* Dorsal-Ventral Axis. *Science* **336**:999–1003. doi:10.1126/science.1219147

Zheng M, Jin G, Zhou Z. 2022. Post-Translational Modification of Lamins: Mechanisms and Functions. *Front Cell Dev Biol* **10**:864191. doi:10.3389/fcell.2022.864191

Zuela N, Bar DZ, Gruenbaum Y. 2012. Lamins in development, tissue maintenance and stress. *EMBO Reports* **13**:1070–1078. doi:10.1038/embor.2012.167